5-2001

The influence of process parameters on filament size distribution

Saybil Nuray Ercan

THE INFLUENCE OF PROCESS PARAMETERS ON FILAMENT SIZE DISTRIBUTION

By

Saybil Nuray Ercan

B.Sc., Boğaziçi University, 1994

M.Sc., Boğaziçi University, 1996

A THESIS

Submitted in Partial Fulfillment of the

Requirements for the Degree of

Doctor of Philosophy

(in Chemical Engineering)

The Graduate School

The University of Maine

May, 2001

Advisory Committee:

Douglas W. Bousfield, Professor of Chemical Engineering and Advisor

Joseph Aspler, Senior Scientist, PAPFUCAN

Patrice Aurenty, Scientist, Sun Chemical

Albert Co, Associate Professor of Chemical Engineering

Edward Thompson, Professor of Chemical Engineering

THE INFLUENCE OF PROCESS PARAMETERS ON FILAMENT SIZE DISTRIBUTION

By Saybil Nuray Ercan

Thesis Advisor: Dr. Douglas W. Bousfield

An Abstract of the Thesis Presented

in Partial Fulfillment of the Requirements for the

Degree of Doctor of Philosophy

(in Chemical Engineering)

May, 2001

Filaments are formed at the exit of rolling nips in some coating and printing operations. The filament size distribution can determine product quality such as gloss. The average filament size is linked to operational difficulties such as misting. The filament size distribution of various fluids and inks is characterized and compared to theoretical model. A high-speed video camera is used to visualize the exit of a rolling nip. The size distribution of the filaments is characterized with image analysis. A laboratory print tester is used with the high speed camera to characterize the size of the defects right after printing. The rheological properties are obtained using a cone and plate rheometer. A novel test is developed characterize the fluids cavitation pressure using a mechanical tester and a closed syringe. Elongational properties are obtained with a falling bob technique.

Fluid rheology has a strong influence on filamentation. The cavitation results do not give a direct correlation with filament volume. The elongational properties of the fluids have a strong effect on filamentation but in a complex manner. **As** printing speed or ink film thickness increases, the filaments increase in average size and in their size distribution. The nip loading does not have a large effect on filament size nor the size distribution. Porous substrates reduces or eliminates the "remains" within the detectable limit.

An empirical correlation is developed to link average filament volume to dimensionless parameters of Reynolds number, Deborah number, and Trouton's ratio. Reasonable correlations are obtained for specific groups of fluids but low correlation is found for the entire fluid set.

A physical model is proposed to predict the occurrence of filamentation and the filament volume. Theoretical predictions are compared to the experimental filament volume for all fluids. The results indicate that a small number of cavities that are formed actually coalesce to form filaments. By altering this fraction linearly with the Trouton ratio, the filament volumes are predicted. The Newtonian model including the elongational effects predicts the filament volume best. The persistent wide scatter in the results compared to the model or the empirical correlation implies that at least one other parameter affects the filamentation process.

ACKNOWLEDGEMENTS

This study was carried out in the Paper Surface Science Program of the Chemical Engineering Department at the University of Maine between October 1996 and December 2000.

I would like to express my sincere gratitude to my thesis advisor Prof. Dr. Douglas W. Bousfield for his continuous guidance, generous support and valuable advice throughout the research.

I wish to express my special thanks to Dr. Joe Aspler, Dr. Patrice Aurenty, Assoc. Prof. Dr. Albert Co, and Prof. Dr. Edward Thompson for the time they have devoted to reading and commenting on my thesis dissertation.

I would like to thank the sponsors of the Paper Surface Science Program for their support throughout this research. I wish to thank Dr. Tamal Ghosh for the comments and data he supplied. Heartfelt thanks are due to the assistants and staff of the Chemical Engineering Department and Pilot Plant for their willingness to understand and help.

I am deeply obliged to Daphné M. Desjumaux for being a very close friend and for her support and encouragement throughout this research.

I am indebted especially to my fiancé Mehmet Mete Altıntaş for sharing all the good and bad moments, for being my friend and for providing me with the encouragement and everlasting support I needed throughout this research and for so many years.

Finally, this work would not have been possible without the patience and everlasting support of my family. This dissertation is dedicated to my family to whom I owe everything.

TABLE OF CONTENTS

LIST OF TABLES

LIST OF FIGURES

NOMENCLATURE

Ca	Capillary number $Ca=\mu u/\sigma$
D	Roll Diameter
De	Deborah Number
F	Force per unit width
g	Gravitational acceleration
h	Film thickness
h*	Dimensionless film thickness
h_i	Initial gap in roll geometry
h_f	Height at nip exit
h_f	Filtercake thickness
h(x)	Distance between rolls
L	Depth of liquid penetration
m	Mass of bob
P	Pressure
P_{atm}	Vapor Pressure
P_e	Exit Pressure
Q	Volumetric flow rate per unit width
Q_e	Volumetric flow rate per unit length at nip exit
r	Radial direction
R	Roll Radius
R_{disk}	Disk Radius

Re	Reynolds Number
R_m	Radius of curvature of the film split meniscus
t	time
Tr	Trouton Ratio
u	Velocity
u_r	Roll surface velocity
V	Volume
V^*	Dimensionless volume
V_M^*	Maxwell dimensionless volume
V_N^*	Newtonian dimensionless volume
V_P	Predicted volume
V_P^*	Predicted dimensionless volume
v_r	Radial velocity
v_y	Penetration velocity
v_z	z-directional velocity
We	Weber Number
x_e	Exit location
x_i	Entrance location
x	x-direction
y	y-direction
z	z-direction

Greek Symbols

ε_p	Void Fraction
ϕ_c	Volume fraction of particles in coating
ϕ_f	Volume fraction of particles in filtercake
λ	Maxwell relaxation time
μ	Fluid shear viscosity
μ_{el}	Elongational viscosity
ρ	Fluid density
τ	Relaxation time
τ_{rz}	Stress in the cylindrical coordinate system
σ	Surface tension

CHAPTER 1: INTRODUCTION

1.1. Coating

Coating flows feature in many industrial processes, most notably in the chemical process industry, with applications ranging from a single decorative layer on packaging, to multiple layer coatings on photographic film. Other examples of coated products are adhesive tape, surgical dressings, magnetic and optical recording media, lithographic plates, paper and fabrics.

Coating flows are small scale, viscous, free-surface flows, in which a film of liquid is continuously deposited on a moving substrate. In general a thin, uniform film of prescribed thickness is desired. In addition the final layer should be free of imperfections and be applied at high speeds. These requirements are difficult to obtain. The industry is looking to science and engineering research to refine their production processes.

Through a combination of mathematical and experimental investigations over a number of years, much insight has been gained into these complex and sensitive flows. However, due to the wide diversity of coating flow applications and products, this field of research is still open, with industrial competition driving technological advancement.

1.2. Roll Coating

Roll coating is a common method to apply coatings to a substrate. This method is used in a wide range of applications such as painting with a roller, textile sizing, printing, and applying coating layers onto various substrates. Coatings and films produced by depositing material in liquid form and then solidifying it are virtual ingredients of such

products as printing and packaging materials, photographic, x-ray and graphic arts films, various specialty films, photoresist preparations, permselective membranes, magnetic and optical disks, conductive wires and optical fibers, protective and decorative surface layers, adhesive coatings, all sorts of laminates and similar composites. In the paper industry, a recent technique to apply pigmented coatings to paper webs involves metering a coated layer on a rubber covered roll that presses the coating against the web in a rolling nip.

Most papermaking, coating and converting operations involve film-splitting: fourdrinier table rolls, press nips, size press applicators, roll applicators for coating and rewetting, and printing presses. Figure 1.1 shows examples of processes that involve a film split

Typically, there are five major classes of roll coaters. These include forward roll coaters, characterized by co-moving surfaces; reverse roll coaters, characterized by counter moving roll surfaces; transfer roll coaters, which are assemblages of four or more forward roll nips; kiss roll coaters (also known as tensioned web arrangements) characterized by the absence of a backing roll at the application nip; and gravure roll coaters, which utilize a gravure roll.

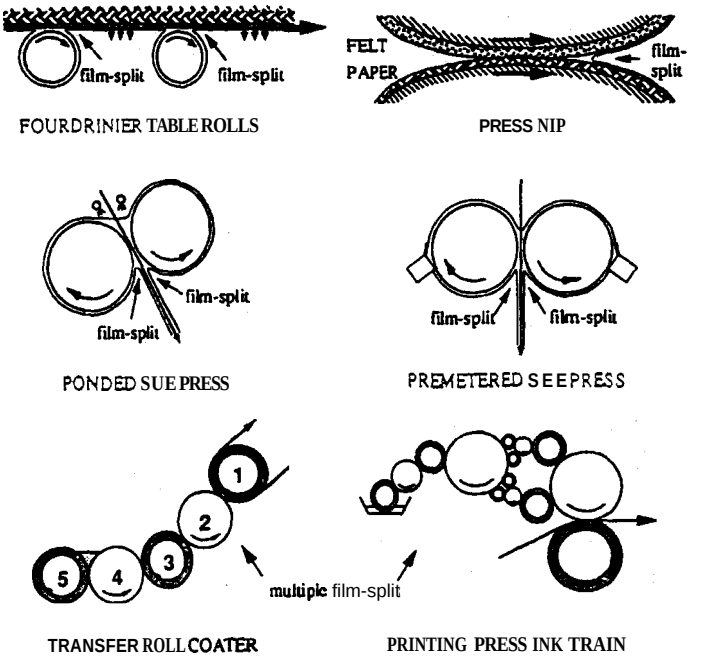

Figure 1.1 : Liquid film-splits in papermaking, coating and converting operations. (Benjamin ***et.*** *al.*, 1994)

Any roll coater can be thought of as an assemblage of gap and nip flows, of which there are eleven types. These unit flows of roll coating are classified in figure 1.2 according to the inflow condition, i.e. flooded, single-film-fed, or double-film-fed; the outflow condition, i.e. flooded, film-splitting or film-transferring; and the relative motion of the rolls – counter-rotating, or forward mode, versus co-rotating, or reverse mode. When the important distinction is drawn between rigid rolls and rolls with a deformable cover of rubber, polyurethane, or other polymer, these unit flows are more than double in number, because one or both rolls of each pair may be deformable. It is how the unit flows are combined that distinguishes one kind of coater from another.

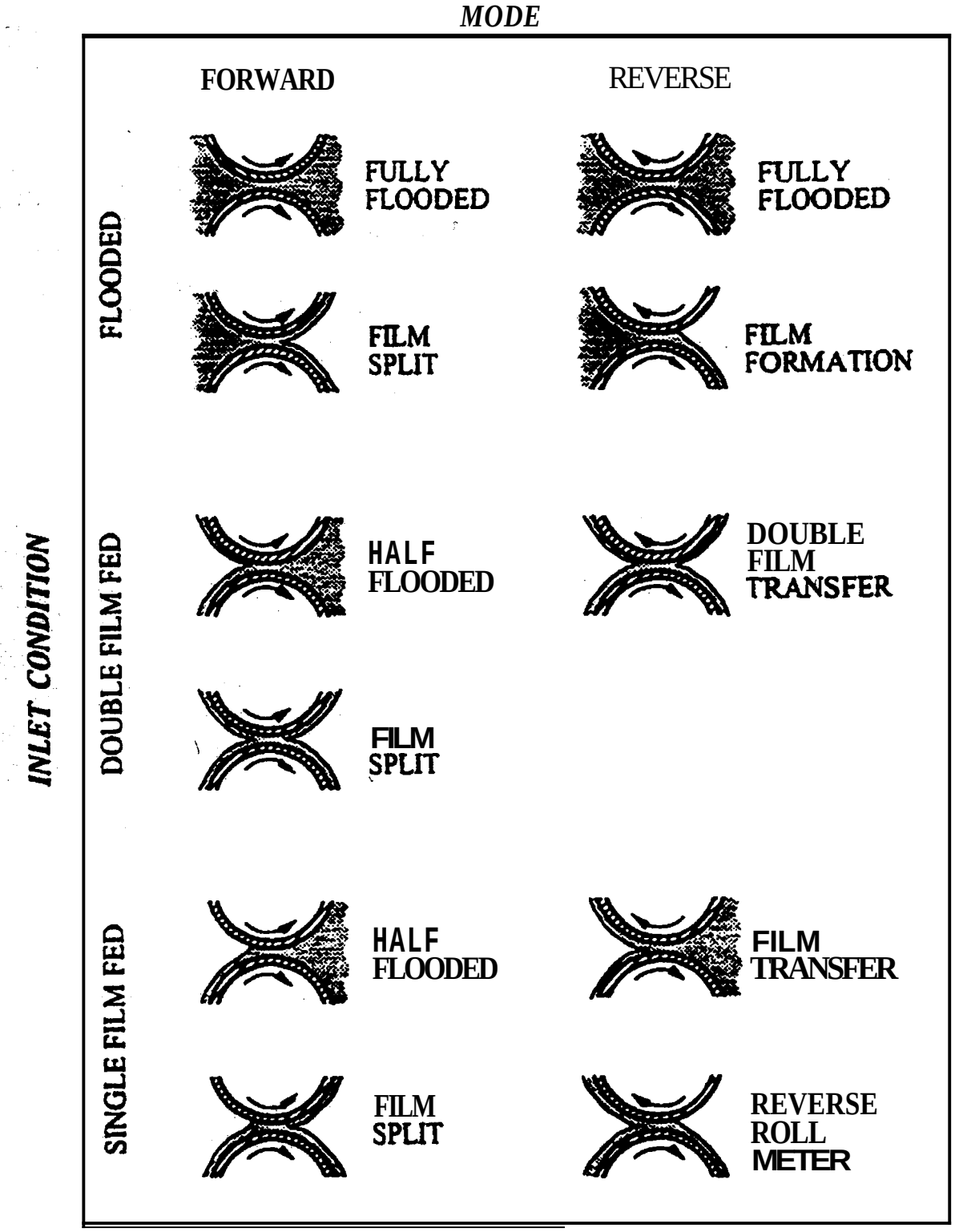

Figure 1.2: Eleven distinct flows between a pair of rolls, also called the hndamental flows of roll coating. (from Benjamin, **1994)**

In any case where thin fluid layers are being separated, a film split will occur. Even in the thin film transfer cases, there is a separation of fluid layers and the possibility of filament formation. Gravure coating generates filaments as liquid is transferred as cells in the roll empty. These filaments should scale with the length scale of the cell.

Coyle *et. al.* (1986,1990) analyzed forward roll coating for laminar flows. The pressure profile and the transfer function were reported. This work does not deal with the filament sizes. However, these studies do describe the pressure distribution inside the nip. Near the nip exit, there is a region of sub-ambient pressure; if this pressure is lower than the vapor pressure of the fluid, cavitation is expected occur.

A simple power-law relationship is usually used to correlate the ratio of the film thicknesses to the ratio of the roll speeds, which actually is a correlation of the experimental data to the theoretical data. (Benkreira *et. al.* 1981; Coyle ***et.*** *al.* 1986, 1987)

In a rolling nip geometry, filaments are produced at the nip exit if the operational speeds are large enough (MacPhee, 1997 a). Nguyen *et. al.* (1994) discusses some aspect of **ink** filaments and splitting characteristics in the nip. The degree of filamentation and filament characteristics may be related to the rheology of the fluid, the printing speed, the substrate properties, the nip loading, and the amount of material fed into the nip. However, there has been no systematic study that integrates the relationship of these parameters to the filament size distribution or the quality of printing and coating in a rolling nip to the filament size.

Misting is a common operational problem at high speeds. **As** the speed increased, misting increased and shifted to a shorter initial period. The rheology of ink is also one of the

parameters that influences misting. As the "quantity" of ink applied was increased the misting quantity increased and the percentage apparently reaches a saturation point (Voet, 1956). Rollers that are not in contact did not show any misting: misting may not be caused by centripetal forces, but exists solely as a result of film transfer. The gap size between the rolls seemed not to have an influence on the misting characteristics (Voet, 1956). Increasing the pigment loading reduced misting but a high load did not seem to eliminate ink misting completely. The other explanation is that additives in the form of particles cause filaments to break sooner. According to Aurenty ***et.*** *al.* (1997) increasing the concentration of the extenders in the ink also increases the elastic nature of the ink. This ensures that the ink snaps at elongation of the ink filament which prevents the formation of ink droplets. The inks varying from short, buttery dispersions to inks of excessive length at the same pigment loading show no significant difference in ink misting (Voet, 1956).

The gloss of a surface is known to depend on the refractive index and the degree of smoothness. The differences in ink gloss will be effected greatly by the degree of smoothness of the surface, as most inks have similar refractive index. The parameters which greatly effect the degree of smoothness are; ink film thickness, printing speed, rheology of the ink, smoothness of the substrate, and the porosity of the substrate. Glatter and Bousfield (1996) have concluded that the printing speed and ink film thickness have a strong influence on the gloss. They have found that high speeds (8 m/s) along with high ink levels *(5* μm) produce an ink film which levels rapidly but subsequently slows down and produces a lower gloss sample.

Generally, in conventional inks, the broken ink filaments, filament "remains", retract on the rolls and flow out to form a glossy film. The gelled inks show such an extremely rapid structural build-up that they cannot flow out. Thus, the retracting filaments are "frozen" in a rough surface pattern, showing matness instead of gloss. Short inks are broken up by shear and need a period of time to recover the structure generally in an order of several seconds, where when the gelled inks are broken up by shear they recover to their original structure in a period of time of a millisecond or less. (Voet, **1956)**

1.3. Coating Defects

Besides the thickness of the coated film, its cosmetic quality is also of importance, and each manufacturer has their own standards of tolerance for frequently encountered defects. Common defects are:

Pin-Holes: Where localized regions of the substrate remain uncoated. This is usually due to non-uniformity, or contamination of the substrate, but may also be due to the bubbles in the coating liquid, due to air entrainment.

Streaks and Drips: Where a coated fill is degraded by careless handling of waste fluid, or as a consequence of centrifugal splashing. Foreign-bodies can also accumulate in the coating system, causing irregularities on the coated film. Streaks may also be formed by what is known as the cascade instability, where the feed to the coating flow varies with time, due to an imbalance of forces at the coating meniscus.

Ribbing or Corduroy: Referring to the transverse variation of film thickness, giving rise to a regular, striated pattern on the coated film. This is a common defect, and

is due to an instability at the coating meniscus, where destabilizing hydrodynamic forces exceed the stabilizing surface tension forces.

All the above defects can be tolerated to some degree, as small amplitude irregularities can settle before drying or curing takes place.

The control and prevention of coating defects is a complicated task, but though careful experimentation and mathematical analysis, operating conditions can be identified to give satisfactory coating quality at sufficiently high rates of application.

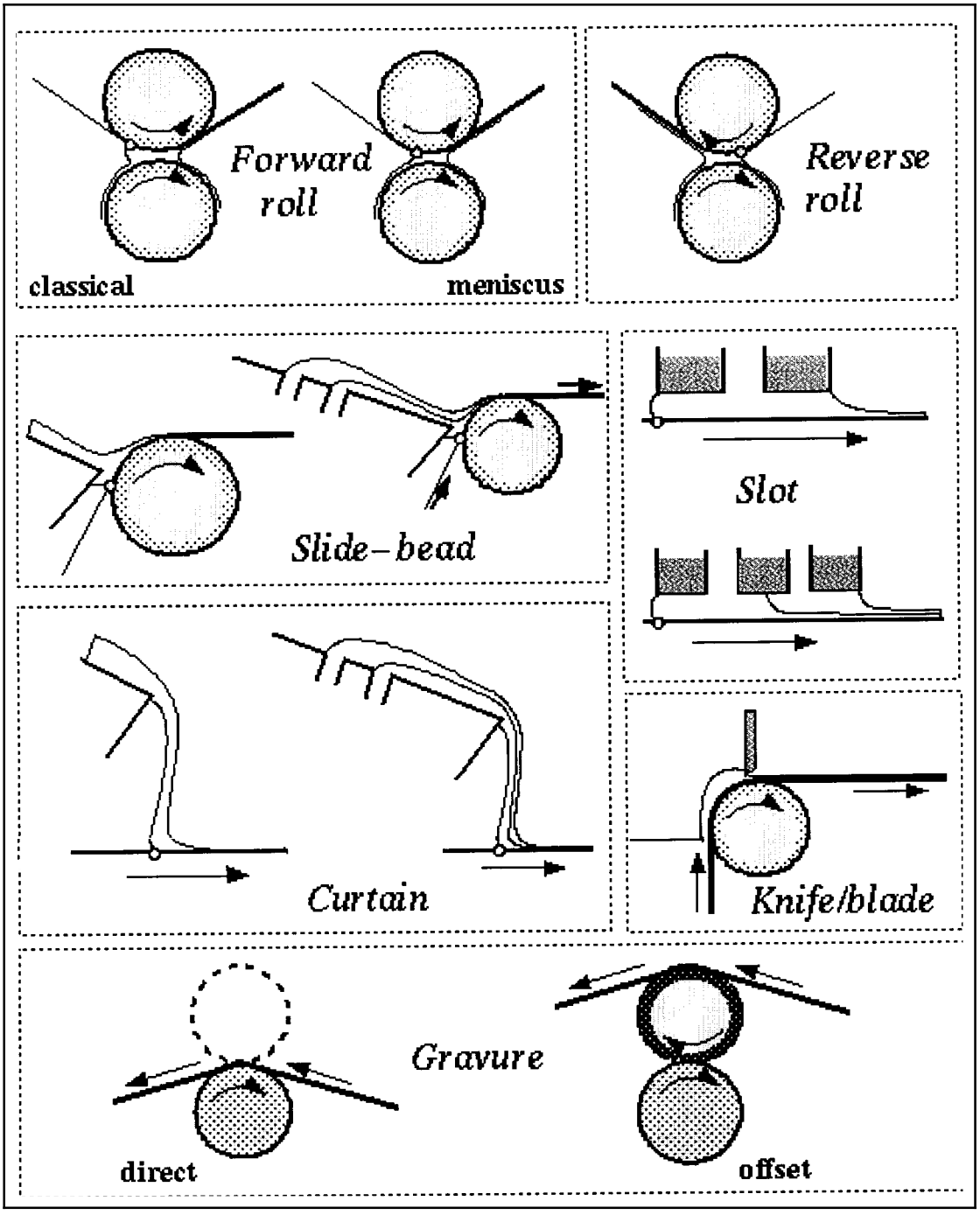

Figure 1.3: Example of different types of roll coaters and coating flows.

As roller surface speed increases, the character of splitting changes due to the onset of a type of hydraulic instability known as ribbing or corduroying. This defect is the formation of equally spaced ridges, parallel to the direction of travel. (MacPhee, 1997 a) Ribbing is a fluid instability, which is well known now and was first investigated by Pitts ***et.*** *al.* (1961) Figure 1.4 shows the different regions of flow. **As** the speed increases, ribbing appears followed by filament formation. This must correlate with the decrease in the pressure in the nip exit and the onset of cavitation.

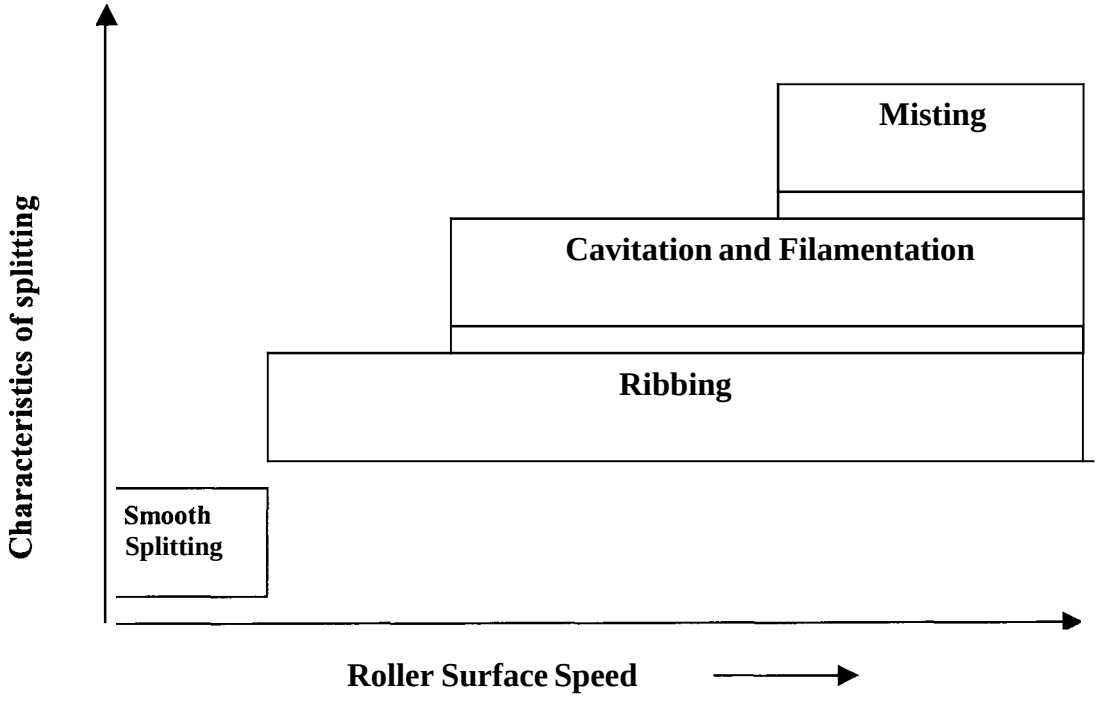

Figure 1.4: Change in character of film splitting at nip exit versus speed (MacPhee, 1997 a)

1.4. Printing

A printing press consists of a series of cylinders that "work" the ink down to a thin, uniform film, by successively splitting ink films. The film is spread over the printing plates on the rotating plate cylinder. In the letterpress printing process raised surfaces receive the ink and the desired image is deposited onto the paper substrate. In the case of offset lithography the image is first offset onto a blanket, and then the image is transferred from the blanket cylinder to the paper in a subsequent printing nip. In either case, the transfer of ink to paper in the printing nip is critical to the resulting image fidelity.

Zettlemoyer (1960) describes the printing nip by considering the flow between two rigid rollers, as shown in figure 1.5. In a nip formed by rigid rollers the pressure increases and peaks and decreases throughout the nip. With presence of a deformable rubber-covered roller, the pressure peak position shifts forward into the nip. The exiting ink film cannot sustain significant tensile forces and the tension created by the extentional flow in the nip exit is relieved by cavitation. The frequency and characteristics of cavitation will determine the filament size. Observations suggest that extentional flow behavior dominates behavior in the separating ink layer. (Pangaloset. *al.*,1985) **As** the fluid exits the nip a number of complex phenomena such as ribbing, web growth, filament formation and misting may occur.

The concept of ink tack is related to the net force or energy developed in the splitting on ink films at the exit of a printing nip. (Zang et. *al.*, 1991). Tack is one of the most important characteristics of an ink, affecting the runnability and printability of papers. Tack may influence filament size.

Aspler (1993) has indicated that under normal printing conditions, less than half the available ink transfers to the paper. Asymmetry increases with ink film thickness and printing speed.

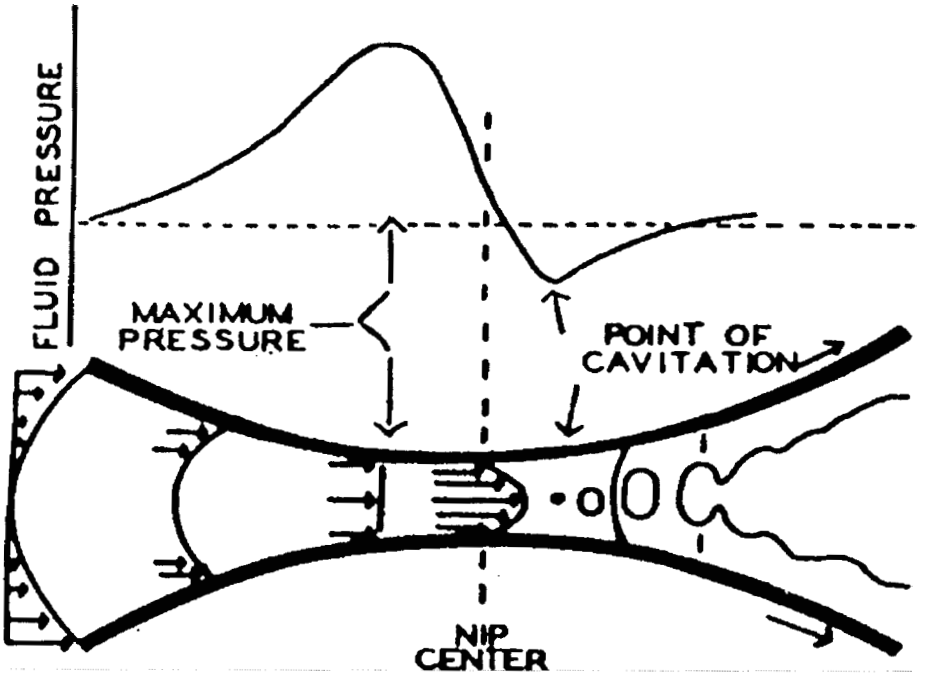

Figure 1.5: Flow in a printing nip and typical pressure profile for rigid cylinders. The arrows indicate the shape of the velocity profile at various locations. (Zettlemoyer, 1960)

Taylor and Zettlemoyer (1958) have found that the surface velocity and the fluid viscosity have an effect on the film split. If the surface velocity and fluid viscosity is low enough, the cohesion of the fluid is great enough to withstand the tension developed, and a smooth film split occurs. At higher speeds and viscosities, the fluid cannot flow rapidly enough to relieve the tension formed as the two geometries separate and therefore,

cavities are formed within the film and an uneven film split occurs causing filaments and filament remains.

Figure 1.5, shows pressure and velocity profiles of this event. At the nip entrance, fluid is dragged into the nip resulting in an increase in pressure. After the nip center, the pressure decreases as the fluid flows toward the exit. If conditions are right, this pressure can drop below the vapor pressure of the fluid to produce cavitation. This is when vapor bubbles form in the liquid. The liquid, which is trapped between the bubbles, is what forms the fluid filament. **As** the fluid is dragged through the nip and farther out the filaments elongate and start to get thinner. As they become thinner there is a point at which they break, this is what is considered the fourth step, the rupture step. The filament break and the remaining part of this fluid, which recoils back toward the surface of the substrate, is what is called the filament "remain" or "residue". These are usually conical shapes that are seen on the surface of the substrate.

De Grâce ***et.*** *al.* (1992) has found that the length of filaments increased as the shear viscosity of the component vehicle of the inks increased. The shear viscosity of the ink (pigment and vehicle) seemed not to effect the length of the filaments at rupture. In this research it was also found that inks with different compositions and of different viscosities, and the oil/resin system all split close to the nip exit when printing thin films of the liquids at high speeds.

Cohu and Magnin (1995) showed that the duration of the shear flow between the rolls is long enough to provide a complete structural breakdown within the paints. It was also found that the high shear-rate steady-state viscosity is relevant to describe the flow properties of the paint during passage between the rolls.

1.5. Metered Size Press

In recent years, metered size press technology has emerged as a versatile coating process capable of applying conventional starch sizing as well as pigmented coatings. In the metered size press, coating is metered onto a transfer roll that applies the coating to the paper web. **As** in printing, misting, in this process can be a serious problem under certain conditions. Roper *et. al.* (1997) linked filament sizes produced in the nip to the misting characteristics of the inks. "Orange peel" patterns may also be related to filament sizes. The conditions that lead to misting and the size of the droplets produced at the nip exit are well characterized by Roper *et. al.* (1997), but the size of filaments produced at the exit of the nip is not characterized.

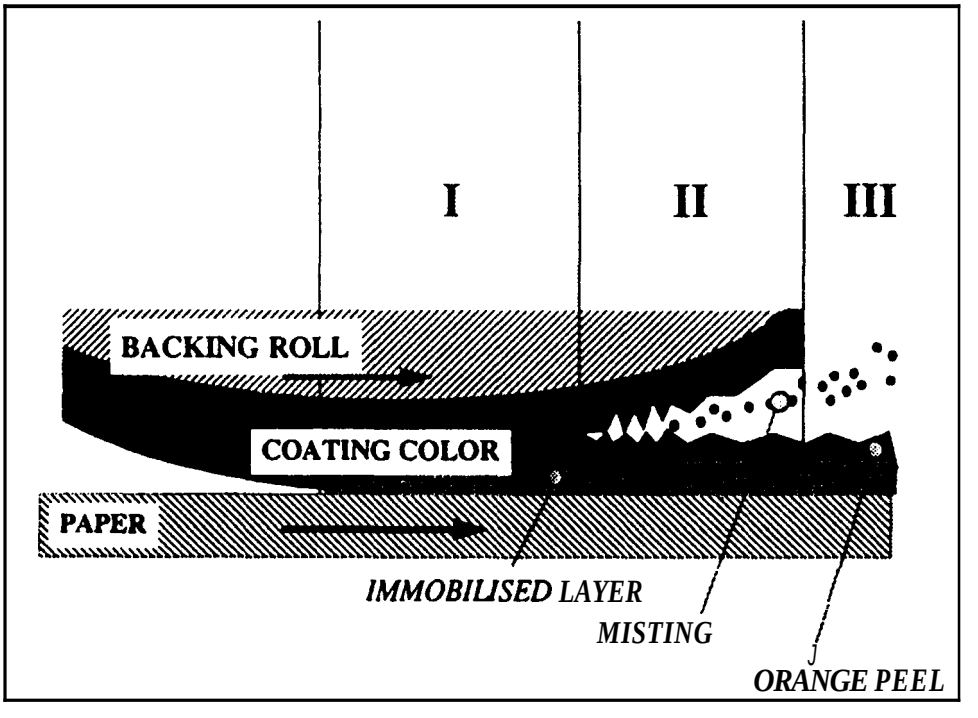

Figure 1.6: Hypothetical model of film splitting. (Roper *et. al.* 1997)

A description of the metered size press was developed by Roper *et. al.* (1997) as illustrated in figure 1.6. This model divides the film splitting process into three regions. The first region, region I, is known as the dewatering region, the coating experiences a pressure pulse which leads to loss of water from the coating into the base paper (Trefz, 1996, Letzelter, 1996). At the interface between the base paper and the applied coating color, an immobilized coating color layer starts to form. The degree of misting and orange-peel formation is controlled by the thickness of the non-immobilized coating layer at the end of the coating application nip (Roper *et. al* 1997). With increasing thickness of the immobilized layer, the non-immobilized coating thickness available for filament formation is reduced. High coating solids and low water retention accelerate growth of the immobilized layer in region I thereby resulting in reduced misting. Confirmation of this has been reported in several studies and current experimental data supports the importance of coating immobilization in the nip for control of misting.

In region II, filaments elongate and break. The excess fluid from breaking of a filament is pulled back onto the web and roll surface by surface tension forces. This occurs in region III of figure 1.6, the relaxation region, which affects the leveling-off of the unevenness of the coating surface. At high coating speeds and if the size of the excess fluid unevenness on the roll surface is large enough, centrifugal forces may be strong enough to overcome the surface tension forces and fling fluid from the rotating roll. From some video images that have been recorded, misting at high speeds seem to show mist droplets separating from the applicator roll at a small distance away from the nip where filaments form (Roper *et. al.,* 1997). Large misting droplets may be generated by centrifugal forces acting on the fluid film on the roll surface and small droplets are generated from the

breakup of filaments at the nip exit (Roper *et. al.,* 1997). Figure 1.7 shows a filament that breaks at two points generating a drop compared to a filament that breaks at one point.

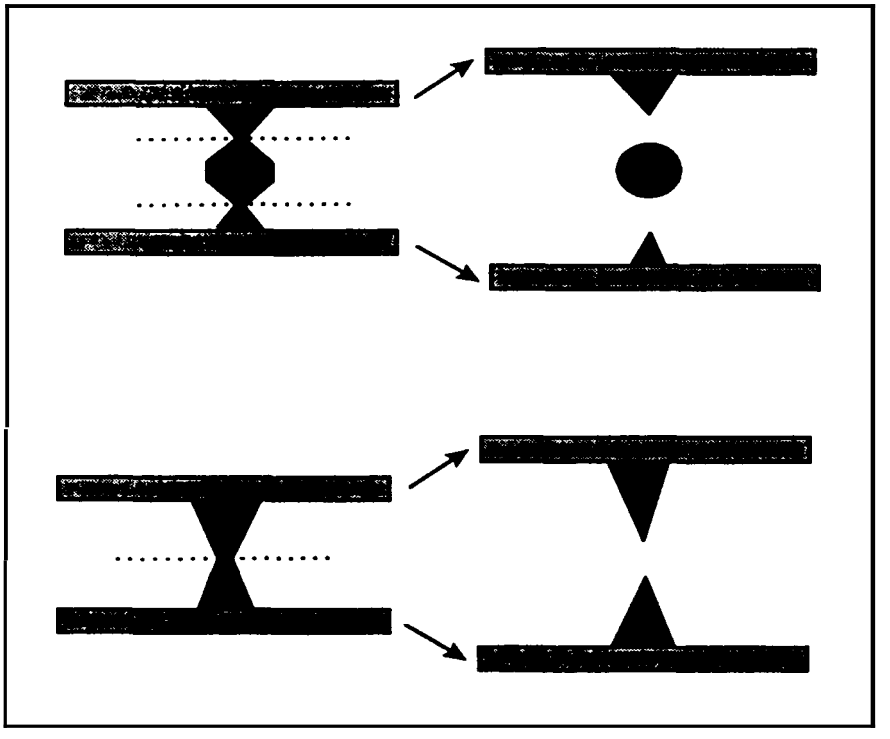

Figure 1.7: Two possible situations for filament breakup (Roper *et. al.,* 1997)

Ninness *et. al.* (1998) proposed a model which described the flow field in the nip of a metered size press. It was found that the pressure field generated in the nip is linked to the amount of penetration in the nip. Ninness *et. al.* (1998) expected that when the pressure in the nip falls below the vapor pressure of water that the liquid layer will cavitate and form filaments.

1.6. Cavitation

Cavitation is defined as the process of nucleation in a liquid when the pressure falls below the vapor pressure (Brennen, 1995), where nucleation is an initiation of a vapor phase. The role of solid particles in producing tensile weakness in the fluid is recognized, but not considered dominant in most flows of interest. Implicit in this description is the presence of inhomogeneity to produce a local "weakness" in the liquid; pure liquid would not cavitate at the expected tensile pressures in either the laboratory or the field. (Rood, 1991)

Cavitation is a process of bubble formation due to a localized reduction in pressure often caused by movement or flow situations. Cavitation can be considered as homogeneous cavitation and heterogeneous cavitation. Homogeneous cavitation is when the cavitation occurs in the bulk solution, where no impurities or defects are present. Heterogeneous cavitation occurs at surfaces or defects in surfaces.

At the nip center, the distance between the two cylinder surfaces is at a minimum. The cylinders rotate with a tangential velocity, which separates the two surfaces. As the fluid emerges into the nip exit, the surfaces of the cylinders recede from each other. The separation velocity and distance between rolls increase with increasing distance from the nip center. A tensile force is applied to the fluid. If the tensile stress is greater than the fluid's vapor pressure, vapor bubbles will form. The tensile stress is relieved by cavitation within the film. At this point, the pressure in the fluid decreases suddenly. (De Grâce, 1991)

1.7. Filament Formation

As the fluid is carried further away from the nip, the surfaces of the cylinders continue to separate and the cavities expand vertically. Filaments of the fluid are formed between the cavities as the cavitation bubbles coalesce. Subsequent cavities and filaments are formed as long as fluid continues to emerge from the nip.

De Grâce ***et. al.*** (1992) has noted that, in the direct measurement of the pressure pulse in a printing nip, the duration of the sub atmospheric pressure pulse during cavitation appears to correspond with the distance in their photographs between the nip exit and the filament rupture.

De Grace ***et. al***. (1992), Thomson and Young (1975), Hayashi ***et. al.*** (1992), Zang ***et. al.*** (1992), Amari ***et. al.*** (1994), Taylor ***et. al.*** (1958), Bery ***et.*** *al.* (1992) and MacPhee (1997) are examples that visually record the filamentation at a printing nip exit. The filaments stretch as they move outward. However, the size of these filaments are difficult to analyze from a side view because they are continually stretching and changing dimensions. De Grace ***et. al.*** (1992) do characterize the location of filament breakup but do not report the size of the filaments.

The filaments elongate and become thinner as they continue their travel away from the nip. The rate at which filaments elongate is equal to the rate at which the plate separation increases. At high rates of film separation, a shorter ink filament is generated at the rupturing point (Hayashi ***et.*** *al.,* 1993). If the ink filament is elongated slowly, a viscous flow occurs. However, as the speed of the ink splitting increases, the ink filaments rupture as elastic materials and are quickly recoiled back onto the ink surface.

1.8.Extensional Flows

Extensional viscosity is a measure of the resistance of a fluid to extensional deformation. In addition, some fluids are "shear-thinning" in extension while others are "shear-thickening". Elongation of the fluid in the nip should be related to the fluids extensional viscosity. There has been no work, to our knowledge, characterizing the relationship between filament size and extensional viscosity.

Ink holdout on paper is assumed to depend on the ink's shear and extensional viscosities and surface pore sizes in the paper. Since ink extensional resistance normally increases as extensional strain rate increases, the impact on ink holdout of extensional behavior should increase at higher printing speeds. This is related to the rheological Deborah number, which is the ratio of molecular relaxation time to flow deformation time. **A** zero Deborah number indicates purely viscous flow and a very large Deborah number corresponds to highly elastic flow. High printing speeds should lead to high extensional rates and high extensional resistance for inks containing long chain resins having comparatively lengthy relaxation times. (Fu, 1994)

There are four techniques for the measurement of extensional viscosity that are applicable to the lower viscosity inks: fiber spinning, opposing jet flow, converging flow, and filament stretching. In fiber spinning extensional rheometry, a filament is generated through a spinneret and is wound **up** by a rotating drum. Pangalos *et. al.* (1985), who used this technique, noticed that changing the composition of the ink caused differences in the extensional viscosity. **An** addition of pitch drastically reduces the extensional stress in an ink, while the addition of resin or carbon black increased it. Pangalos *et. al.* (1985)

also noticed that black inks have rheological properties that are strongly dependent on shear rate and time.

Considering the flow of a filament that is being stretched by a falling cylinder. The simple elongational flow happens in the filament of length L and at time t. From the conservation equation one can write the elongational rate, $\dot{\varepsilon}$, as:

$$\dot{\varepsilon} = \frac{-2V_r}{r} \tag{1.1}$$

where r is the filament radius and V_r is the radial velocity.

The elongational viscosity, η_e is defined as :

$$\eta_e = \frac{T_{11}}{\dot{\varepsilon}} \tag{1.2}$$

where T_{11}, the total stress, for a Newtonian fluid neglecting the interfacial surface tension is:

$$T_{11} = 3\eta_o \dot{\varepsilon} \tag{1.3}$$

η_o is the Newtonian shear viscosity.

A simple relationship for a Newtonian fluid can be obtained as follows:

$$\eta_e = 3\eta_o \tag{1.4}$$

This expression is commonly known as the Trouton expression. Non-Newtonian fluids are not expected to follow this law.

1.9. Rupture

The fluid film splits as the filaments rupture, probably through tensile failure. The length of the filaments, for an ink, at rupture may be considered to be a measure of the "shortness" of an ink. The ruptured filament segments recoil towards the cylinder surfaces. In printing nips, the splitting process continues until all of the ink on the image area on the printing form has passed through the nip.

De Grâce ***et.*** *al.* (1992) has observed an increase in the rupture length of the filament with an increase in the amount of fluid fed. This is believed to be due to the increase in filament volume which permitted the filaments to elongate to longer lengths before their rupture, which caused the ink film split to occur farther from the nip center. **As** the speed was increased it was seen that the rupture length of the filament and the distance from the nip center had decreased. The reason for this type of behavior is believed to be due to an increase in the tensile forces applied to the filaments, and to an increase in the rate of filament extension (filament acceleration).

1.10. Substrate Characteristics

Aspler (1993) and Aspler ***et. al.*** (1994) show that the substrate used for printing changes the pressure field in the nip and cause different printing defects. Porous substrates may reduce the pressure swings in the nip and change the film-split conditions. Aspler ***et. al.*** (1994) shows that a porous substrate reduces the negative pressure pulse in the nip. The porous substrate may cause a shift in mechanism from a cavitation phenomena to a capillary film split as studied by Coyle ***et. al.*** (1986). The substrate is expected to change the filamentation process and filament size.

1.11. Summary

Although much work is available to understand the basics of coating flowing in the rolling nips, the conditions to cause ribbing, filament formation and misting, no systematic work has tried to characterize the filament size at the nip exit. Several have photographed the filaments, but their size dependence on process conditions and rheology have not been reported.

This thesis will characterize the important rheological parameters that determine the size distribution of the filaments at the exit of a rolling nip. The experiments were done by using a high-speed video camera with high magnification lenses to visualize the exit of the nip on a roll system. The length and diameter are measured from a stopped video image. Assuming a cylinder geometry, these dimensions are converted into a volume. Empirical correlations are given to predict average filament size. A physically based theoretical model is proposed to predict filament size and is compared with experiments.

CHAPTER 2: EXPERIMENTAL METHODOLOGY

In this chapter, the five experimental tests will be described. Twenty-two different fluids are analyzed, seven of these are Newtonian fluids, eight are non-Newtonian, and seven are real inks. The procedures and set-ups described below are done on each of these fluid types. **All** of the techniques require data analysis. The results for each of these types of fluids will be discussed in chapters 3-5. In chapter 6, the effect of substrate, speed and nip loading for a specific fluid will be discussed.

2.1. Rheological Tests

The rheological characteristics of the fluids used are analyzed using a constant stress rheometer (BOHLIN CVO). **A** stress sweep and oscillatory tests are performed. These are done by performing the yield stress, constant stress viscometry, and oscillatory tests that come standard with the rheometer, on the fluids analyzed. The cone-plate geometry is used with an angle of **4"** and a cone base diameter of 40 mm. The gap is 150 μm. The amount of fluid needed to obtain correct results is 1.3-1.5 cm^3. The fluid is placed in the middle of the bottom plate with a plastic syringe. The top cone is adjusted by the built in procedure to come down towards the bottom plate and stop at the appropriate gap.

The yield stress procedure requires an input of start stress (0.06 Pa) and end stress (500 Pa) with a sweep time (500 sec) and gives an output of shear stress versus shear rate and intrinsic viscosity. The constant stress viscosity characterizes the steady shear viscosity of the fluid as a function of shear rate. For the oscillatory tests, the frequency range (0.1-30 **Hz)** is given and the frequency sweep type (up/down). The loss modulus

(G''), storage modulus (G') and phase angle (δ), where tan(δ)=G"/G', the loss factor, are obtained. All of the measurements are done at room temperature.

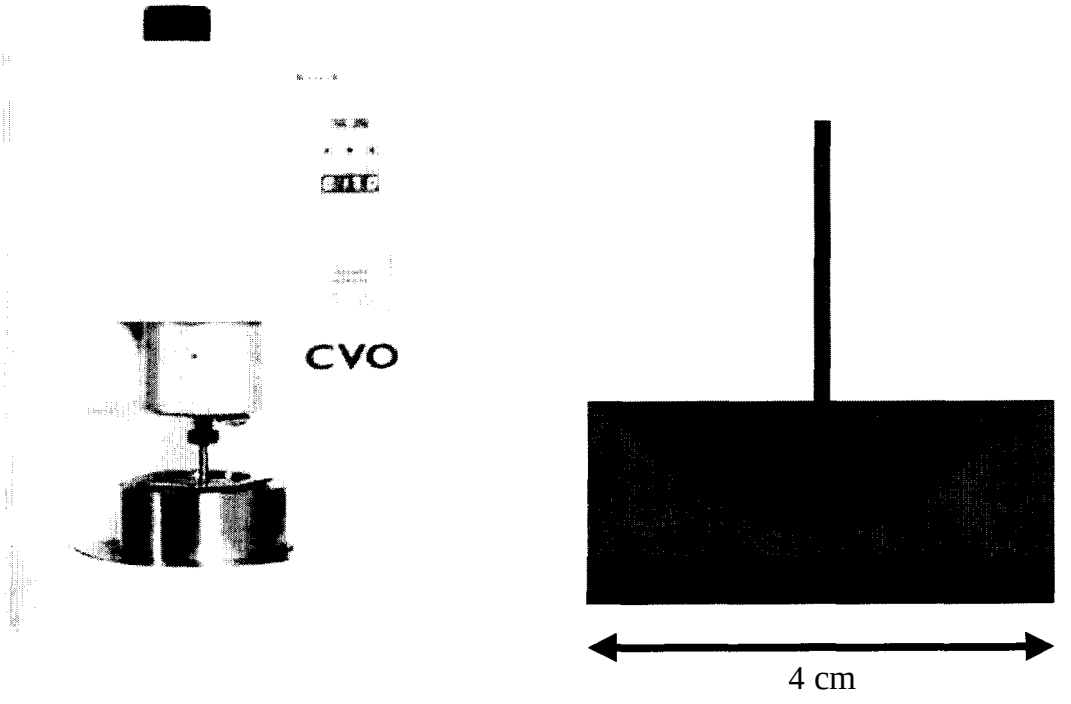

Figure 2.1 : Bohlin Rheometer Set-Up with Schematic of Geometry

2.2. Cavitation Analysis

Cavitation is known to be associated with filament formation. Therefore, a new test is proposed to characterize the ease of cavitation or the tensile properties of the fluids. One cubic centimeter (1 cm^3) of fluid is placed in a plastic syringe, that has one end open, with either a spatula or having the syringe vacuum in the fluid by pulling the plunger. The procedure of filling the syringe depends on how viscous the fluid is. Care is taken to remove all air bubbles, and for some samples, the syringe is left open overnight to allow

air to escape before being sealed. The open end of the syringe is sealed by melting a piece of plastic onto this open end. The end of the syringe is pushed completely to make sure that there is no leakage of fluid out of the syringe and pulled to make sure that there is no leakage of air into the syringe. After these vacuum tests, the syringe is mounted in a mechanical tester (model 5564, Instron Corp.) as depicted in figure 2.2 with the clamps provided. The syringe is pulled at a speed of 0.1 *mm/min*, for a time period of 600 seconds or more. The load versus time data is obtained. The load is converted to a tensile pressure knowing the cross sectional area of the syringe as:

$$P_s = \frac{T}{A} \tag{2.1}$$

where P_s is the pressure inside the syringe, T is load that is evaluated by the mechanical tester and **A** is the cross sectional area of the syringe.

The results are shown as pressure as a function of time. However, the actual pressure inside the syringe is not measured directly.

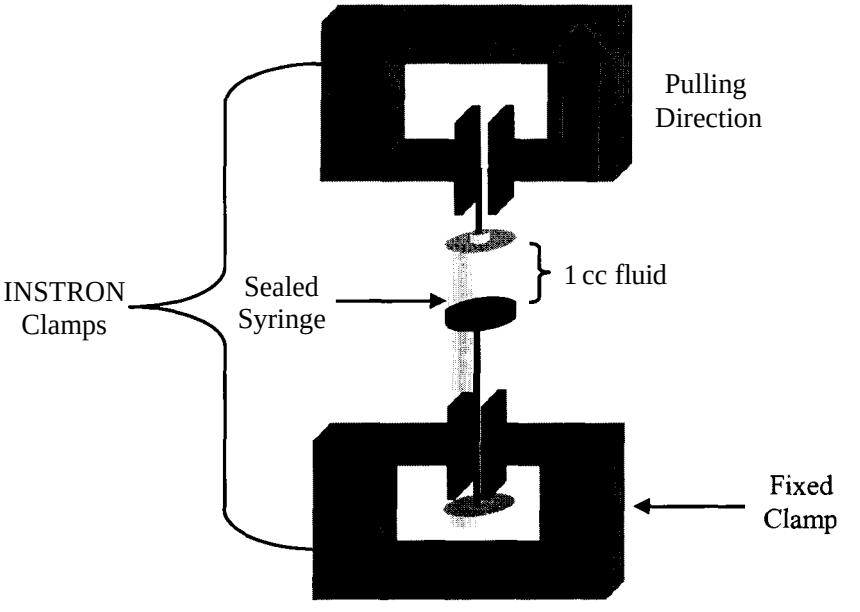

Figure 2.2: INSTRON Experimental Set-Up

2.3. Elongational Viscosity Analysis

The apparent elongational viscosity data is obtained using the novel apparatus shown in figure 2.3. The fluid is put between the two screws depicted in the figure. Enough fluid is put between the screws to allow a disk of fluid to be formed between the two screws. The bottom screw is held in position with a magnet. The position of the magnet is accomplished by a magnetic field. The bottom screw is allowed to drop by turning off the magnetic field as soon as the high-speed video camera is ready for recording Sample figures and the calculation technique is described in detail in Appendix A.

These experiments are done by using a high-speed video camera (Encore MAC-2000, Olympus America Inc.) with high magnification lenses (Kilfitt, ZOOMAR) to visualize the motion of the filament elongation. The high-speed video camera recordings are done at a speed of 500 frames/sec with a shutter speed of 20X and played back at a speed of 1

frame/sec. Lighting is provided by using a fiber optic lighting system (model 180, Dolan-Jenner Ind., Inc.); the images are stopped by using the high-speed camera. Images of the filament elongation are transferred to a standard VHS video tape. The length and diameter of the filament at each frame, approximately every **2** ms, are measured from a stopped video image. **A** typical image and how the measurements are carried out are given in Appendix A figure **A.**1.

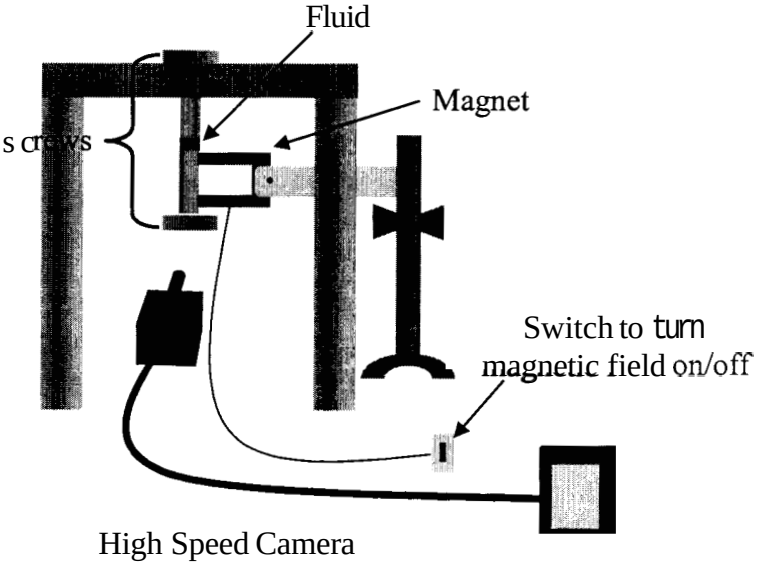

Figure 2.3: Elongational Viscosity Experimental Set-Up

Once the images are recorded the event is played back, as indicated above, at 1 frame/sec where each frame is approximately **2** milliseconds. The filaments length and diameter at that time is measured and recorded. This is done for each frame until either the end of the filament is not seen on the screen (the elongation length can not be measured) or the filament breaks before elongating that far. From this data the apparent elongational viscosity can be calculated.

The parameters needed to calculate the apparent elongational viscosity are the filament force and the elongational rate. The filament force equation needs the bob acceleration value. This value is obtained by first plotting the filament length versus time, the equation of the derivative the filament length versus time data will give the bob velocity. Plotting the bob velocity versus time and taking the derivative of the curve that fits this data gives the bob acceleration, a, which when used in the equation given below gives the filament force value:

$$F_L = m(g - a) - F_d \tag{2.1}$$

Assuming that there is no drag force, $F_d=0$, the force on the fluid, F_L is calculated. Where m, is the screw mass and g, is gravitational acceleration.

V_r, the radial velocity is found by plotting the radius values versus time and taking the derivative of the curve that best fits the data and which will give us the equation for the radial velocity. The elongational rate, ε, is obtained using the radial velocity from the equation depicted below. Where r, is the filament radius at each time frame.

$$\varepsilon = \frac{-2V_r}{r} \tag{2.2}$$

Using the filament force value, F_L, and the elongational rate, ε, the apparent elongational viscosity for the fluids can be evaluated using the equation below:

$$\eta_e = \frac{(F_L - \pi r \sigma)}{\pi r^2 \dot{\varepsilon}} \tag{2.3}$$

2.4. Filaments and Filament Remain Analysis

Using the rolls of an ink distribution device (IGT AE Reprotest B.V., Model # 87.406.Z.2424), shown in figure 2.4, the volume of the filaments formed and the filament "remains" are determined. These experiments are done by using a high-speed video camera (Encore MAC-2000, Olympus America Inc.) with high magnification lenses (Kilfitt, ZOOMAR) to visualize the exit of the nip on an IGT roll system. The high-speed video camera recordings are done at a speed of 500 frames/sec with a shutter speed of 20X and played back at a speed of 1 frame/sec. This frame speed and shutter speed is used for the convenience of lighting and slowing down the motion. Lighting is done by using a fiber optic lighting system (model 180, Dolan-Jenner Ind., Inc.); the images are stopped by using the high-speed camera. Side images of the roll are transferred to a standard VHS video recorder. The length and diameter are measured from a stopped video image. Assuming a cylinder geometry, these dimensions are converted into a volume. A sample figure and calibration is given in Appendix B figure B.1 and B.2. Filaments that form early in the nip and break will be missed by this method. Therefore, this method should be assumed to capture the large side of the size distribution.

The roll surface velocity is 0.34 m/sec. Film thicknesses from 1-5 μm are characterized. The top roll is replaced with a roll made out of Plexiglas with a diameter of 60 mm as shown in figure 2.4. This allows light to pass through the nip for better illumination. The

thickness of the roll and the strip that is being recorded is 2 mm, which is the depth of focus of the lens that is being used. The back thick strip is made to be able to help the fluid spread on the rolls for a constant and homogeneous fluid thickness. The thicknesses of the fluid on the roll is calculated by weighing the inked roll and clean roll and subtracting the different weights, dividing the weight difference by the density of the fluid will give us the volume of fluid on the roll, and finally dividing this volume by the total surface area of the Plexiglas roll ($50.9\ cm^2$) will give us the fluid film thickness on the Plexiglas roll. The top roll weighted 161.727 grams. The ink is distributed on the rolls for 15 minutes. The top roll is contacted to the distribution roll. Images are obtained within 10 seconds after the Plexiglas roll is in contact with the other rolls.

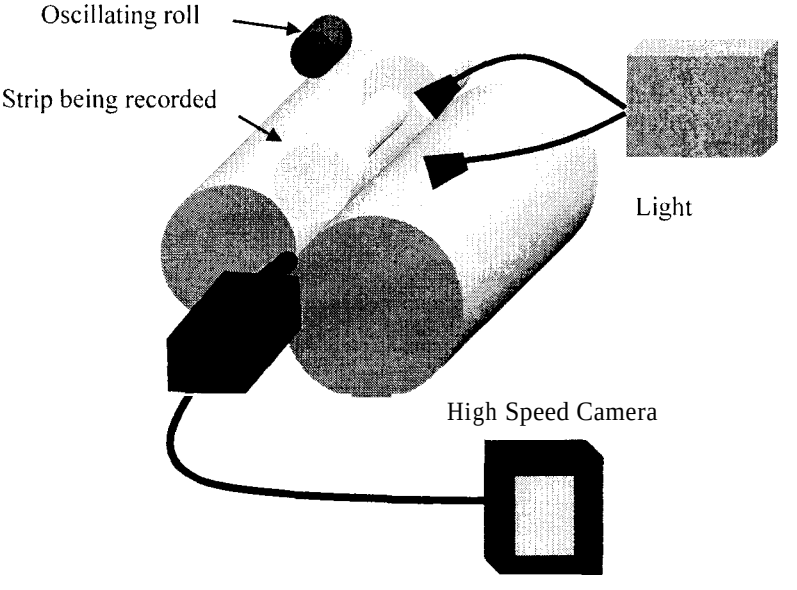

Figure 2.4: IGT Experimental Set-Up

2.5. Analysis of Filament Remains

A CCD camera (Model No. SSC-S20, Sony Corp.) with high magnification lenses (ZOOM 6000 11, D. **O.** Industries) is used to visualize the exit of the nip on a laboratory print tester (KRK). Lighting is adjusted to cast a shadow across the substrate at a 45º angle to produce shadows and bright spots on the ink film features as shown in figure 2.5. The goal is not to see the filaments but to analyze the level nature of the final film. The "remains" of the filaments or "hills" on the substrate after the nip are assumed to give an indication of the filament size distribution instead of viewing the filaments directly. Using the results from the IGT roll system the filament characteristics can be determined for different parameters. The parameters to change are the roll speed, the fluid film thickness, the substrates and the nip loading.

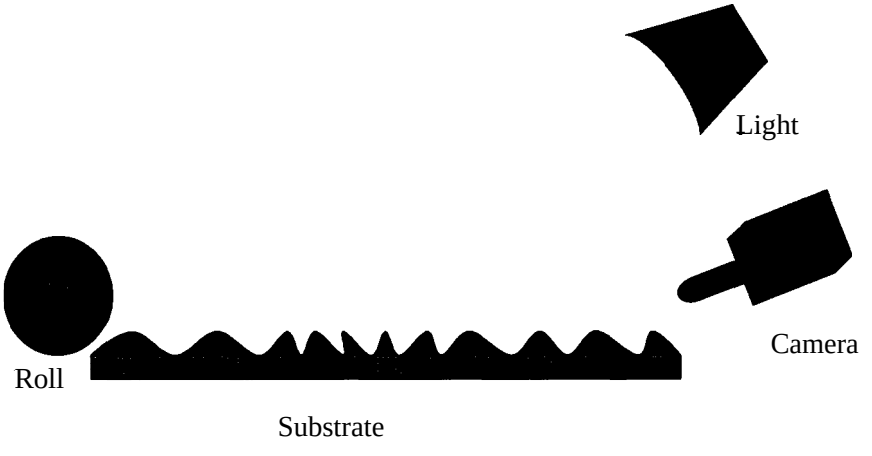

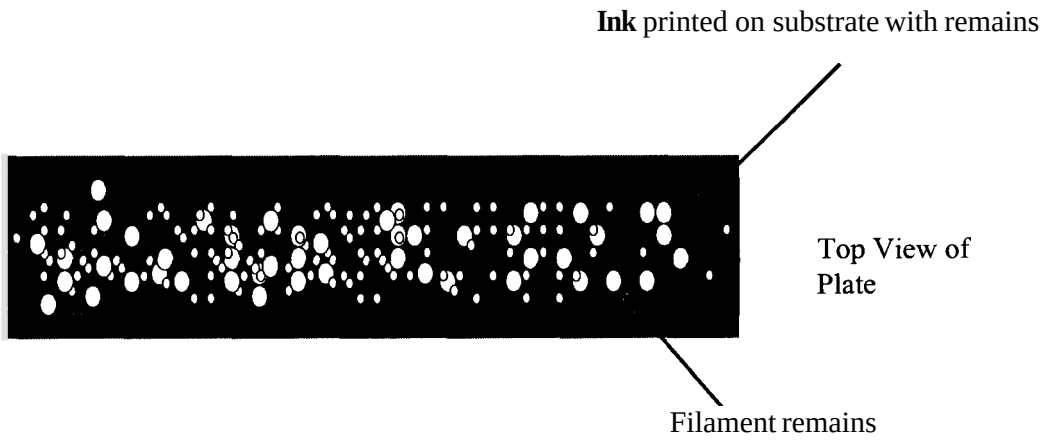

Figure 2.5: KRK Experimental Set-Up

Printing with the KRK printing unit, the substrate is varied which gives an idea about how the substrate effects the filament characteristics. Also different types of fluids are used during the IGT roll system and the KRK printing unit to distinguish the effect of fluids on filamentation. The speed at which printing is done is varied to see the effect of speed, as well as changing the ink film thickness and nip loading, to analyze the effect of ink film thickness and nip loading respectively.

The nip parameters that are varied are speed **(2,** 4, and 8 m/sec), film thickness (1.5, 3.0, and 5.0 μm), and nip loading (doubling and halving the loading). The types of substrates that are used are Mylar, rough plastics, porous plastics and paper. The fluids that are analyzed are Newtonian, shear-thinning inelastic, Boger (constant viscosity, elastic) and model fluids.

CHAPTER 3: NEWTONIAN FLUIDS

A set of Newtonian fluids were selected for initial tests. These fluids did have a constant shear viscosity over a range of shear rates. However, these fluids did show some small elastic properties at high frequencies. Therefore, these fluids are not truly Newtonian. This issue seems to influence the results and cause the analysis of the results to be less clear.

3.1. Materials Used

Seven fluids are analyzed; four different silicone oils (Dow Coming Corp.) and three pick test oils (PTO1 and PTO2, IGT Reprotest Inc. PTO3, Research North America, Inc.). The silicone oils are polydimethylsiloxane where the pick test oils are polyisobutylene. The viscosities for the silicone oils are reported as 12, 100, 300, and 600 Pa-s and these are denoted as SO1, SO2, SO3, and SO4, respectively. The pick test oils also had viscosities around 10, 126, and 50 Pa-s and are denoted PTO1, PTO2, and PTO3, respectively. Since the oils denoted with the numbers one and two have approximately the same viscosity values these fluids are considered as pairs and their filamentation behavior are compared.

3.2. Rheological Results

Figure 3.1 shows that the silicone oils and pick test oils have a constant shear viscosity near the expected value for a wide range of shear rates. The pick test oil one (PTO1) has a viscosity lower than the silicone oil at 9.5 Pa-s. PT02 has a viscosity of 120 Pa-s which

is higher than the silicone oil at 100 Pa-s. The other oils denoted as PTO3, S03, and S04, all found to have viscosities, 56 Pa-s, 276 Pa-s, and 571 Pa-s, respectively. Figure 3.3 shows the frequency sweeps of the storage and loss moduli for the silicone oils and the pick test oils. These results show, that over the entire frequency range, these fluids are dominated by viscous behavior with a phase angle above 85° at 1 Hz frequency. However, at higher frequencies, the phase angle can drop especially for the silicone oils.

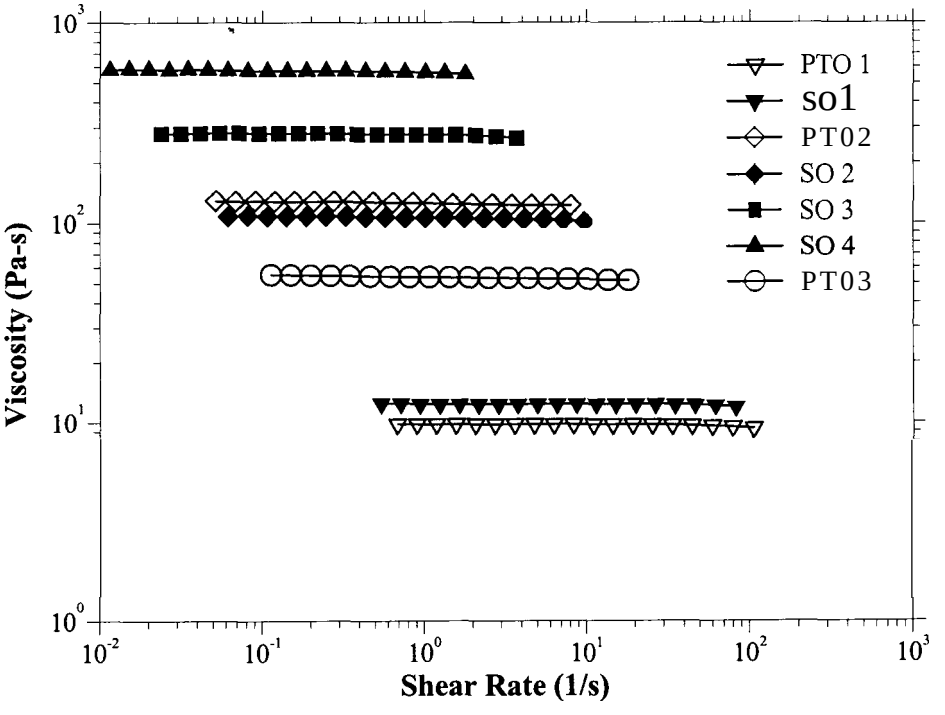

Figure 3.1: Steady shear viscosity versus shear rate values for the simple fluids

As can be seen from figure 3.2 a-b, both pairs of fluids (SO1 - PTO1 pair and SO2 - PT02 pair) have a higher viscous modulus than an elastic modulus over the entire frequency range. The other oils show the same trend where the viscous modulus is higher than the elastic modulus. At low frequencies, for all seven fluids, the viscous effect is quite dominant, for example for silicone oil one at 1 **Hz** frequency the G'/G" ratio is approximately 0.003, but at higher frequencies, the elastic modulus does approach the viscous values, at 30 **Hz** this ratio increased to 0.270 implying that the elastic modulus showed a great increase. It is noticed that with an increase in viscosity for a specific type of fluid, for example, the silicone oils, the trend of the elastic modulus approaching the viscous modulus seems to increase.

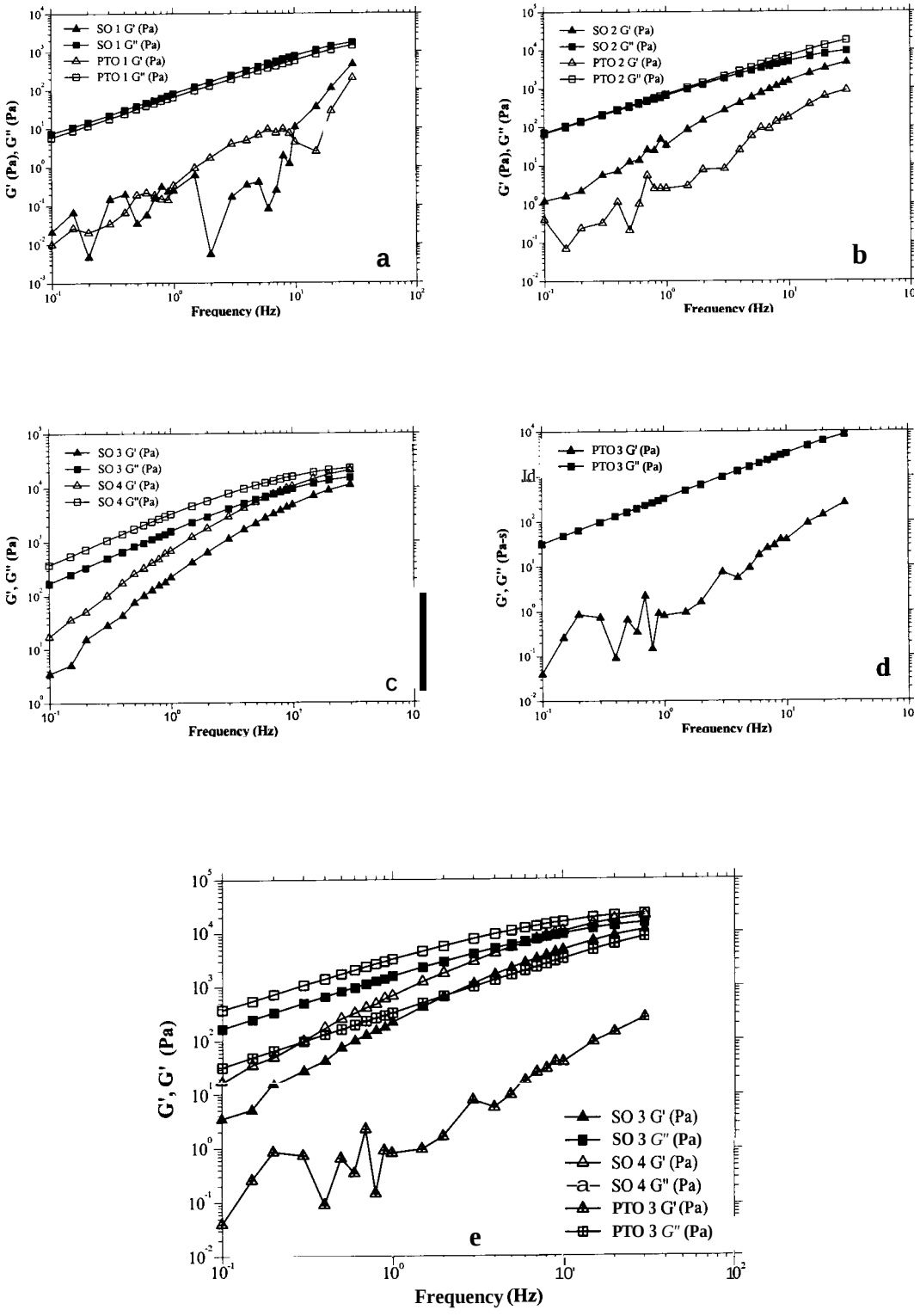

Figure 3.2: Oscillatory results for the simple fluids for a) SO1 and PTO1 and b) SO2 and PT02 c) SO3 and SO4 d) PT03 e) S03, **S04,** and PT03

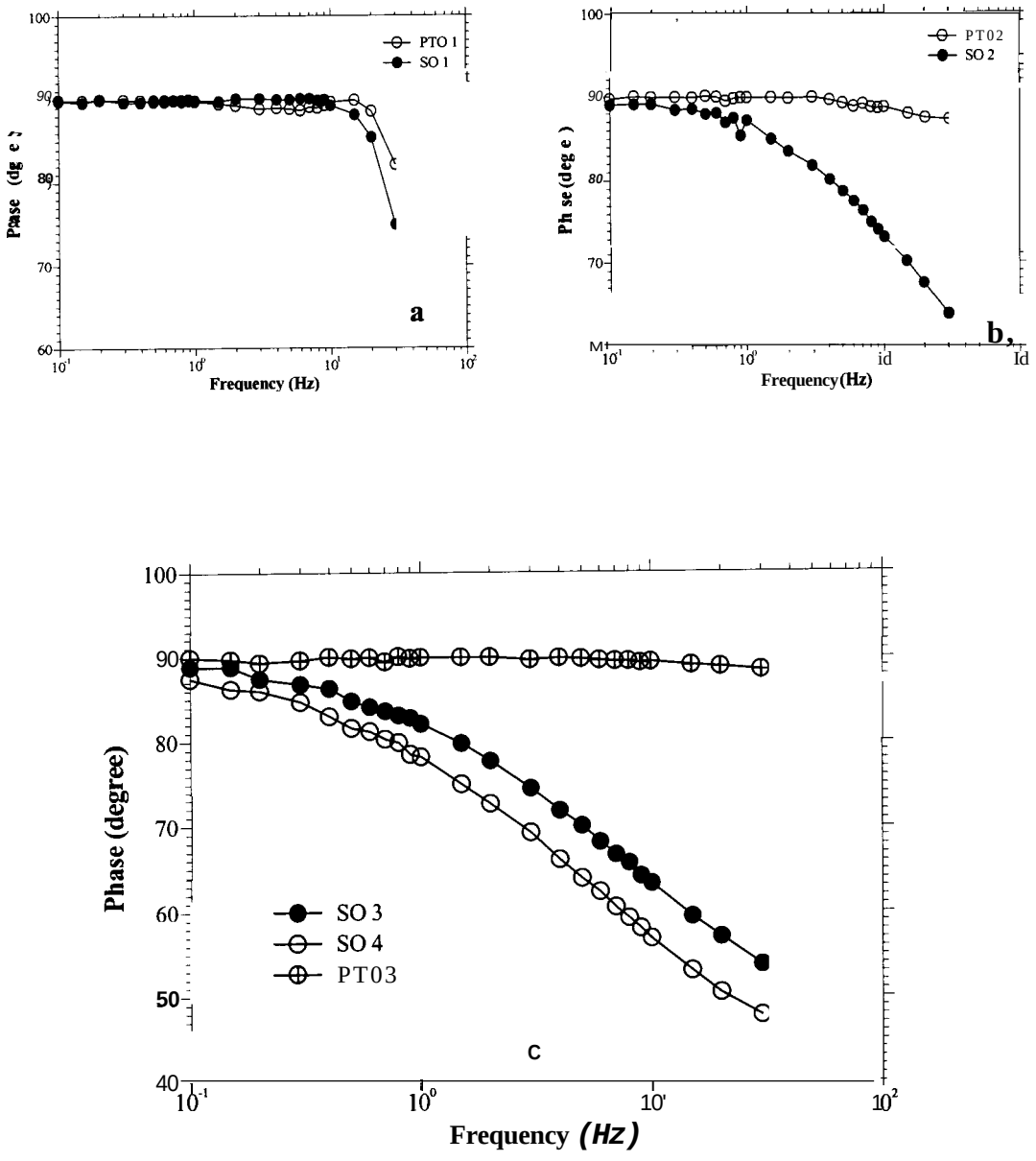

Figure 3.3: Phase angles for the oils

Figure 3.3 shows the phase angles for these fluids. The phase angle is near 90º for most cases, but at high frequencies, the value drops for then silicone oils. Still the phase angle is large and SO1 would be considered to have mostly viscous behavior, but a significant difference is seen in figure 3.3-b between PT02 and S02. When the other fluids are taken into consideration it is seen that the pick test oils tend to have a phase angle for the whole frequency range of approximately 90º where the silicone oils tend to drop with an increase in frequency. For the silicone oils, as the viscosity of the fluid increases, the phase angle decreases with frequency and drops at a lower frequency value. This may reflect that higher molecular weight polymers are being used that can store energy.

3.3. Tensile Test Results

The results from the tensile tests are reported in figure 3.4 for the two pairs of pick test oils and silicone oils. The pressures reported should be thought of as the pressure below atmospheric; an increase in pressure is actually a pressure drop from atmospheric. **As** expected, the pressures did not drop below 100 kPa except for PTO1, but in both cases, the silicone oils show a lower pressure. Pressures over 100 kPa indicate an extra resistance to the motion of the syringe, possibly friction of the syringe, because these fluids should have some small but finite vapor pressure. This result indicates that the silicone oil has a behavior that allows for cavitation at a lower pressure. This may cause vapor bubbles to from earlier in the nip and result in smaller filaments.

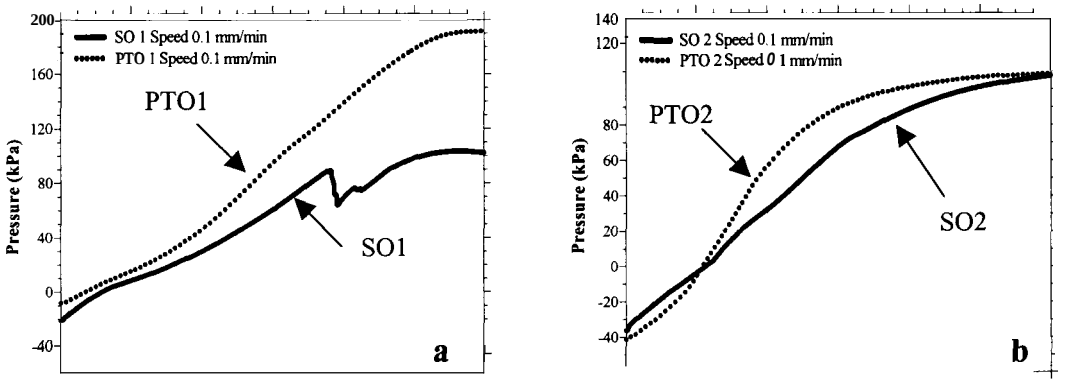

Figure 3.4: Pressure versus time graphs obtained from the tensile test for a) PTO1 and SO1 and b) PT02 and S02.

3.4. Elongational Results

The elongational viscosities of the pick test oils correlates well with their shear viscosity as reported in table 3.1. In the previous section, section **3.2,** it was indicated that the pick test oils seemed to a have a phase angle all in the 90º region which indicated that their viscous behavior was dominating, whereas for the silicone oils the phase angle seemed to drop, indicating that they have a more elastic behavior than the pick test oils. For PT02 and PT03 their elongational viscosity values seem to correlate well with the Trouton ratio which indicates that for a Newtonian fluid the elongational viscosity should be three times its shear viscosity. Whereas for the silicone oils it seems like the only one out of all four which is SO2 comes close to a factor of three. Assuming some of these fluids might have elastic behavior may be why the Trouton ratio of three does not apply for all of the seven fluids.

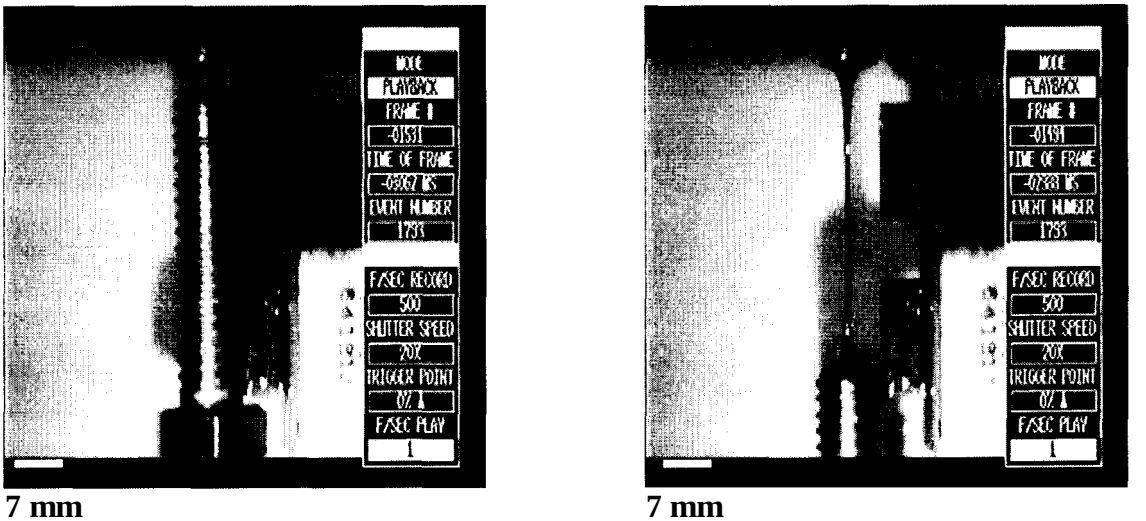

Figure 3.5: Images of PT03 at a a) very short time of elongation b) longer time of elongation

If the plots in figures 3.6 and 3.7 are compared, it can be seen that the lower viscosity silicone oils tend to decrease in extensional viscosity with extensional rate and come to a equilibrium value whereas the silicone oil with the highest viscosity values tends to show an increase in elongational viscosity with extensional rate and than come to a steady value. This fluid is the only one out of all seven which showed an increase and then a steady value, all of the other fluids tended to decrease with elongational rate. From figures 3.6 and 3.7 except for PT03 all six fluids approached the theoretical Trouton ratio where the extensional to shear viscosity ratio is three. In these two graphs this theoretical line is also shown.

Comparing the two pairs of oils (SO1 – PTO1 and SO2 – PTO2) a direct correlation with the average filament volumes and the extensional rates of the fluids can not be detected. The oils with low viscosities seemed to show the same filament volume or at least according to the frequency plot they fell in the same range but comparing their

extensional values to the other pair they do not fall on top of each other as well as the oils with the higher viscosities. The higher viscosity fluids showed a drastic difference in filamentation but as indicated above their extensional viscosities are very close in value. In general looking a table 3.1 with increasing elongational viscosity there seems to be a decrease in average filament volume. The only fluid that does not obey this trend is pick test oil two.

Table 3.1 : Average filament volume for the oils with their viscosity values and apparent elongational viscosity values at higher extensional rates

Fluid	Viscosity (Pa-s)	App. Elong. Vis. (Pa-s)	Avg. Filament Vol.*10^3 (mm^3)	V* *10^{-3}
SO1	12	123	5	78
SO2	106	365	0.6	10
SO3	300	236	0.7	12
SO4	600	351	1	16
PTO1	10	78	7	103
PT02	126	**345**	11	170
PT03	50	191	5	80

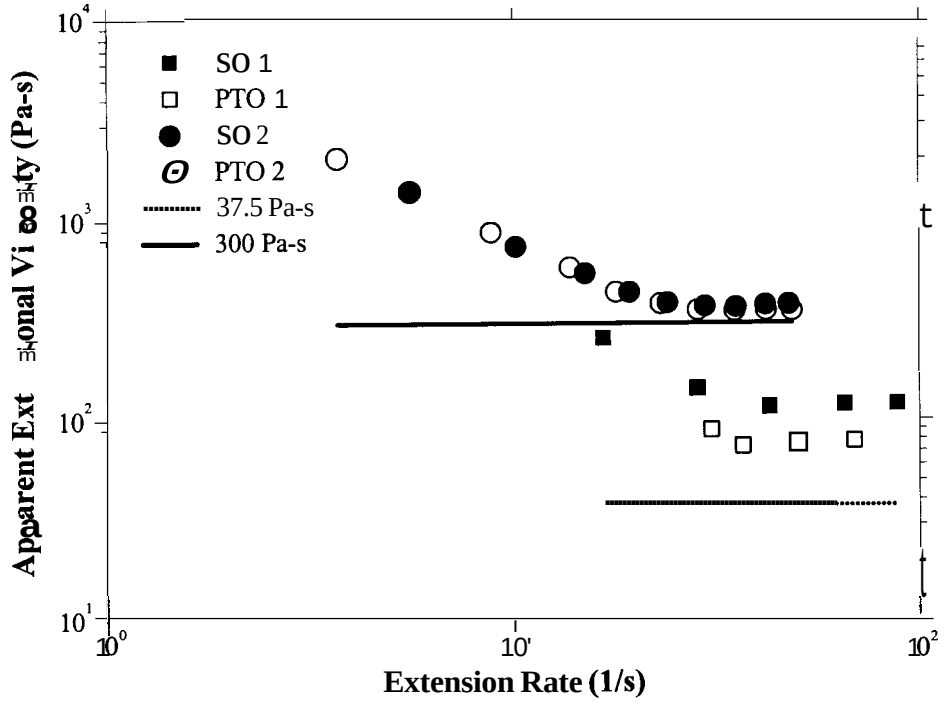

Figure 3.6: Apparent elongational viscosities for the two pairs of silicone and pick test oils and their theoretical elongational viscosity of a Trouton ratio of three times their shear viscsoity. 37.5 Pa-s being the theoretical for 12.5 Pa-s fluids and 300 Pa-s being the theoretical value for the 100 Pa-s fluids.

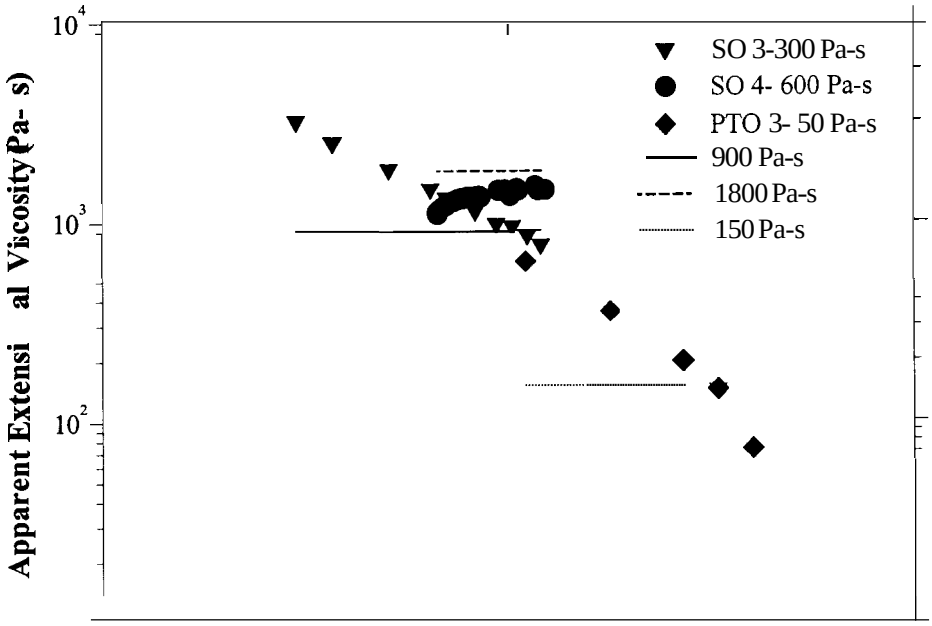

Figure 3.7: Apparent elongational viscosities for the silicone and pick test oils and their Trouton ratio of three times their shear viscsoity. 900 Pa-s being the theoretical for 300 Pa-s silicone oil, 1800 Pa-s being the theoretical value for the 600 Pa-s silicone oil and 150 Pa-s being the theoretical for 50 Pa-s pick test oil.

Theoretically, according to Trouton's ratio, the elongational viscosity of a Newtonian fluid should be three times it shear viscosity. The constant lines found in figure 3.6 and 3.7 represents the theoretical Trouton's ratio elongational viscosity values for the fluids plotted on the graphs.

3.5. Filamentation Results

Although the two pairs of fluid (SO1 - PTO1 and SO2 - PTO2) have nearly the same constant shear viscosity and are essentially viscous Newtonian fluids, they showed a drastic difference in filamentation. Figures 3.8 a-d show the images that are obtained with the high speed video camera for these two pairs of fluids. There is a reflection of the image off the bottom roll that can be eliminated from the analysis. From images such as in figures 3.8 a-d, the filament volumes for all of the fluids are calculated. From these images, it is seen that the pick test oils form larger filaments that elongate more than the silicone oil. The action of recoil also seems to differ for these two types of fluid. The silicone oil has a tendency to spring back rapidly compared to the pick test oil. Where the pick test oil tends to leave peaks on the roll surface. Therefore, the silicone oil doesn't leave as many visual remains or peaks on the surface as does the pick test oil. This was noticed for all seven fluids analyzed.

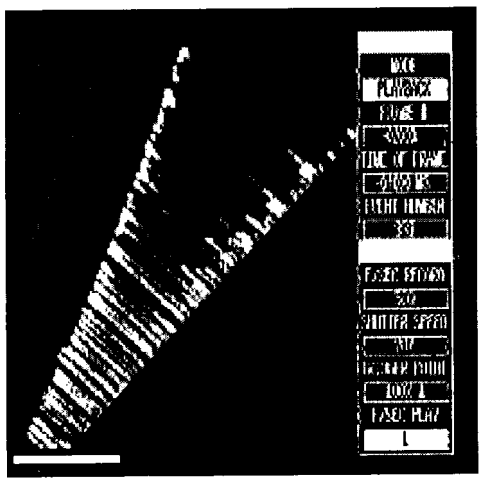

0.5 mm

a

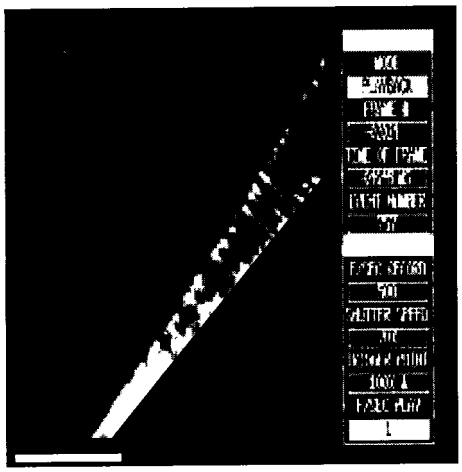

0.5 mm

b

0.5 mm

c

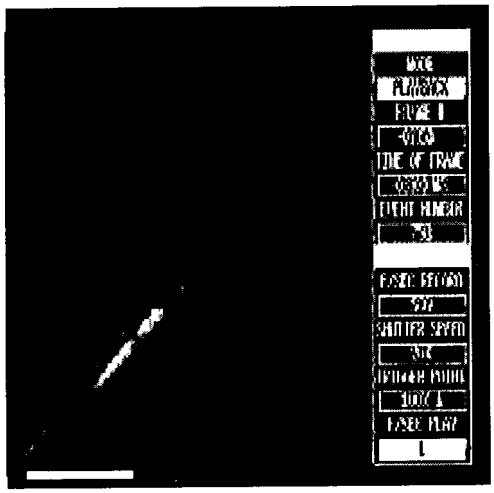

0.5 mm

d

Figure 3.8: Filamentation images of pick test oil PTOl (a) and silicone oil SO1 (b) pick test oil PT02 (c) and silicone oil SO2 (d) with film thickness of ~4μm.

The average filament volume for these two pairs of oils were measured for a number of frames. Figure 3.9 was obtained by normalizing the data and changing the values to a frequency distribution. The SO1 and PTOl (12.5 Pa-s) pair did approximately fall in the same average size region, whereas the SO2 and PT02 (100 Pa-s) pair where different.

The size distribution for the SO1 and PTOl are approximately in the same range where the SO2 and PT02 are different. Table 3.2 reports the average filament size for each fluid. **As** can be seen from the graphical representation, PT02 has the widest distribution and SO2 has the narrowest. This distribution may be an artifact that the method does not pick up the small filaments and can hardly see the filaments for S02. When we compare the fluids looking at the same type of fluid but with different viscosities we can see that with the pick test oil an increase in viscosity (PTOl - PTO2) showed an increase in the average filament volume as when we compare the silicone oils, an increase in the viscosity (SO1 - S02) showed a decrease in the average filament volume. In general, the pick test oils showed a larger filament volume than the silicone oils.

When silicone oils are compared an increase in viscosity caused an increase in average filament volume, but the increase is small compared to the change in viscosity. The phase angles of these seven fluids are different at high frequencies. SO1 has a phase angle of 90" up to the higher frequencies. The other three silicone oils have a drop in phase angle at earlier frequencies. This would indicate that the other three silicone oils may have some elastic effects in the nip and that an elastic behavior leads to smaller filaments by "fracturing" the fluid. **As** for the pick test oils the phase angle was always greater 85º, except for PTO1, which dropped at the higher frequency. PTOl might have a small elastic effect because of this drop where the other two oils do not show this type of drop. Therefore, a logical increase in the average filament volume with an increase in viscosity for these two pick test oils is reasonable. The V* values in table **3.2** are obtained by dividing the average filament volume by the cube of the film thickness.

Table 3.2: Average filament volume for the oils and their dimensionless volume (average volume/cubic film thickness)

Fluid	Viscosity (Pa-s)	Film Thickness (μm)	Avg. Filament Vol.*10^3 (mm^3)	V* *10^{-3}
SO1	12	4	5	78
SO2	106	4	0.6	10
SO3	300	4	0.7	12
SO4	600	4	1	16
PTO1	10	4	7	103
PTO2	126	4	11	170
PTO3	50	4	5	80

From the steady shear viscosities, SO2 and PT02 are the same. However, SO2 does have a higher elastic modulus for all frequencies compared to the PTO2, and this difference is around a factor of ten. SO2 does have a lower pressure in the tensile test. This lower pressure may indicate that SO2 can form vapor bubbles earlier in the nip, leading to smaller filaments.

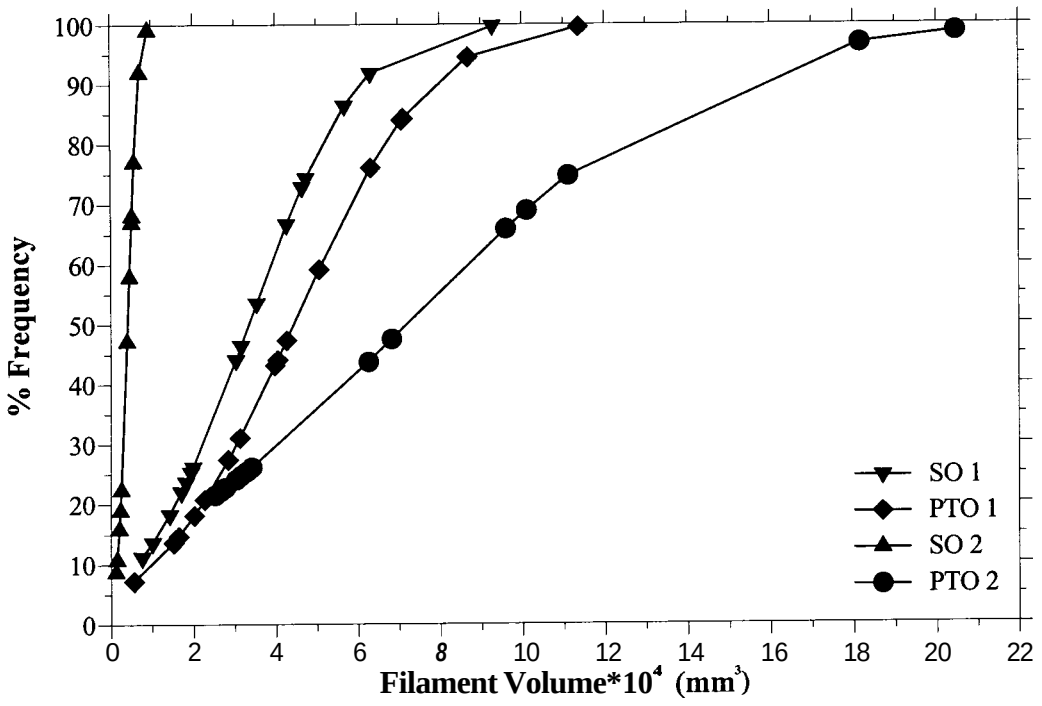

Figure 3.9: Frequency plot for the four simple fluids compared

3.6. Filament Remains

Only PT02 is tested with this procedure. PT02 is printed on Mylar at three different speeds and three different film thicknesses. From figure 3.11 the effect of speed and film thickness on this specific fluid with a smooth nonporous substrate can be seen. PT02 did not transfer to the substrate well and had a tendency to pull up the substrate rather than transferring to the substrate. From figure 3.10 this can be seen, the dark area in the images are the areas were the oil seems to print and the light areas are the nonprinted areas, areas were the fluid is not transferred to the substrate.

From the graph given below we can see that the size of the filament remains increase with an increase in film thickness. Keeping in mind that this specific fluid did not transfer as well as the others and that this fluid is a test oil, it can also be noticed that as the printing speed is increased, comparing 0.5 m/s and 4 m/s, there is an increase in the average volume, but as we go up to a higher speed, 8 m/s the volume seems to decrease. An increase in speed in this type of fluid tended to prevent it from transferring to the substrate and the fluid was more likely to stay on the printing roll.

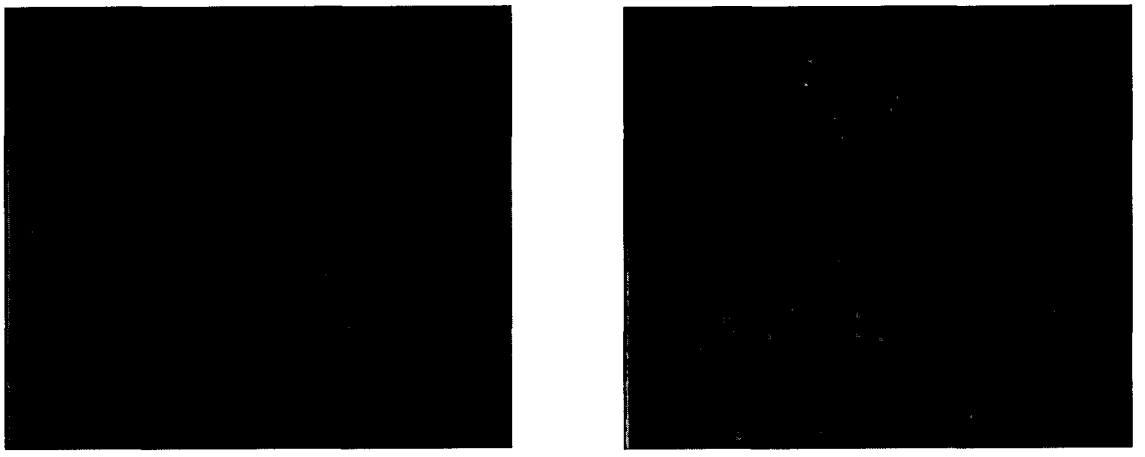

a **b**

Figure 3.10: Pictures captured from video of PT02 printed on Mylar substrate. Frame (a) shows a **3** micron film printed at 4m/s. Frame (b) shows a 5 micron film printed at 8m/s. The total width of the images is **2** mm. The time after printing is 0.5 seconds.

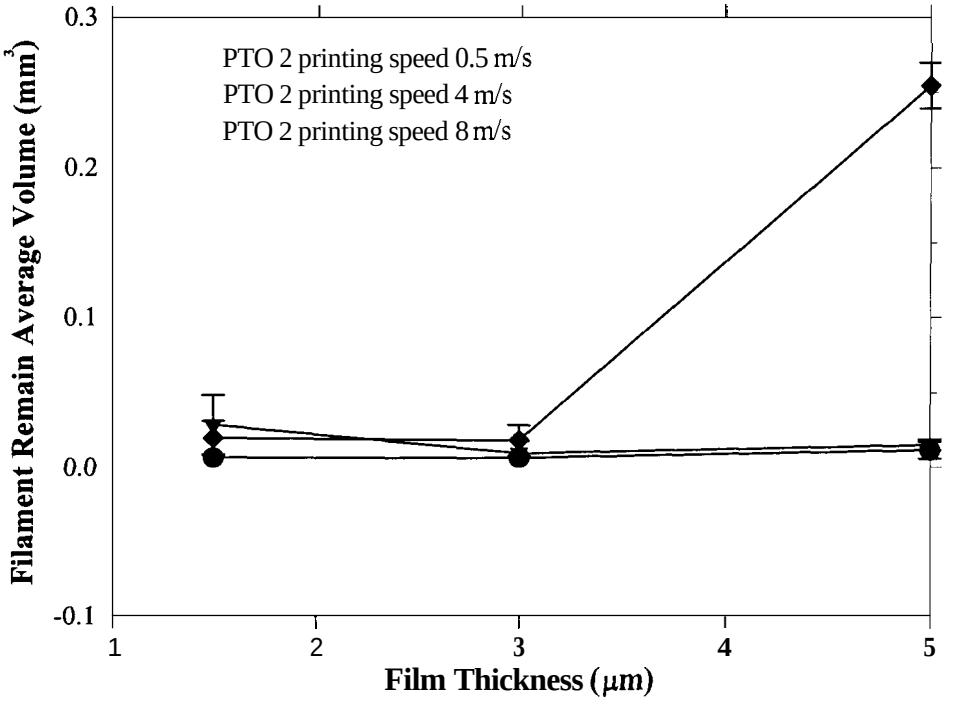

Figure 3.11: Average volume of the filament remains of PT02 printed on Mylar versus the film thickness of the oil on the substrate

3.7. Summary

Fluid rheology is found to have a significant effect on filamentation and the resulting size distribution in a complex manner. Increasing the viscosity of pick test oils increase the average filament size, while the opposite result is found for silicone oils. The low pressures in a tensile test indicated small filament sizes for pick test and silicone oils. For all fluids, increasing the elastic nature of the fluid resulted in smaller filaments. The elongational properties of the fluids seem to have an effect on filamentation but a simple relationship is not clear.

CHAPTER 4 : NON-NEWTONIAN FLUIDS

4.1. Introduction

A group of non-Newtonian fluids were selected for a full analysis of their filamentation behavior. Eight different types fluids were analyzed in this section. The filament remain analysis was not done on these fluids.

4.2. Materials Used

The carboxylmethylcellulose (CMC) solutions were prepared by mixing the dry powder with three times the weight of methanol. This mixture is added to water to obtain the desired concentration. Therefore, for a 2% CMC solution using 2 grams of CMC ***6*** grams of methanol is needed. After making sure that the alcohol has completely dissolved the CMC, to add up to a 100 grams of solution deionized water is added. 100 grams minus the amount of CMC, 2 grams, and minus the amount of alcohol, ***6*** grams, would give the total amount of deionized water needed, in this situation 92 grams. The solution is let to stir until the CMC has completely dissolved in the water this may take up to two hours. **As** the concentration of the CMC is increased the time of mixing must be increased. Two types of CMC were used. A medium molecular weight CMC (9M8, Hercules) with a 0.9 degree of substitution and a high molecular weight CMC (7H, Hercules) with a 0.7 degree of substitution.

The Boger fluid were prepared using the procedure found in Nguyen (1990). The Boger fluids are prepared using polyisobutylene (prod#18 1498, Aldrich Chemical), kerosene

(prod#329460, Aldrich Chemical) and polybutene (prod# 388688, prod#388637, Aldrich Chemical). Two different Boger fluids were prepared, therefore, two different polybutenes were used to change the viscosities of the solutions. The polyisobutylene was cut into small pieces and dissolved in kerosene. The weight percentage of the polyisobutylene in the total solution is aimed to be 0.244%. The kerosene percentage aimed for is 6.98%. The kerosene polyisobutylene solution was stirred mildly for a period of 3 days using a magnetic stirrer to obtain homogeneity. After this solution has been stirred for three days it is diluted with polybutene. The polybutene percentage in the solution should be around 93%. The final solution is stirred for another 3 or 4 days with a magnetic stirrer.

The other two samples used were corn syrup (Karo light corn syrup, CPC International Inc.) and polyacrylamide (prod#3434949, Aldrich Chemical). The tests done on the CMC 7H solution were the rheological, and filamentation tests. The rheological, tensile, filamentation and elongational tests were done on all of the other seven fluids.

4.3. Rheological Results

Figures 4.1-4.3 show the steady shear viscosity curves for the eight different fluids. The oscillatory curves are shown in figures 4.4-4.6. Figure 4.1 shows that the CMC solutions are shear thinning and that an increase in concentration causes an increase in the viscosity value. The 7H CMC, although it has the same concentration as the lowest 9M8 CMC, falls between the 3.5% and 6.2% 9M8 CMC solutions.

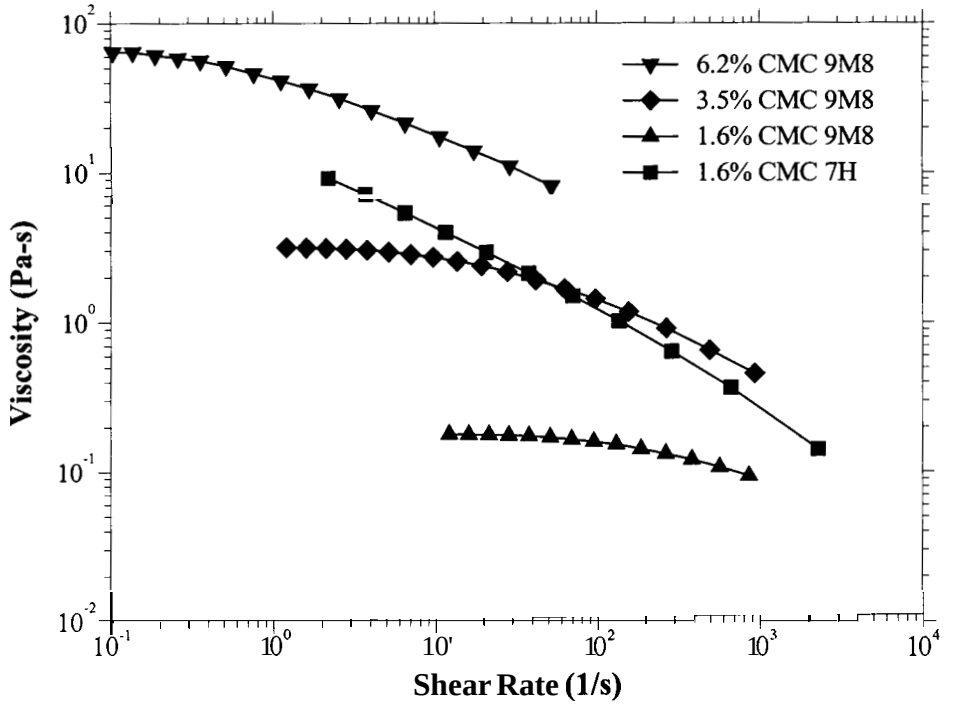

Figure 4.1: Steady shear viscosity versus shear rate values for the CMC solutions

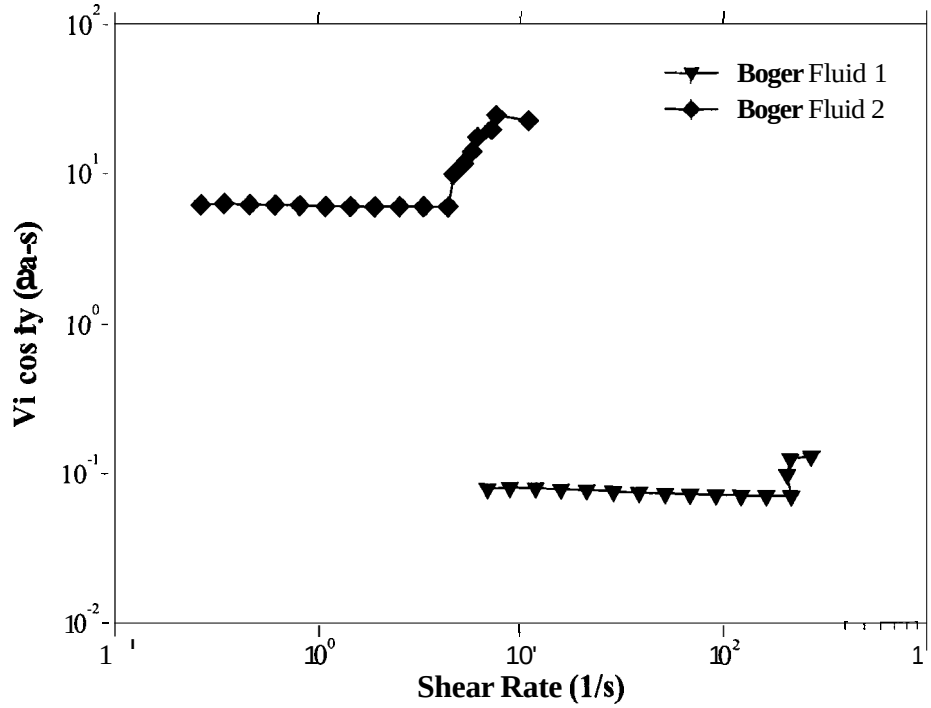

Figure 4.2: Steady shear viscosity versus shear rate values for the Boger fluids

Figure 4.2 shows that the Boger fluids have a constant shear viscosity at low shear rate values, but an apparent increase in viscosity at high shear rates. This increase in viscosity may be an artifact of an elastic-vortex type instability. The first Boger fluid was diluted with a high molecular weight polybutene compared with the second which caused its viscosity to be greater than Boger fluid one.

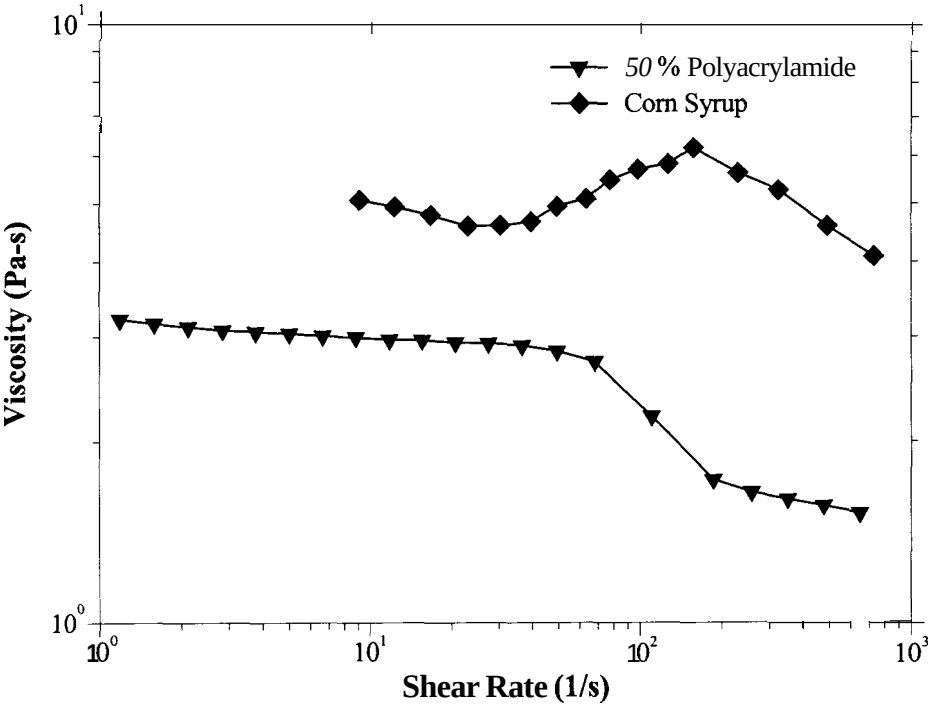

Figure 4.3: Steady shear viscosity versus shear rate values for corn syrup and polyacrylamide

Figure **4.3** shows the steady shear viscosity curve for the corn syrup and polyacrylamide. For the polyacrylamide, a typical constant shear viscosity at low shear rates, a shear-thinning region, and a constant shear viscosity at a higher shear rate is found. The corn syrup has a constant steady shear viscosity, with **an** increase in viscosity with an increase in shear rate, and decrease at higher shear rates. This behavior happens in a small range, between *5-6* Pa-s. Therefore, the corn syrup can be considered to have a constant viscosity.

For the CMC solutions, there is an increase in storage and loss moduli with an increase in the concentration. In general, for all four CMC solutions, the loss modulus is larger than the storage modulus, but in all four cases there is a frequency at which the two moduli cross-over. This point is known as the relaxation frequency. For all CMC solutions, this point seems to be above 15 Hz. For the 9M8 CMC solutions, as the concentration of the CMC increases, the curves become smooth or because the error in the measurement is smaller compared to the signal. **At** low frequencies, with an increase in concentration, the elastic modulus approaches the viscous modulus value. At the same concentration, we notice that the high molecular weight CMC has a higher moduli compared to the medium molecular weight CMC.

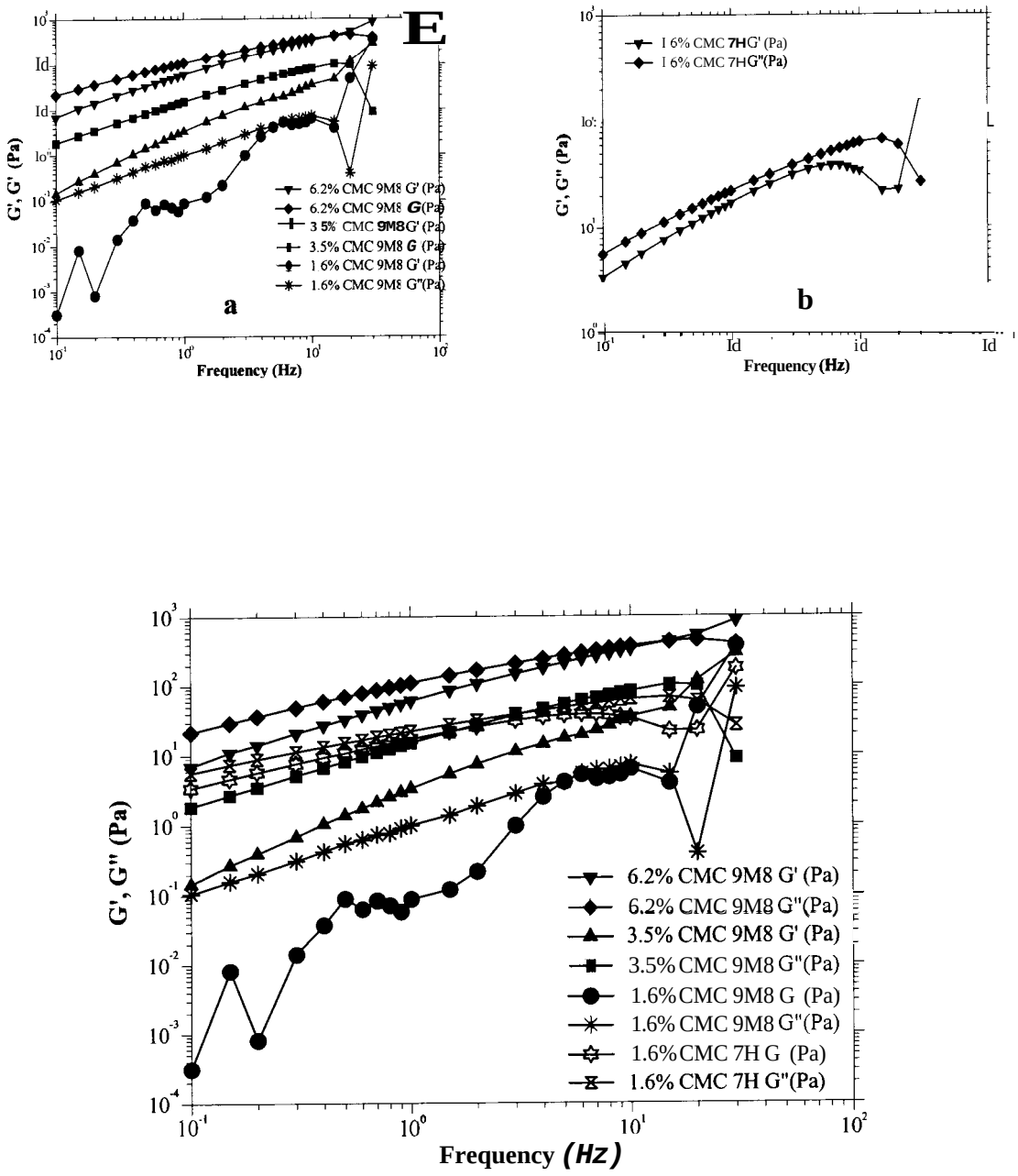

Figure 4.4: Oscillatory results for the a) 9M8 CMC b) 7H CMC c) all CMC solutions

Figure 4.5 shows the oscillatory results obtained for the Boger fluids. Although these fluids are known to be elastic fluids with a constant viscosity, the dominating modulus is the loss modulus. For Boger fluid one, the elastic modulus approaches the viscous modulus at a frequency of **2** Hz. For Boger fluid two, around a frequency of 10 Hz there is a sudden drop in the elastic modulus but rapidly starts to approach the viscous modulus this might just be noise. This fluid does not seem to have the elastic modulus dominate over the viscous modulus in this frequency range. At higher frequencies the elastic modulus does start to dominate and for this fluid the relaxation point was found to be around the 41 Hz point.

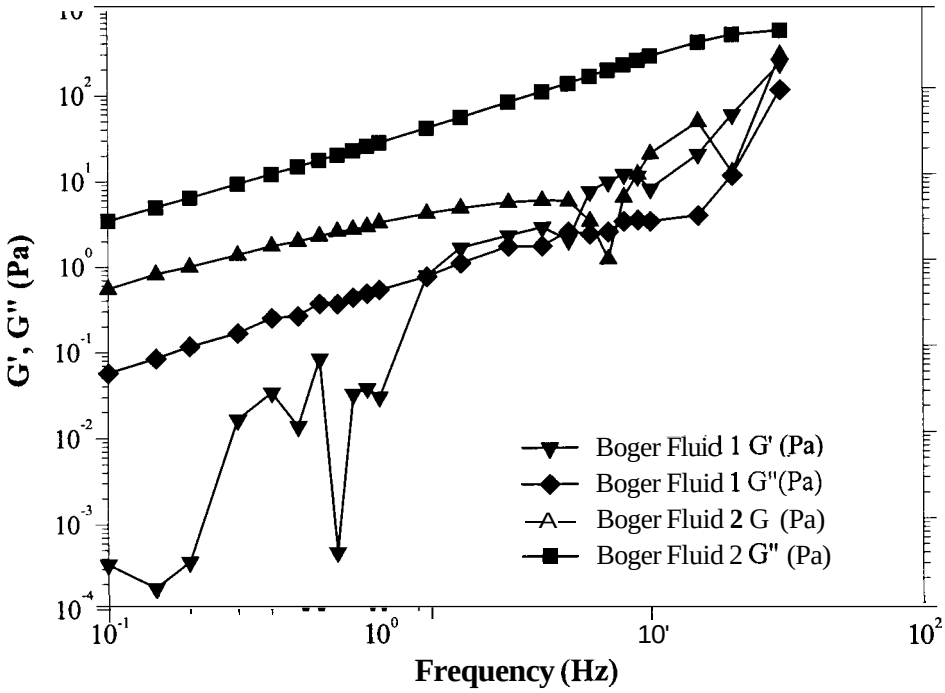

Figure 4.5: Oscillatory results for the Boger fluids

Figure **4.6** shows that the corn syrup is elastic. This fluid is the only fluid which had a storage modulus larger than the loss modulus. The polyacrylamide has a large loss modulus at low frequencies, but at higher frequencies, the elastic modulus approaches the viscous modulus. At a frequency of around 30 **Hz** the two moduli are equal.

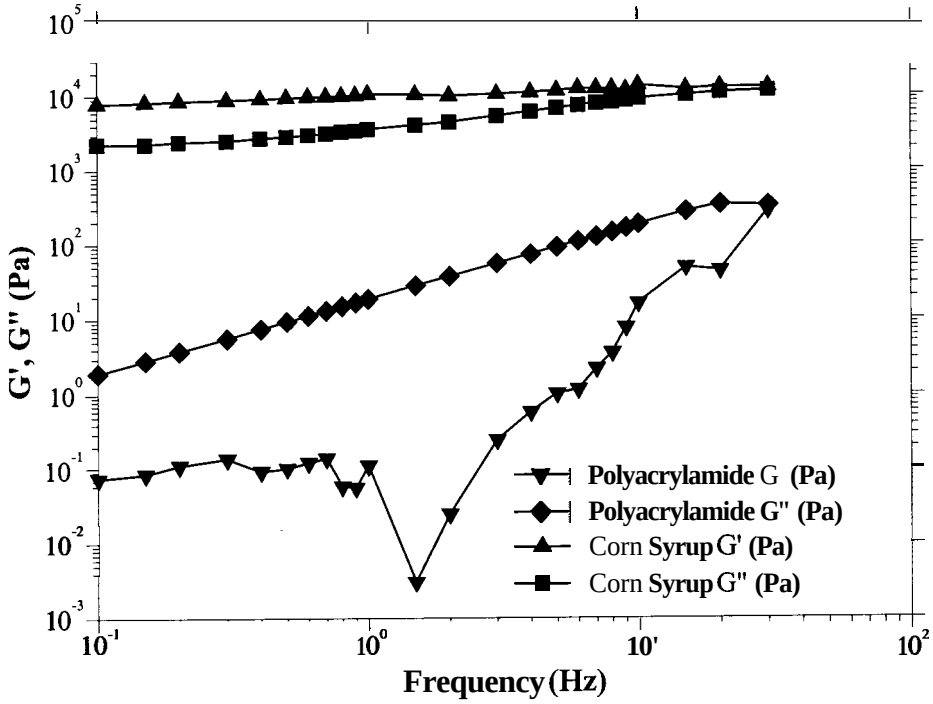

Figure 4.6: Oscillatory results for corn syrup and polyacrylamide

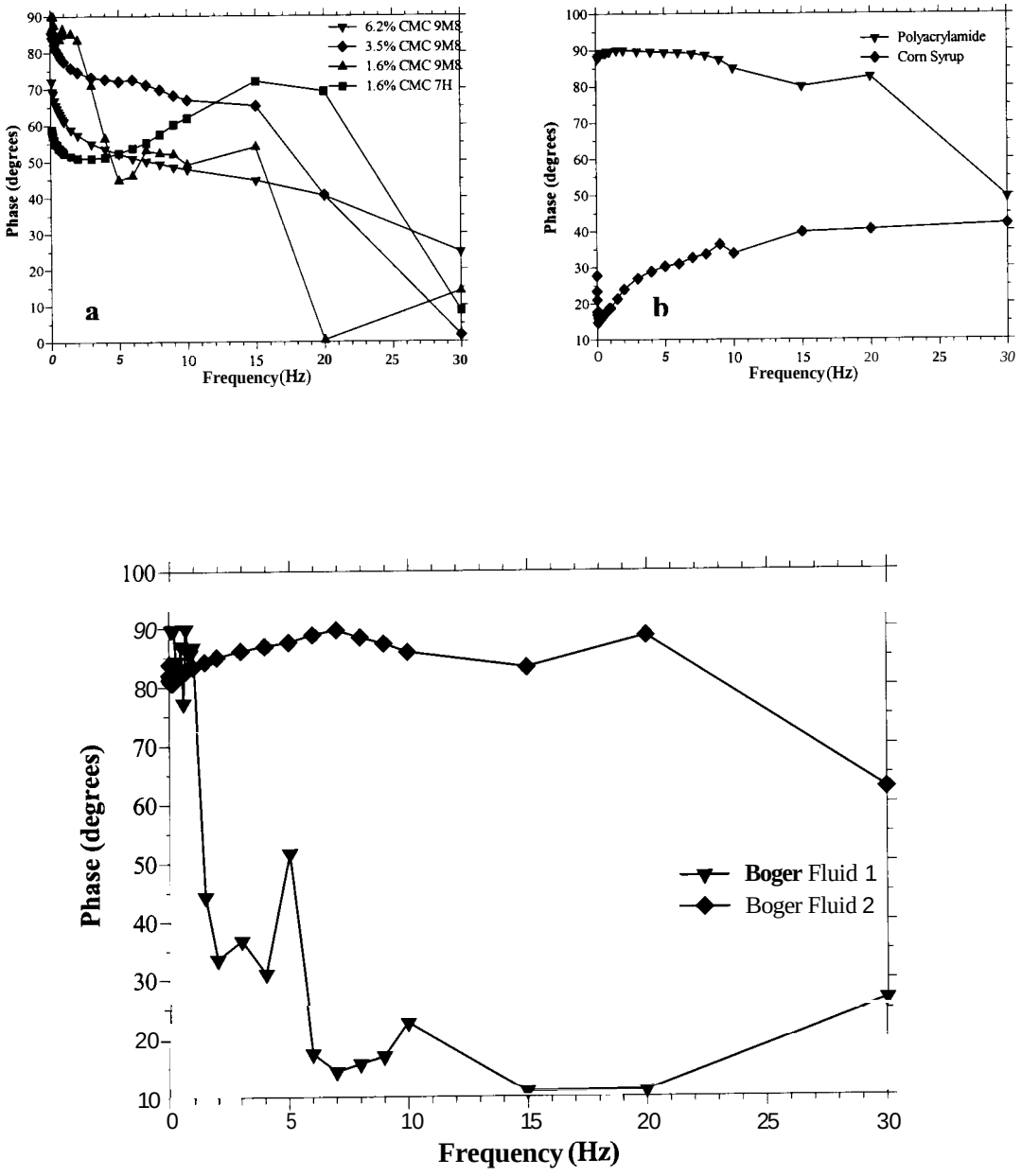

Figure 4.7: Phase angle results for the a) CMC solutions b) Polyacrylamide and Corn **Syrup** c) Boger fluids

The phase angle for the CMC solutions show the same trend where at low frequencies, as the CMC amount is increased in the solution the phase angle is lower. 3.5% and 6.2% CMC 9M8 do decrease with an increase in frequency where 1.6% CMC 7H increases with an increase in frequency. After a frequency of 15 Hz all four solutions show a drop in phase angle. Polyacrylamide has a phase angle around 90" where Corn Syrup has a low phase angle, indicating that it is more elastic. At a higher frequency, around 30 Hz the two fluids phase angles start to approach each other. Boger fluid 1 has a lower phase angle compared to Boger fluid 2. Boger fluid 2 has a phase angle above 80" up to a frequency of 20 Hz than a drop whereas Boger fluid 1 drops to low phase angles at a frequency of 1 **Hz** and stays in the low phase angle region at higher frequencies.

4.4. Tensile Test Results

From figure 4.8 an increase in CMC concentration decreases the steady pressure value of the tensile test. The decrease in pressure correlates well with the concentration of the CMC. This result indicates that an increase in CMC causes the fluid to cavitate at a lower pressure. The CMC may act as nucleation sites for cavitation.

Figure **4.9** shows the pressure values obtained for the four fluids. Boger fluid 1 needs to approach higher pressure values to cavitate. Corn syrup which had a higher storage modulus throughout the whole frequency sweep test, needed less pressure to cavitate then Boger fluid one but still more than the other two fluids. Polyacrylamide needs the lowest pressure to cavitate. A correlation with the parameters are not seen with these types of fluids. For the Boger fluids the one with a higher elongational viscosity needs less pressure to cavitate. For the polyacrylamide and corn syrup pair, polyacrylamide has a

higher elongational viscosity and needs to approach a lower pressure for cavitation. Comparing the fluids in pairs, a higher elongational viscosity concluded to a lower pressure for cavitation.

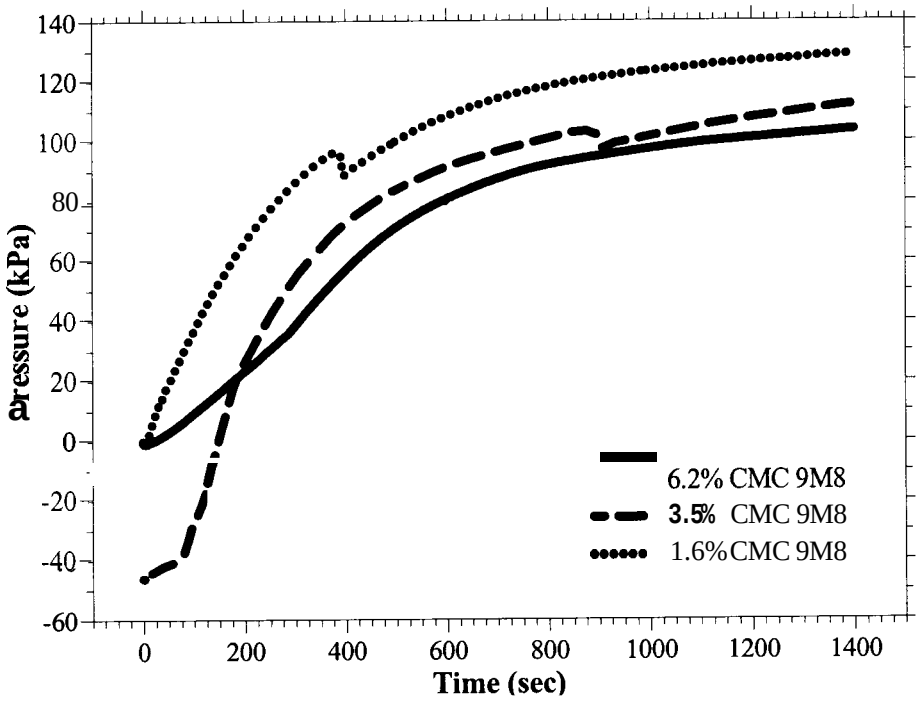

Figure 4.8: Pressure versus time graphs obtained from the tensile test for the CMC 9M8 solutions

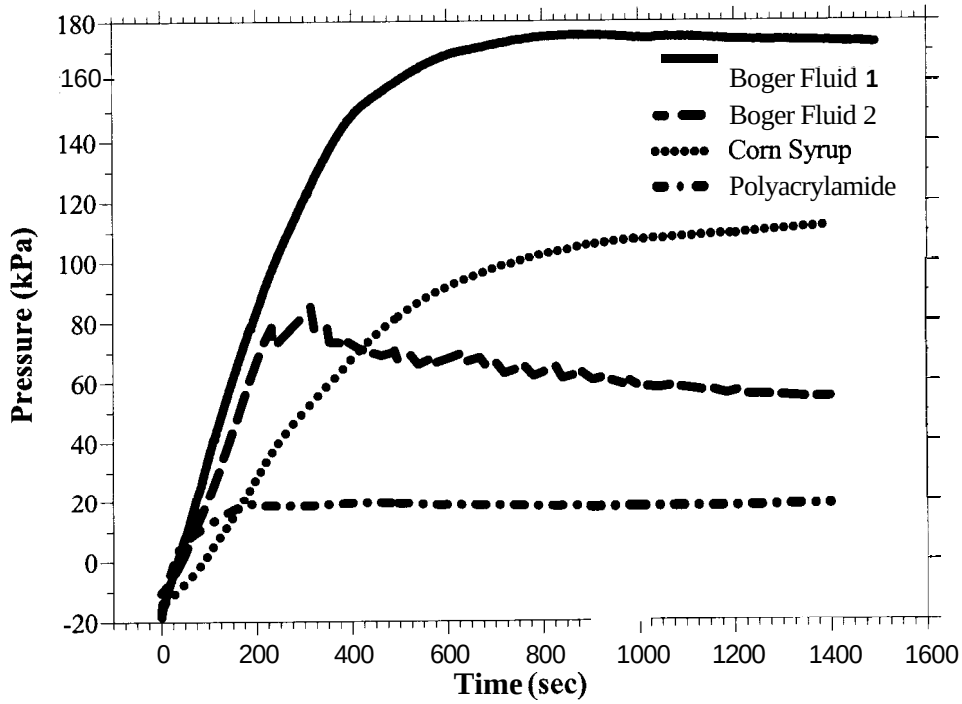

Figure 4.9: Pressure versus time graphs obtained from the tensile test for the other fluids

4.5. Elongational Results

These eight fluids had different elongational viscosity values. Figure 4.10 shows the three CMC 9M8 solutions apparent elongational viscosity values found at different elongational rates. **A** steady clear value is not obtained, but at $100\,s^{-1}$, these fluids seem to have a steady value. The 6.2% CMC 9M8 solution was the only fluid out of these three that had an increase in apparent elongational viscosity with extension rate up to an equilibrium value. The decrease seen in figure 4.10 in the apparent elongational viscosity for 1.6% CMC 9M8 can be due to shear effects occurring during the experiment. The

Trouton ratios, using the plateau values are 504.5, 15.9, and 0.72 for the 1.6, 3.5, 6.2 % CMC, respectively. The relaxation time is the inverse value of the frequency (f) multiplied by 2π at which the loss G" modulus and storage G' modulus are equal. For some fluids, G' and G" had to be fit to a function and "f" found due to extrapolation. The G"/G' values for the four fluids at 1 Hz seems to correlate well with their filamentation values, with a decrease in G"/G', indicating the fluid becomes more elastic an increase in the average filament volume is noticed. The G"/G' values for 1.6%, 3.5 %, and 6.2% CMC at 1 Hz are 11.37, 4.52, and 1.82, respectively.

Table 4.1 : Average filament volume for the fluids with their film thickness, shear viscosity, apparent elongational viscosity, cavitation pressure, and relaxation times

Fluid	Film Thickness (μm)	Avg. Filament Vol.*10^3 (mm^3)	Viscosity (Pa-s)	App. Elong. Vis. (Pa-s)	Cavit. Pressure (kPa)	Relax. Time (s/rad)
1.6% 9M8 CMC	1.7	2		112	129	0.014
3.5% 9M8 CMC	1.8	3	3	48	112	0.009
6.2% 9M8 CMC	2	6	64	46	103	0.011
Boger Fluid 1	2	7	0.1	2304	173	0.121
Boger Fluid 2	0.5	13	7	2814	56	0.004
Corn Syrup	2.5	9	6	20	112	0.005
Polyacrylamide	2	4	2	991	19	2.463

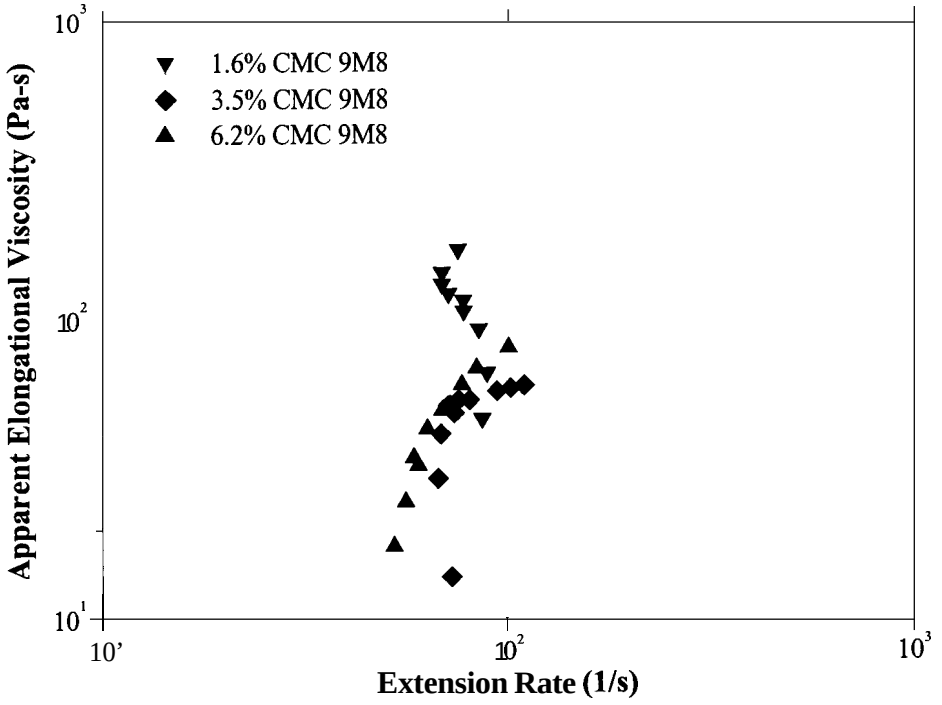

Figure 4.10: Apparent elongational viscosities for the CMC solutions

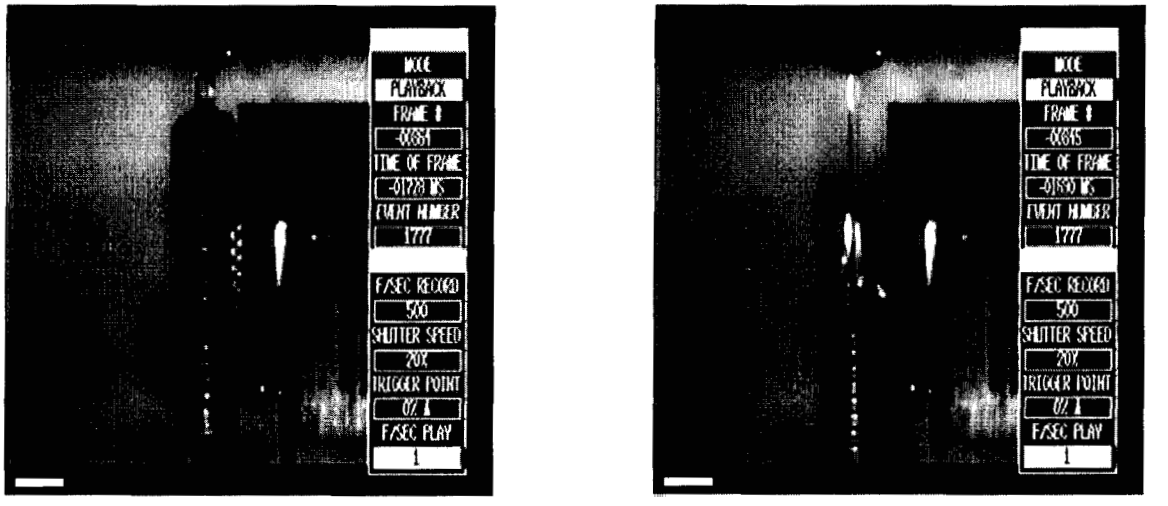

7 mm **7 mm**

a **b**

time=26 ms **time= 64 ms**

Figure 4.11 : Images of Boger Fluid **2** at a a) very short time of elongation b) longer time of elongation

The two Boger fluids have large elongational viscosities as expected. Figure **4.1**1 shows actual images of these elongational tests. These images agree with others in literature (Matta, 1990). The first Boger fluid seems to have a plateau at 3 s^{-1} of 2300 Pa-s, but shear thins at higher extensional rates. This fluid is difficult to select a value for the extensional viscosity. The average of the high extensional rate apparent elongational viscosities were averaged to obtain a single value. The second Boger fluid has a plateau value around 90 Pa-s. these values are in the same range as others have reported. (Matta, 1990)

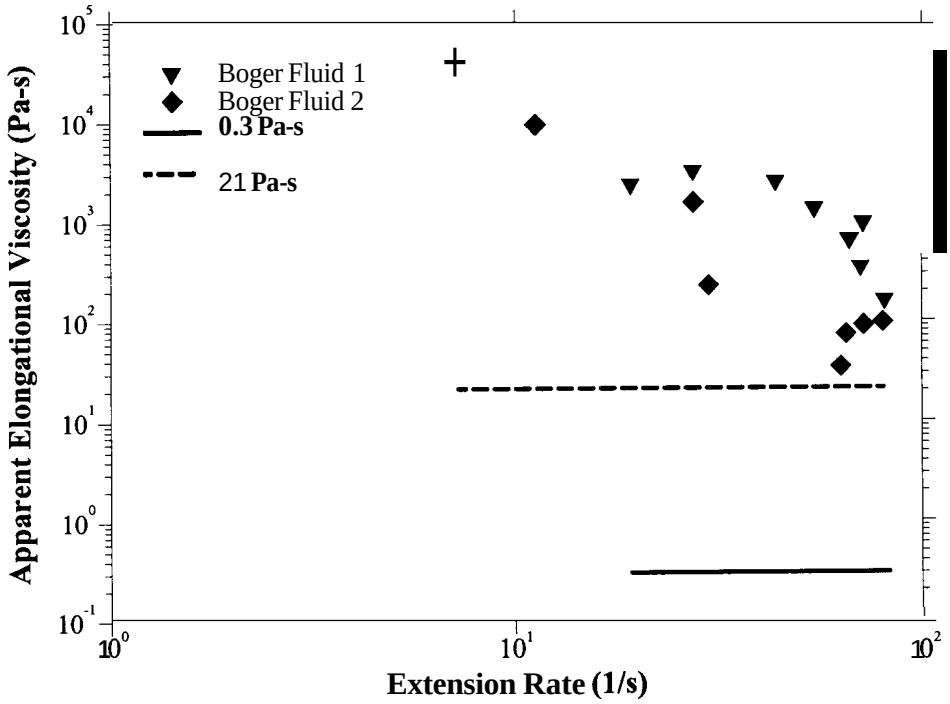

Figure 4.12: Apparent elongational viscosities for Boger fluids and their theoretical elongational viscosity of a Trouton ratio of three times their shear viscsoity. 0.3 Pa-s being the theoretical for Boger fluid 1 and 21 Pa-s being the theoretical value for Boger fluid 2.

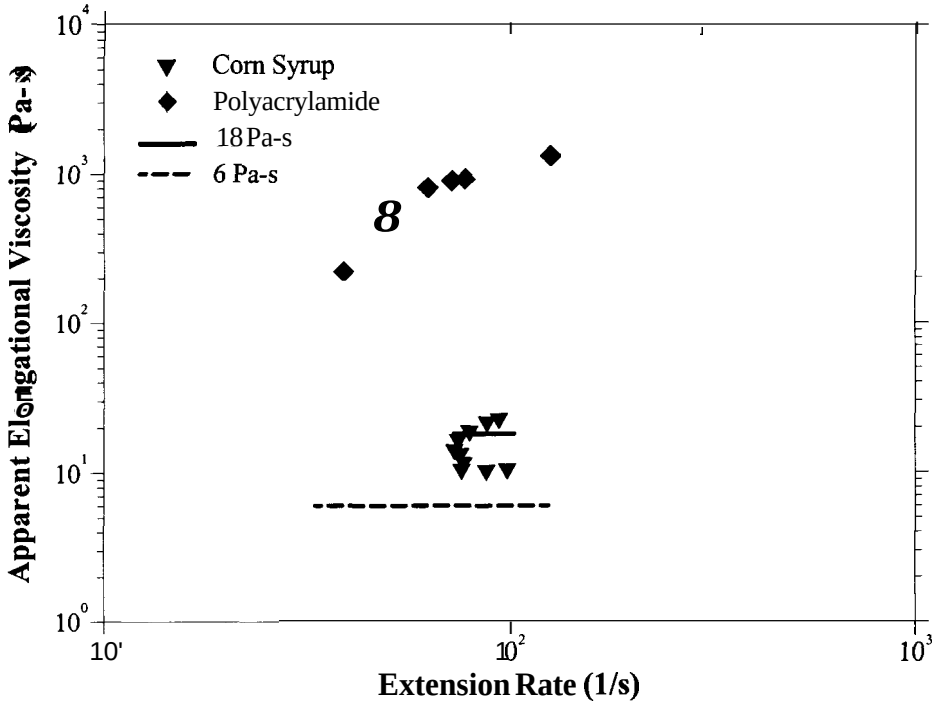

Figure 4.13: Apparent elongational viscosities for Corn Syrup and Polyacrylamide and their theoretical elongational viscosity of a Trouton ratio of three times their shear viscsoity. 18 Pa-s being the theoretical for Corn Syrup and 6 Pa-s being the theoretical value for Polyacrylamide.

Figure **4.13** shows the results for corn syrup and polyacrylamide. Corn syrup did not show a typical curve that would be expected from an elastic fluid. The oscillatory results show that corn syrup has elastic behavior and the polyacrylamide is viscous, yet the elongational viscosities are opposite of what might be expected. The G"/G' values for the four fluids at 1 Hz seems to correlate well with their filamentation values, with an increase in G"/G', indicating the fluid becomes less elastic a decrease in the average

filament volume is noticed. The G"/G' values for corn syrup, Boger Fluid 2, Boger fluid 1 and polyacrylamide at 1 **Hz** are 0.340, 8.619, 17.7, and 167, respectively.

4.6. Filamentation Results

Table 4.1 shows all of the fluids with their viscosity values, film thicknesses and average filament volume values. All of these fluids were analyzed close to **2** μm film thicknesses. For the shear-thinning fluids, the low shear viscosity is given. The three CMC solutions show an increase in the average filament volume with an increase in their concentration. The frequency sweep tests indicated that these fluids were dominated by their viscous modulus.

The other four fluids do not show a trend with their filament volume values and their shear viscosity values. As for the polyacrylamide and corn syrup, an increase in viscosity did show an increase in the average filament volume.

The CMC solutions formed larger filaments as the apparent elongational viscosity and cavitation pressure increased. A decrease in cavitation pressure for the Boger fluids meant an increase in filament volume where for the apparent elongational viscosity, the opposite trend was observed. For polyacrylamide and corn syrup an increase in cavitation pressure and decrease in apparent elongational viscosity showed larger filaments.

4.7. Summary

The CMC solutions show a correlation with their steady shear viscosity values and their average filament volume values but this correlation does not hold for the other fluids. The

filament volume increases with increasing apparent elongational viscosity. The Boger fluids have large apparent elongational viscosities, and filament volume values, but the other fluids have high Trouton ratios and small filament volumes. **A** good correlation with elasticity and average filament volume is not obtained. With increasing elasticity the average filament volume increases for both the CMC solutions and the other four fluids.

CHAPTER 5 : INKS

5.1. Introduction

Inks consist of materials: pigments, resins and oils. Pigments are the contribution of color to imaging. Pigments are a solid phase and the vehicle is a liquid, but a liquid of very special nature: It must remain a liquid on the press and yet be completely dry on the substrate.

The pigments and vehicles of the ink are combined by dispersing. Pigments and vehicles have different functions. The pigments contribute not just the color of the printed image, but also many other features of the printed product for quality. The vehicle is basically responsible for the adhesion of the printed image onto the substrate. It is also responsible for the type of drying and the speed of drying of the ink.

Other ingredients may include driers, though, not in all types of inks, wetting agents, anti-skinning agents, waxes and sometimes perfumes.

5.2. Materials Used

Five model inks were provided by Sun Chemical Corp.. These inks had different vehicle concentrations or chemistry. Model Ink **A** and Model Ink D have the same vehicle in different concentration amounts. The other three inks have different vehicle chemistry. The inks are denoted Model Ink **A-E.** The other two inks are a standard cyan process ink which will be denoted as Process Ink (Capiplus III Process Cyan, Flint Ink Corp.) and a 25% carbon black ink provided by Sun Chemical Corp. which will be denoted Model Ink

I. In one of the sections there is an ink named Model Ink II which is an 18% carbon black ink again provided by Sun Chemical Corp..

5.3. Rheological Results

The results obtained in this section of this chapter are obtained using the Bohlin CVO rheometer using the procedures described in chapter 3 section 3.2.

The misting factors for these five inks are supplied by Sun Chemical and are reported in table 5.1. The mist factor is found by holding a piece of white glossy paper vertically behind the rollers and another one horizontally below the rollers in an inkometer. The inkometer is run at 3000 RPM for 1 minute, at 90°F, with 2.4-2.5 grams of ink sample, with appropriate precautions. The mist rating is determined by measuring the optical density on the sheet of paper using a densitometer (a reflectance measurement). Several measurements are made and an average was provided by Sun Chemical.

Figure 5.1 shows that these five inks have similar steady shear behavior with a low shear rate Newtonian plateau and shear-thinning behavior at moderate shear rates. The same trend for the process ink is seen in figure 5.2. the model ink I seems to show the same Newtonian plateau and than a shear-thinning behavior but the Newtonian plateau seems to be at lower shear rates. Figure 5.3 shows the storage and loss moduli for these inks over a range of frequencies. Figures **5.4** and 5.5 show the phase angle and the low shear stress results. At high shear rates, the high misting inks **(A** and C) seem to have lower viscosities compared to the other inks, but this difference is rather small. These inks do not show yield stress behavior as others have noted, but with our rheometer, we are able to characterize low shear rate viscosities. Note that a yield stress would be expected if

data under 1 s^{-1} were not available and the data was extrapolated back to zero shear rate. Otherwise, if the storage modulus at the highest frequency is compared to the mist ratings, there is a good correlation between small storage modulus and high misting factor and large filaments. The loss and storage modulus for Model Ink I is much higher than that of the Process Ink. In figure 5.4, there is a fair correlation between a high phase angle and a high misting factor, with the exception of ink C. This ink also had a low viscous modulus and therefore gave a low phase angle. In general, there is a correlation between the elastic nature of the ink and the decrease in filament size and misting. This trend agrees with the silicone oil and pick test oil results, where the increase in elastic nature of the silicone oil results in smaller filaments.

In figure 5.5, it is hard to see any correlation with low shear rate behavior and misting factor.

Table 5.1: Mist rating properties for the model inks.

	Vis. (Pa-s)	App. Elong. Vis. (Pa-s)	Mist Factor	Phase Angle (°) at 1 Hz	Average Filament Volume *10^3 (mm^3) Film Thickness		
					1μm	3 μm	5 μm
Model Ink A	333	369	34.9	76.8	8.2 ± 7.0	2.5±1.4	10.7±5.8
Model Ink B	318	512	1.36	71.3	1.1h0.6	1.4h0.6	15.2h19.6
Model Ink C	121	438	20.1	71.0	2.3h1.5	4.8h4.3	4.9±5.5
Model Ink D	598	290	8.7	74.8	0.8h0.4	1.7h1.6	7.6h7.4
Model Ink E	251	217	**NA**	71.6	1.8h1.0	2.4h1.6	6.0±4.0

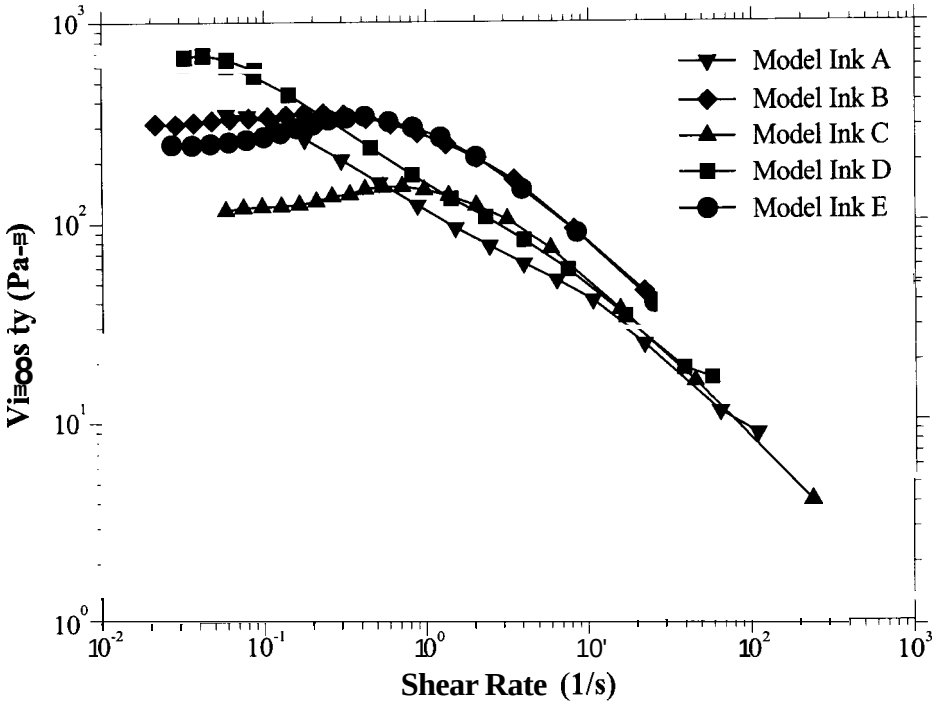

Figure 5.1: Steady shear viscosity versus shear rate values for the five model inks

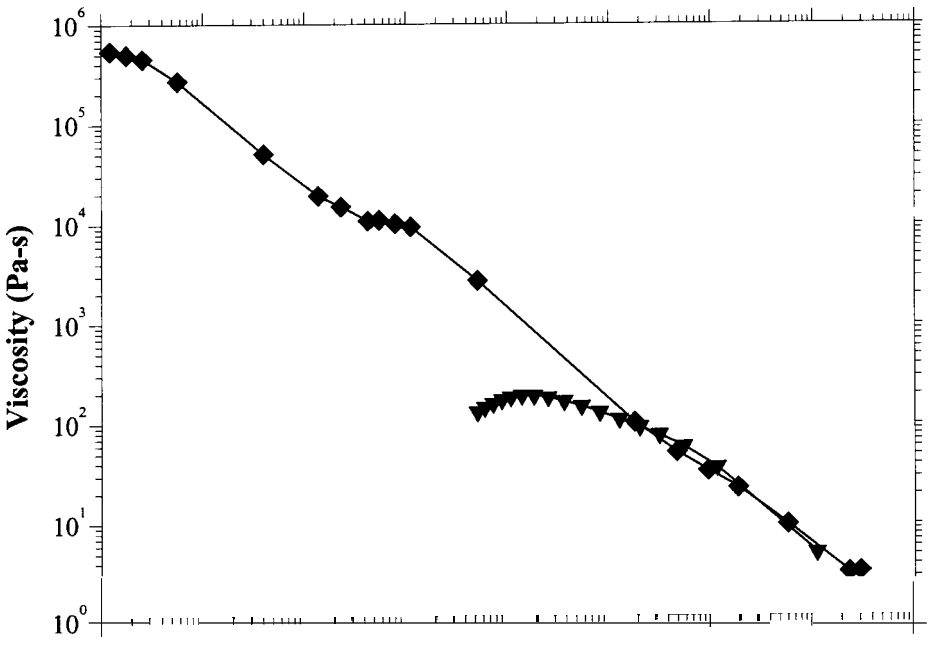

Figure 5.2: Steady shear viscosity versus shear rate values for Process Ink and Model Ink I

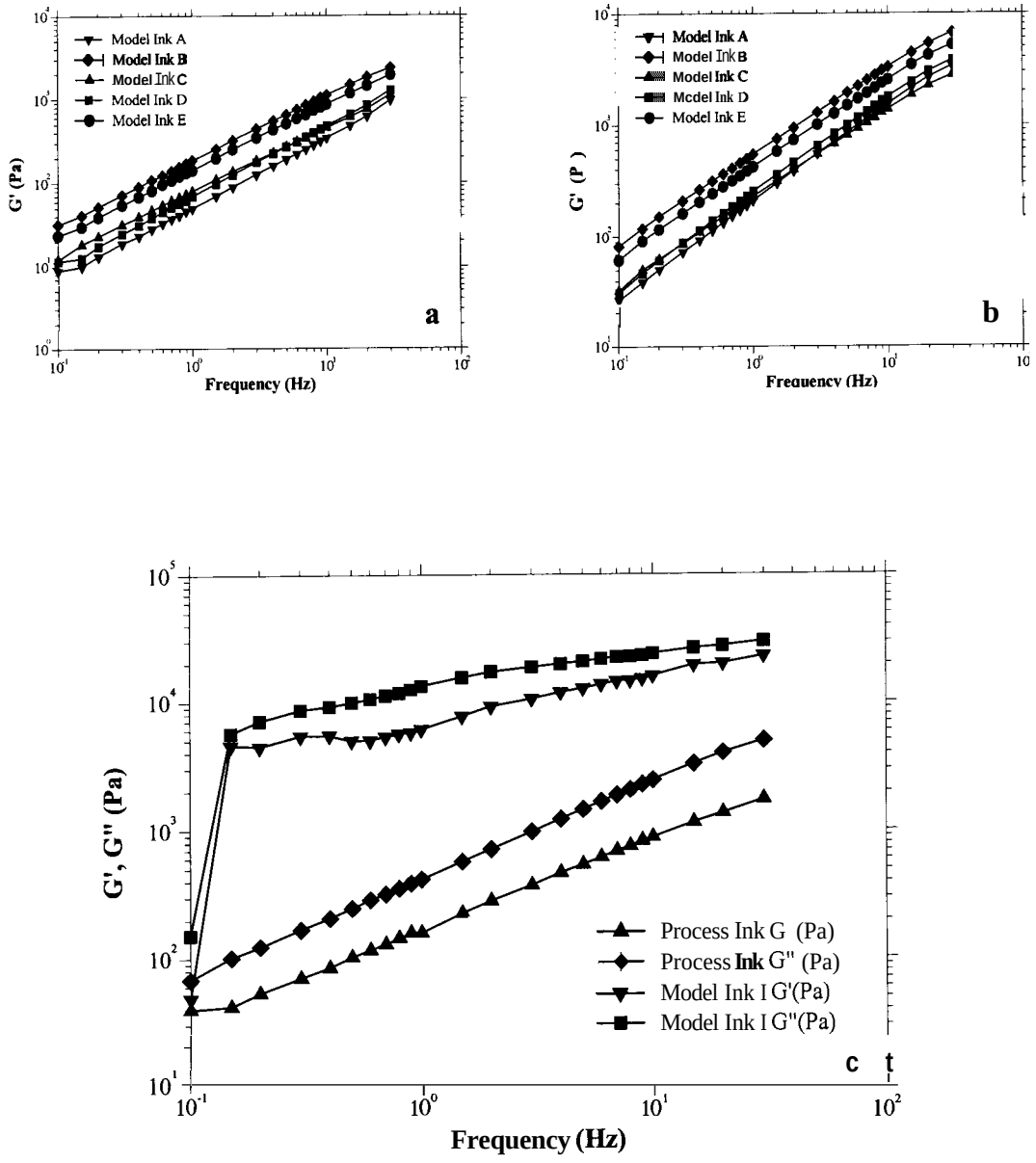

Figure 5.3: Oscillatory results for the five model inks a) elastic modulus and b) loss modulus c) oscillatory results for Process Ink and Model Ink I

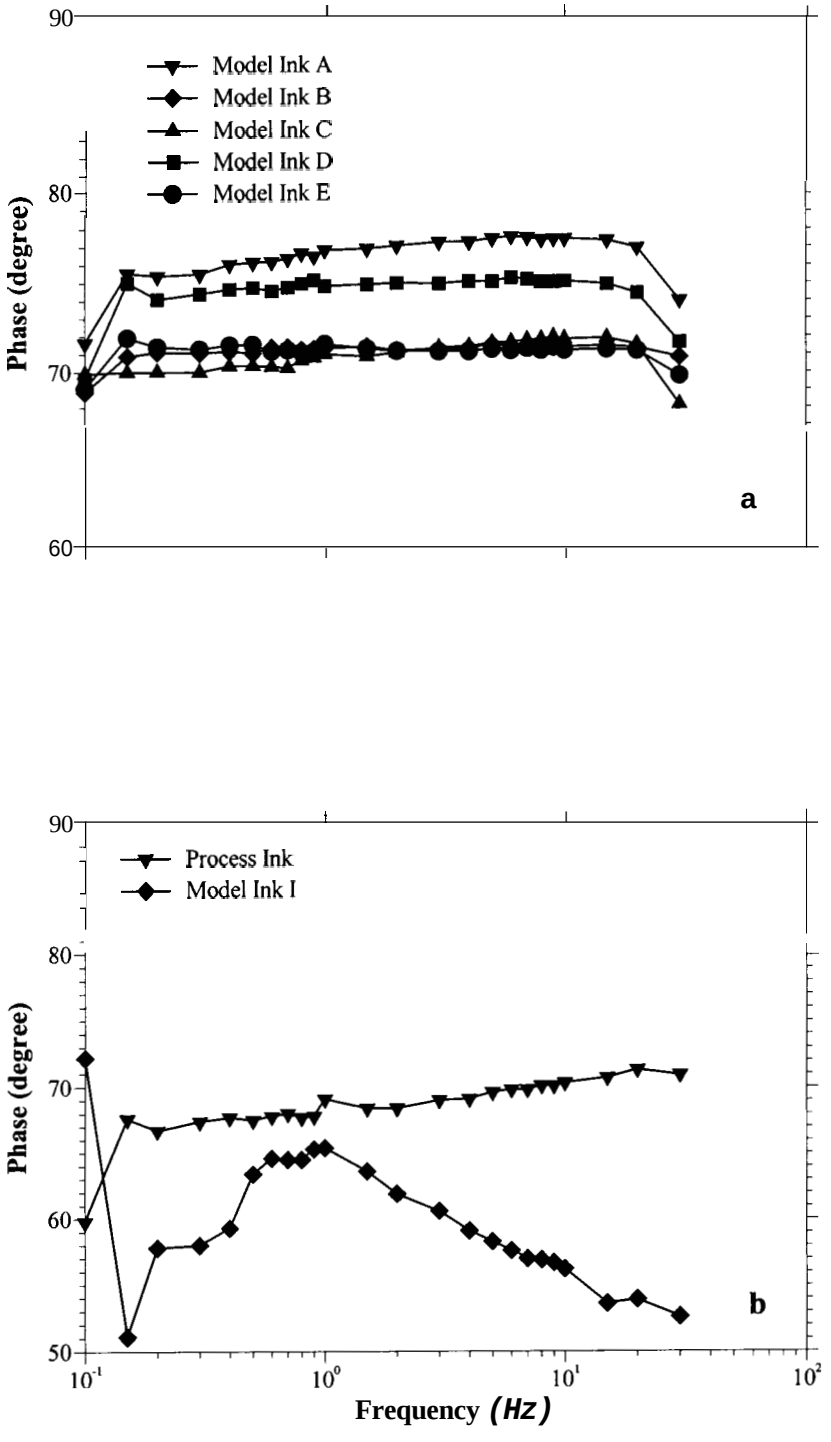

Figure 5.4: Phase angles values for a) model inks **A-E** b) Process Ink and Model Ink I.

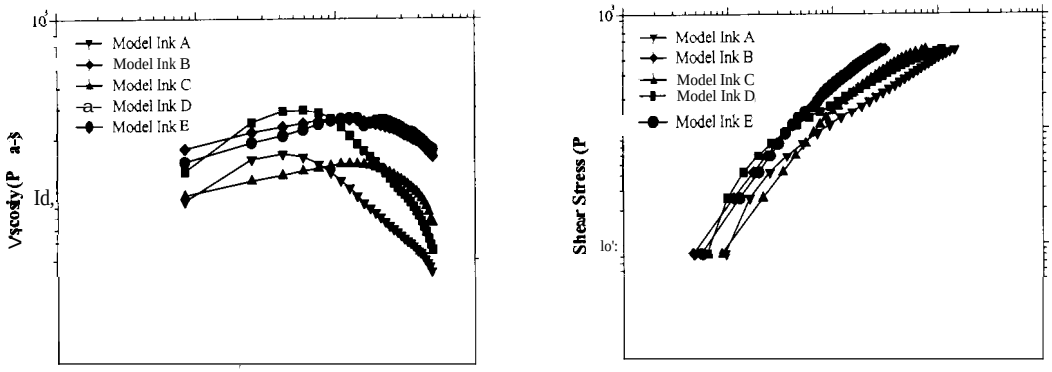

Figure 5.5: Low stress results.

5.4. Tensile Test Results

Figure 5.6 shows the results of the tensile test for the model inks. In all cases, the pressure goes above 100 kPa. This indicates that there is some resistance in the syringe motion, because the pressure cannot drop below vacuum inside the syringe. The shapes of the curves are often not the same from run to run, possibly causes by different resistance to motion of the syringe. However, the general ranking of the fluids do seem constant, with **A,** C, D, and B, ranking from low to high pressure. Ink E did not fall in the same rank from run to run. However, when looking at this ranking with the misting factors, a clear trend emerges: low tensile pressures tend to generate larger mist factors.

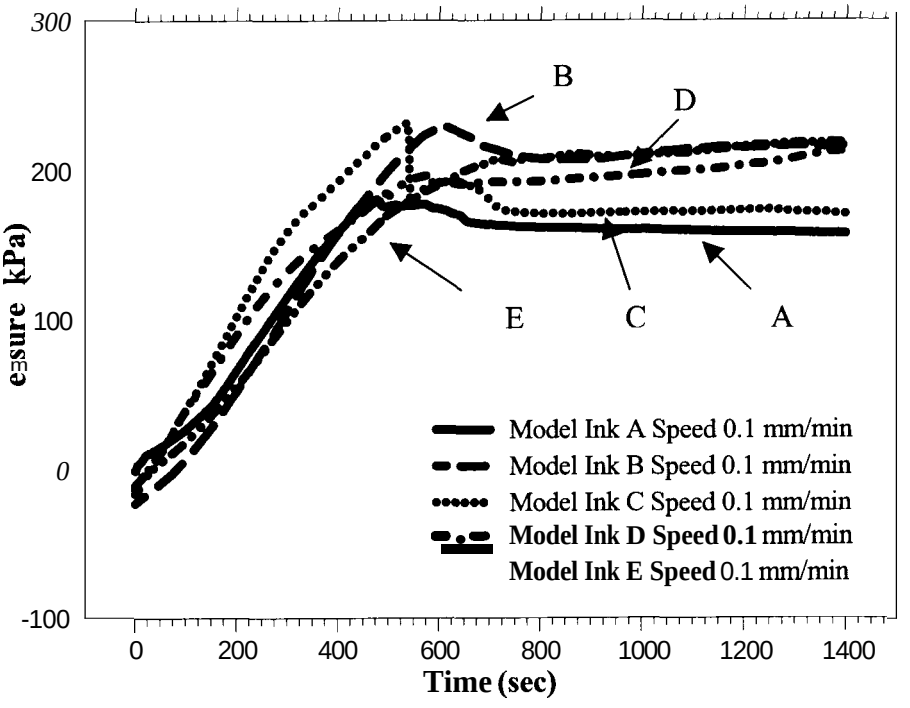

Figure 5.6: Pressure and time results for 0.1 mm/min pulling rate

Figure 5.7 shows the results for the other two inks, Process Ink and Model Ink I. The process ink needs to approach higher pressures to be able to cavitate compared to model ink I. Model ink I did form smaller filaments compared to the process ink which indicate that the fluids having lower pressure values would cavitate farther in the nip and form smaller filaments, but this is not the case with the Model inks **A-E.**

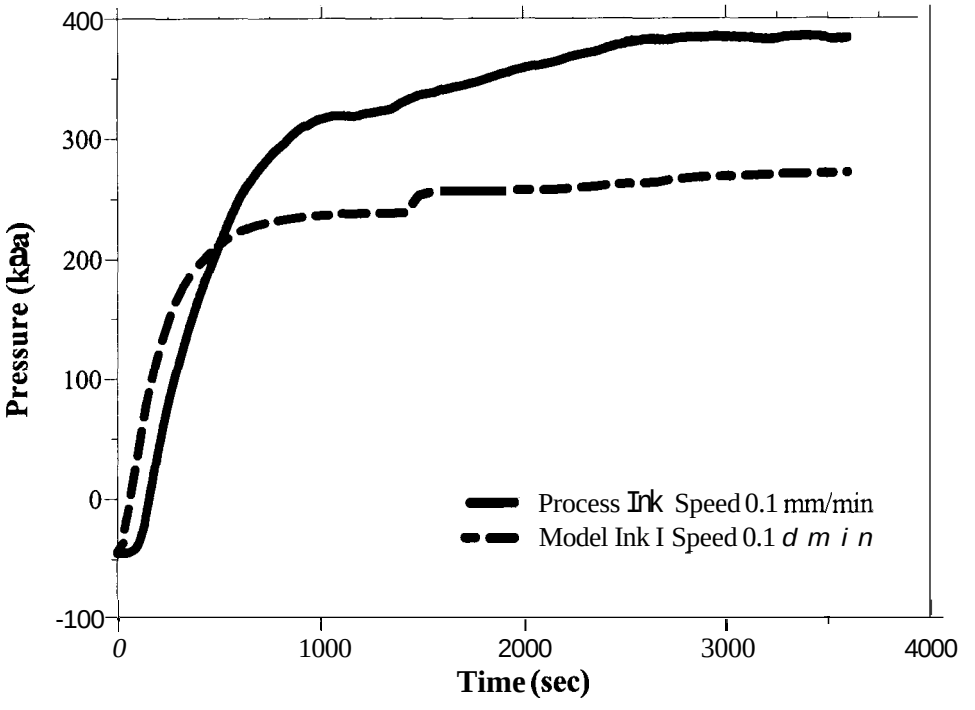

Figure 5.7: Pressure and time results for 0.1 mm/min pulling rate

5.5. Elongational Results

The results obtained in this section of the chapter are from the elongational viscosity procedure described in chapter 3 section 3.6. **A** sample image of a filament at short time and long time is given in figure 5.8.

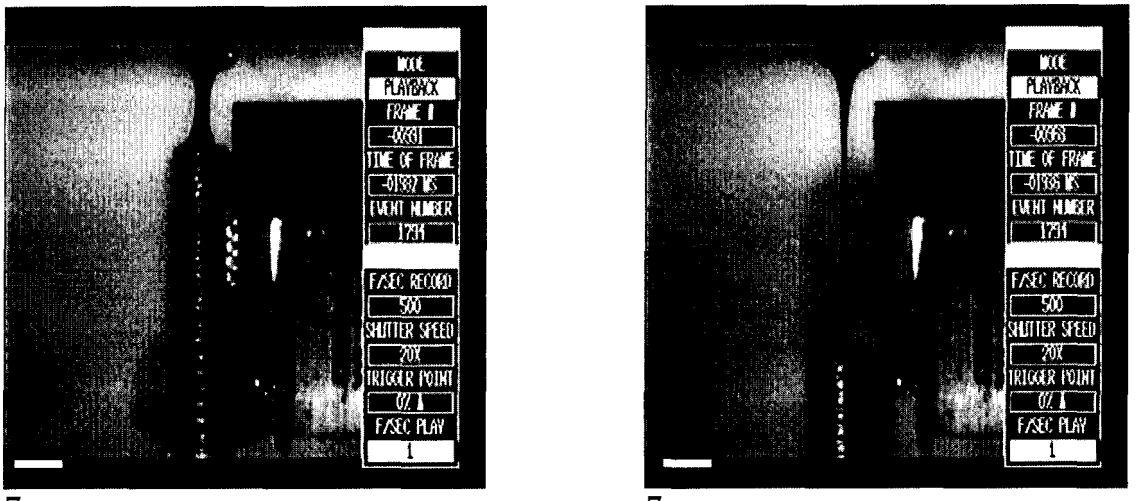

Figure 5.8: Images of Model Ink **A** at a a) very short time of elongation b) longer time of elongation

Table 5.2 has the shear viscosity values, elongational viscosity values and the average filament volume values. From this table a direct correlation with the elongational viscosity and the filament volume is not found. With some of the inks we do see what was seen with the shear viscosity that the filament volume seems to increase with a decrease in elongational viscosity but this trend does not apply for all inks, therefore, a conclusion can not be made. These fluids are all shear-thinning fluids as can be seen from their shear viscosity curves given in the appendix figure **A.2-A.4** is a plot of apparent elongational viscosity versus extension rate and from this figure we see a thinning behavior of the fluids. This would indicate that the fluids elongate which would imply that they would form filaments that are elongated; because of this elongation and thinning with elongation, the filaments would have a very thin radius which would still form filaments with a small volume value.

Table 5.2: Average filament volume for the fluids with their viscosity values and apparent elongational viscosity values at higher extensional rates

Fluid	Viscosity (Pa-s)	App. Elong. Vis. (Pa-s)	Avg. Filament Vol.*10^3 (mm^3)	V* *10^{-3}
Model Ink A	333	369	8	8200
Model Ink B	318	512	1	1100
Model Ink C	121	438	2	2300
Model Ink D	598	290	0.8	800
Model Ink E	251	217	2	1800
Process Ink	147	199	4	4000
Model Ink I	25760 25760	33	4	4000

5.6. Filamentation Results

The filamentation results are the results obtained from the IGT set-up described in section 3.4. For the Process Ink and a Model Ink I the filament volume and spot volumes were calculated and compared. The results found were done manually and using image analysis. The two results obtained were compared. The calculations for the spot volume were done by using a calibration value obtained from the bead image given below (figure 5.8). The original bead diameter is known and a light reflection coming in at a 45^o angle was measured and this calibration value was used. From this it was again seen that for the Process **Ink,** as the film thickness increased the filament volume increased, as did the spot volume. When the ratio of filament volume to spot volume is taken it was seen that for these three thicknesses (1, 3, and 5 μm) they tended to be in the range of a ratio

value of 1.7-2.0. This was something that we thought could be interesting to take into consideration.

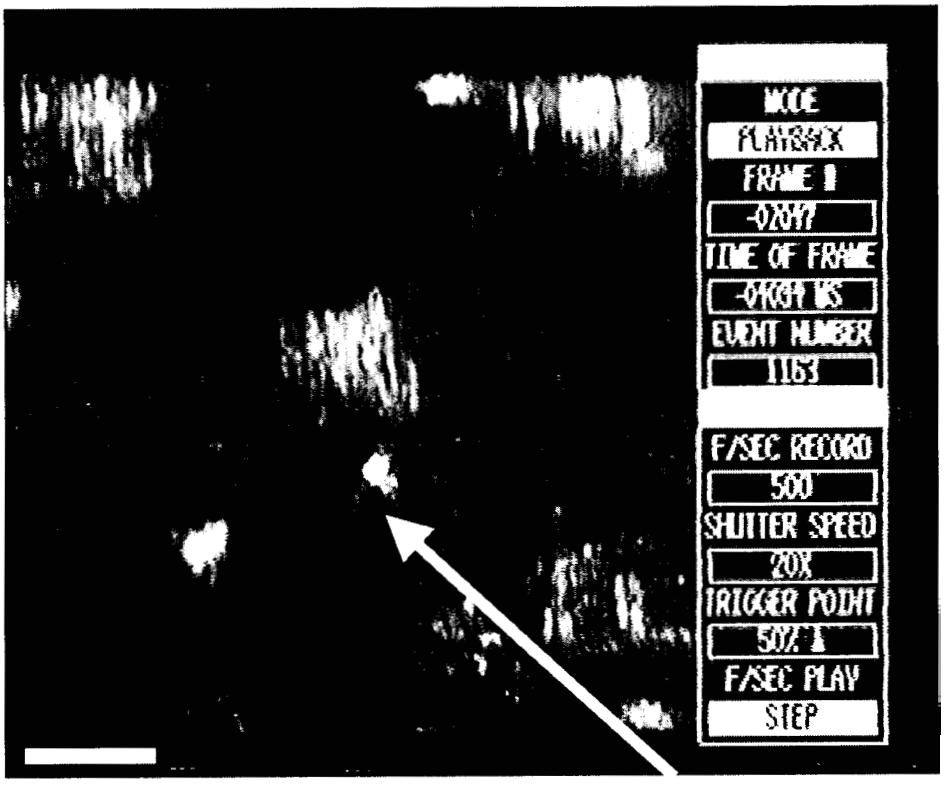

0.5mm **0.5 mm diameter bead**

Figure 5.9: Image used to figure out the calibration of a 45° lighting on the images.

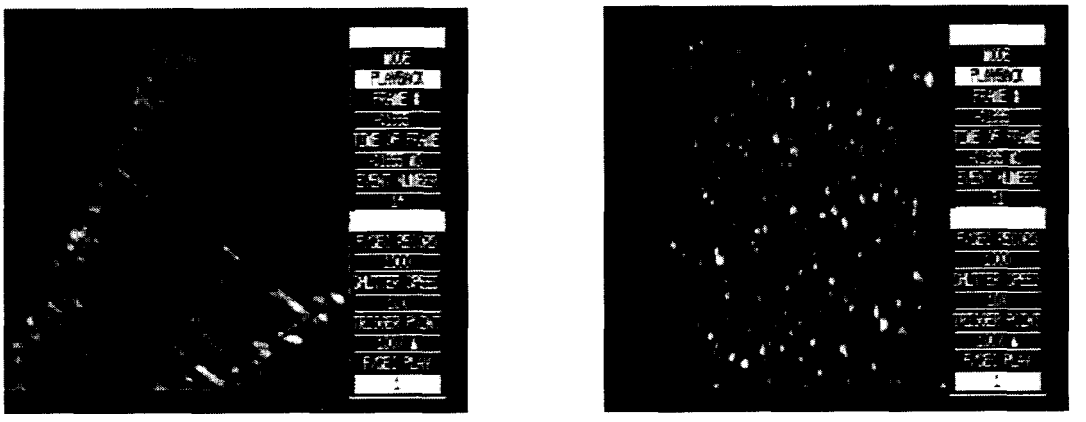

(a) **(b)**

Figure 5.10: Pictures captured from video of ~ 34 μm cyan ink on the IGT rolls. Frame (a) shows a side view of the strip showing the cones. Frame (b) shows a front view of the strip showing the spots.

Table 5.3: Cone-Hemisphere Relationship for three different inks with –34 μm film thickness

	Cyan Ink	**Model Ink I**	**Model Ink II**
Cone Volume (mm^3)	0.00408	0.00024	0.00034
Hemisphere Volume (mm^3)	0.00012	0.00023	0.00012
Ratio (cone vol./h.s vol.)	34.65	1.03	2.88

Figure 5.10 (a) shows the side view seen on the IGT rolls and figure 5.10 (b) shows the spots seen when looking directly on the rolls. Table 5.3 shows the cone-hemisphere relationship found for three different types of ink. A one-to-one ratio was expected but this was seen only in the Model I type of ink. These three inks have different rheological properties, it can be seen visually that the recoiling back onto the roll of these three inks are different. It was observed that the cyan ink has a tendency to fall over after breakage whereas the other two types of ink snap back rapidly sometimes it is difficult to see the cones that are formed. The behavior described explains the results: a high ratio would be expected if a filament volume fell over because its volume would look larger than if it snapped back.

The result in table 5.3 changes the emphasis of this whole project. At first, the spots after printing were thought to indicate directly the filament size. However, the way filaments either fall over or snap back to the roll changes its volume on the roll. Therefore, looking at the filaments would give us a better idea of the filamentation process. Manual measurements are needed to measure filament size for each type of ink or fluid.

Table 5.4: Manually Measured Filament Volumes for Process Ink

Film Thickness (pm)	1	3	5
Avg. Fil. Vol. (mm^3)	0.004	0.010	0.020
Std. Dev. (mm^3)	0.003	0.008	0.013
C.O.V. (%)	82	74	64

Table 5.5: Manually Measured Spot Volumes for Process Ink

Film Thickness (pm)	1	3	5
Avg. Fil. Vol. (mm^3)	0.002	*0.005*	0.010
Std. Dev. (mm^3)	0.002	0.007	0.015
C.O.V. (%)	101	129	154

Table 5.6: Manually Measured Filament Volume to Spot Volume Ratio for Process Ink

Film Thickness (pm)	Fil. Vol./Spot Vol.
1	1.709509536
3	1.895043715
5	2.076496848

Table 5.7: Manually Measured Filament Volumes for Model Ink I

Film Thickness (μm)	1	3	5
Avg. Fil. Vol. (mm^3)	0.004	0.006	0.009
Std. Dev. (mm^3)	0.002	0.004	0.005
C.O.V. (%)	56.6	**74.2**	51.6

Table 5.8: Manually Measured Spot Volumes for Model Ink I

Film Thickness (μm)	1	3	5
Avg. Fil. Vol. (mm^3)	0.007	0.011	0.034
Std. Dev. (mm^3)	0.008	0.012	0.031
C.O.V. (%)	118.9	110.3	90.3

Table 5.9: Manually Measured Filament Volume to Spot Volume Ratio for Model Ink I

Film Thickness (μm)	Fil. Vol./Spot Vol.
1	0.578217588
3	0.508542155
5	0.257213325

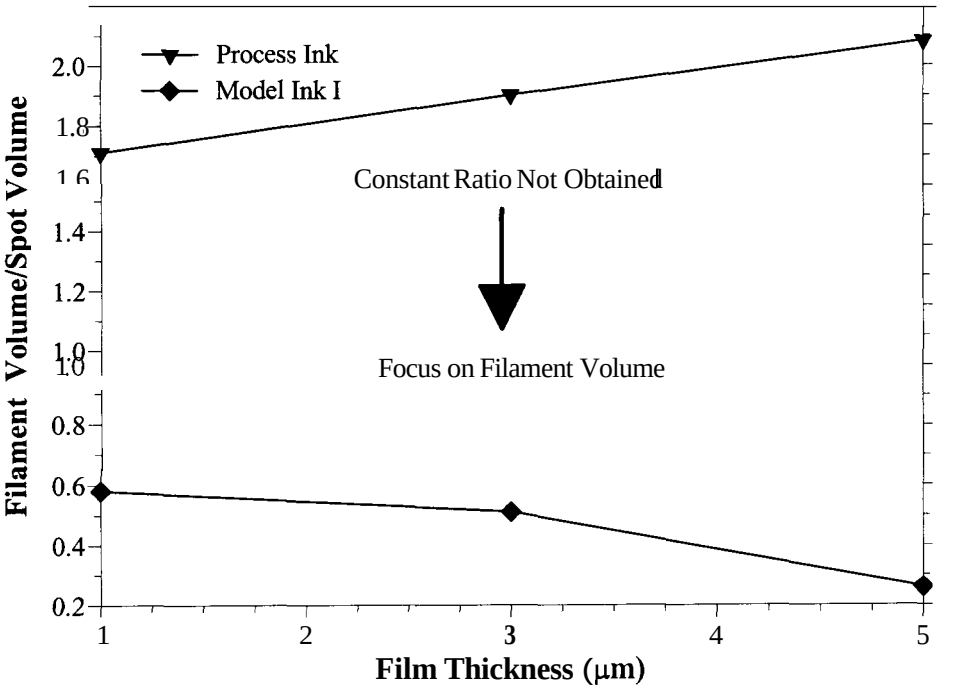

Figure 5.11: The plot of filament volume to spot ratio. This value is not constant therefore focus is given to filament volume.

Table 5.1 shows the mist rating factors for the inks, the phase angle, and the filament volume size characterized from the video images. The standard deviation of the filament volume is noted and should be thought of as the distribution of filament sizes produced. The standard deviation can be quite large, because a few filaments much larger than the average can cause a wide distribution. **An** interesting result is obtained for Model Ink **A:** this ink has the most viscous behavior and is the ink that generates the largest filaments at 1 μm ink film thickness and has the highest misting rating.

For the 1 μm film thickness, there is an expected relationship between the mist factor and the average filament volume: large filament sizes leads to high misting. However, for the

larger film thicknesses, this trend does not hold. Figure 5.12 shows the trends for the three film thicknesses.

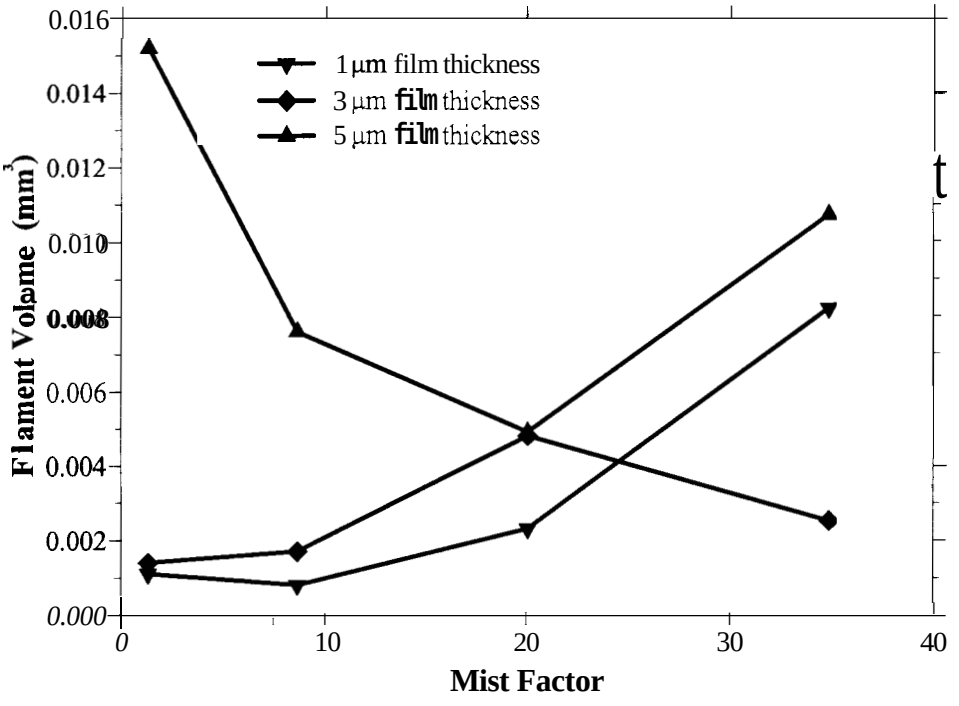

Figure 5.12: Filament volume versus mist factor at different film thicknesses for the model inks.

5.7. Filament Remains

The analysis of filament "remains" (residues) are obtained with the procedure described in section 3.5 using the KRK laboratory print tester.

The Process Ink and Model Ink I were printed on Mylar using the KRK Print Tester at three different speeds (0.5, 4, and 8 m/s) (0.5 m/s to be able to compare with the IGT results 0.34 m/s) and three different film thickness (1.5, 3, and 5 μm) 4 runs each to be able to average the values. These images have been recorded and analyzed.

Table 5.10: KRK runs of Process Ink Printed on Mylar. Image Pro Analysis Results

Speed (m/s)	**0.5**			**4**			**8**		
Thickness (μm)	**1.5**	**3**	**5**	**1.5**	**3**	**5**	**1.5**	**3**	**5**
Run1	0.00955	0.03187	**0.44632**	0.03767	0.02224	0.2964	0.04171	0.0369	**0.20077**
Run2	0.01954	0.02146	0.02819	0.01836	0.04803	0.16479	0.08197	**0.34754**	0.24044
Run3	0.00805	0.01569	**0.01519**	**0.0166**	**0.13006**	**0.02326**	**0.05342**	**0.07317**	0.04731
Run4	0.00799	0,02007	**0.03998**	**0.01722**	**0.10181**	**0.16244**	**0.01628**	**0.06811**	**1.17076**
Average	**0.01128**	**0.02227**	0.014	**0.02246**	**0.07554**	**0.16172**	**0.04834**	**0.13143**	**0.41482**
		Average	**0.10873**						

Table 5.11: KRK runs of Model Ink Printed on Mylar. Image Pro Analysis Results

Speed (m/s)	0.5			4			8		
Thickness (μm)	1.5	3	5	1.5	3	5	1.5	3	5
Run1	**0.01949**	**0.0098**	**0.0098**	0.0742	0.01744	0.01596	0.0104	0.03947	0.02461
Run2	0.01659	0.00979	0.01107	10.04804	0.01908	10.01267	10.09443	**12.37014**	0.01357
Run3	0.0116	0.02028	0.02582	**0.15587**	0.01367	0.00906	**0.63568**	0.02185	**5.90127**
Run4	0.0147	0.01299	0.01536	**019025**	0.0181	0.01863	**1.42149**	**1.16353**	**3.52956**
Average	**0.01559**	**0.01321**	**0.01551**	**0.11709**	**0.01707**	**0.01408**	**0.5405**	**0.89875**	**2.36726**

When the above results are compared with the IGT results, a direct correlation is not obtained. The results in bold indicate that Image-pro might have picked an image that was not a filament remain. This was found by comparing all four runs. When comparing these results with the manually obtained IGT results we can see that for the Process Ink at thicknesses 1 and 3 μm, the KRK results seem to be larger by a factor of approximately 5, as for a thickness of 5 μm this factor is approximately 1.35 (when bold value is not taken into consideration). **As** for the Model Ink I at a thickness of 1 μm this factor is approximately 2, for 3 μm it is approximately 1.2 and for 5 μm it is approximately 0.5. We can see that there is not a consistency in this factor value.

5.8. Summary

Fluid rheology is found to have a significant effect on filamentation and the resulting size distribution in a complex manner. Increasing the viscosity of the five model inks seemed to show a decrease in the average filament size, besides model ink **A.** This trend was not seen for the process ink and model ink I. The low pressures in **a** tensile test was related small filament sizes for the process ink and model ink I, but the opposite result is found for inks **A-E.** For all fluids, increasing the elastic nature of the fluid resulted in smaller filaments. For both the model fluids and the inks, the trend of increasing elasticity to reduce filament size is seen. This result is the opposite of the expected result, because elastic fluids often have high elongational viscosities. However, if the elongation rate is rapid enough, the material can act as an elastic solid and a fracture of the material may occur. This fracture may lead to small or no filaments.

CHAPTER 6: FILAMENT REMAIN SIZE IN PRINTING

The technique and procedure described in section 3.5 is used to determine the effect of printing parameters on filament size remains. The pressure of the nip, the speed of printing, and the ink film thickness are changed, and the effect of these parameters on the filament size distribution was analyzed. Different substrates are used to determine the effect of the substrate properties on filament residue size. The "remains" of the filaments or "hills" on the substrate after the nip are assumed to give an indication of the filament size distribution instead of viewing the filaments directly. Therefore, the results reported here is the size of the features on the ink film shortly after printing.

6.1. Materials Used

A plastic film (Mylar), coated and uncoated cellophane, coated paper, newsprint, copy grade paper, light-weight-coated basepaper, and thin cardboard are used as substrates with one standard process ink (Capiplus III Process Cyan, Flint Ink *Corp.).* The inks used in the second part are the standard process ink and two inks with different rheological properties denoted as Ink **A** and Ink B (Sun Chemical Inc.)

6.2. Effect of Printing Speed and Ink Film Thickness

Figure 6.1 shows the effect of printing speed on the filament remains for an ink film thickness of 5 μm printed on the laboratory print tester. Figure 6.1 (a) and (b) compares speeds of **2** and **8** m/s, respectively. The image taken at low printing speed has smaller

features compared to the high printing speed case. The average size increases with speed and the size distribution also increases.

Similar results are obtained when comparing thin and thick ink films as shown in figure 6.2 (a) and (b). **As** the amount of ink fed to the nip increases, forming a thicker ink film, the filaments formed become larger. The computed average filament "remains" sizes are larger with increasing film thickness. The effect of ink film thickness is also found with the IGT roll system; filaments break farther from the nip and the size and size distribution increases with increasing film thickness.

Table 6.1 compares, in the first three columns, different thicknesses of ink. **As** the thickness of the ink increases, the average of the width of the features increases. The standard deviation is a measure of the size distribution. The standard deviation and the coefficient of variation increase for an increase in ink film thickness. Therefore, as ink film thickness increases, the average size of the features and the size distribution increase.

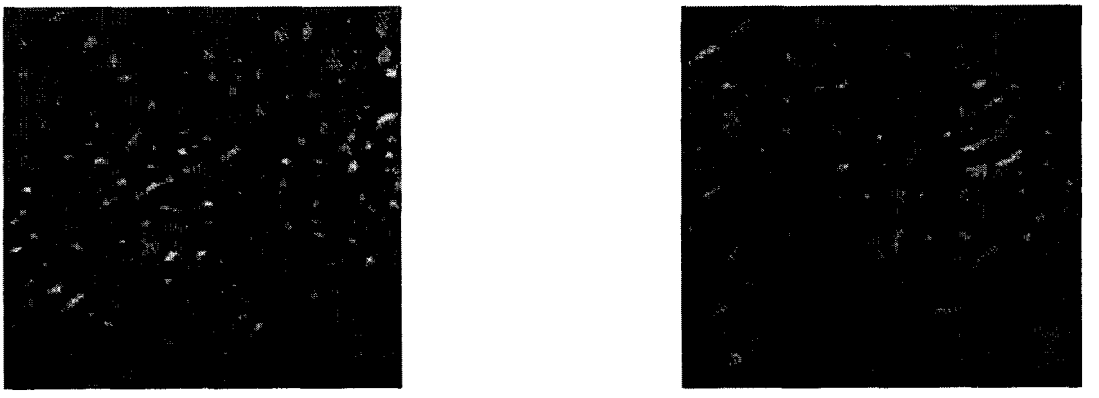

a b

Figure 6.1 : Pictures captured from video of process ink printed on Mylar substrate. Frame (a) shows a 5 micron film printed at 2m/s. Frame (b) shows a 5 micron film printed at 8m/s. The total width of the images is 2 mm. The time after printing is 0.5 seconds.

Table 6.1: Diameter of remains for two ink film thicknesses and speeds for the process ink.

Speed	**4 m/s**	**4 m/s**	**4 m/s**	**8 m/s**
Film Thickness μm	5.0	3.0	1.5	1.5
Average Size μm	154.5	46.4	38.3	63.2
Std. Dev. μm	87.5	18.6	11.0	28.4
Coef. Of Var. (%)	55.0	40.0	28.6	44.0

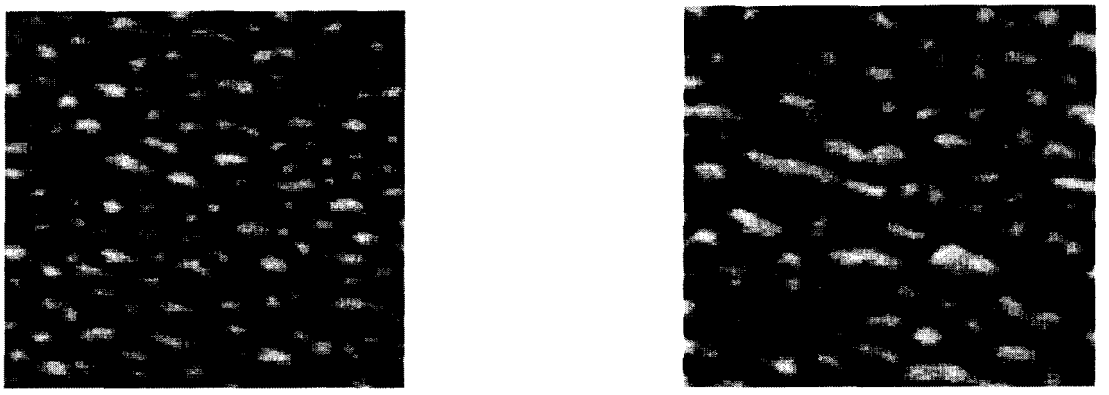

a b

Figure 6.2: Pictures captured from video of process ink printed on Mylar substrate. Frame (a) shows a 3 micron film printed at 2m/s. Frame (b) shows a 5 micron film printed at 2m/s. The total width of the images is 0.6 mm. The time after printing is 0.5 seconds.

The last two columns of table 6.1 show that an increase in speed causes an increase in the width of the features and an increase in standard deviation. The coefficient of variation has also increased for an increase in speed. Therefore, the size and the size distribution increases with the printing speed.

The results above compare to previous found results looking at the side of the nip. De Grace ***et. al.*** (1992) found that with increasing ink film thickness, the filaments break farther from the nip, but with increasing speed the film split moves closer to the nip. The behavior with increasing speeds must indicate a strong cavitation event which can occur at random locations in the film. Glatter (1996) and Thomson (1975) confirm that at higher printing speeds there are a greater number of small and large filaments. This greater number of large filaments must cause the size and the size distribution to increase. These trends might be explained in terms of the pressure distribution in the nip. At higher speeds, the pressure at the nip exit decreases to values well below the vapor pressure of the ink. If an element of ink sees a rapid drop in pressure well below its

vapor pressure, we would expect a homogeneous "boiling" of the fluid rather than a region of the film which is able to cavitate. Therefore, as speed increases, the film splits closer to the nip and at many random locations. As more ink is fed to the nip, the pressure field decreases and the location of splitting moves away from the nip. Therefore, the size distribution will scale with the ink film thickness.

6.3. Effect of Ink Characteristics

The results shown in table 6.2 are obtained using the IGT rolls from which the filament remains where directly observed on the rolls within 0.1 seconds. The filament volume did not correspond nicely with the filament remains seen on the rolls. **A** ratio of filament volume to spot volume was taken and a constant ratio was not obtained. A ratio of **2** was thought to be obtained thinking that the filament would split in half after elongation. Again there is an increase in the filament size distribution as the ink film thickness is increased.

The two inks tested, ink A and ink B, are selected because they have different rheological properties. This initial test is to see if the rheology of the inks had any influence at all on the filament size distribution. *Ink* B is more viscous and elastic compared to ink **A.** Dynamic tests after shear with these inks show that ink B recovers rapidly from shear, as measured by its elastic modulus, compared to ink A. Table 6.2 shows that ink B results in larger features compared to ink **A** and compared to the process ink under the same conditions. Comparing the two images in figure 6.3, it can be seen that ink rheology has a significant influence on the film split and the elongation of the filaments.

Table 6.2: Remain Sized for the different inks on IGT rolls.

Ink Type	Process Ink	Process Ink	Ink A	Ink B
Film Thickness (μm)	27.5	55	55	55
Average Size (μm)	56.4	63.4	59.7	77.9
Std. Dev. (μm)	22.3	24.6	25.1	36.0
Coef. Of Var. (%)	39.6	39.3	42.0	46.2

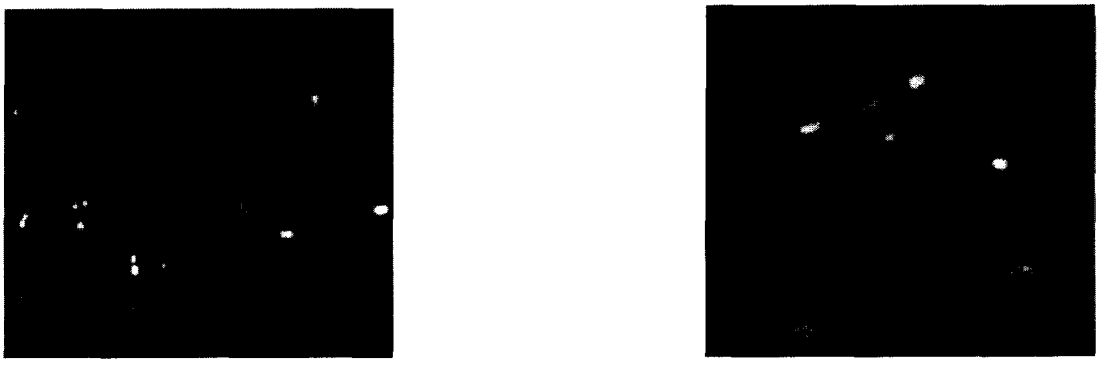

Ink A **Ink B**

Figure 6.3: Pictures captured from video of printing on IGT rolls of two different inks with different misting characteristics with constant thickness and constant speed. The width of the images is 2 mm.

6.4. Effect of Nip Loading

Changing the nip loading does not show a great effect on the average width of the features nor the size distribution as reported in table 6.3; the difference between the two average width is small compared to the effect of speed and ink film thickness on the filament size and filament size distribution. However, other conditions may cause nip loading to become more important. In addition, the range of nip loading reported here may be small compared to industrial conditions.

Table 6.3: Remain sizes for different nip loadings.

	Process Ink	**Process Ink**
Nip Loading (kg/cm)	50	100
Time after print (sec)	0.5	0.5
Film Thickness (pm)	1.5	1.5
Average Size (μm)	38.3	35.6
Std. Dev. (pm)	12.5	7.3
Coef. Of Var. (%)	32.4	20.3

6.5. Effect of Substrate Characteristics

Aspler (1993) and Aspler et. al. (1994) show that the substrate used for printing; changes the pressure field in the nip and cause different printing defects. Changing the printing substrate did cause different average sizes of filamentation. Many substrates did not show

any features on the scale we can detect, such as newsprint, uncoated and coated cellophane, LWC basepaper, copy grade paper, and thin cardboard. Plastic film and a 180 pph latex level coated paper did have features that we could detect with our optical system. The porous substrates either cause filament remains to be smaller than our system can detect or eliminate them completely.

From table **6.4,** we see that larger features are seen on the coated paper than the plastic film. The latex level of the coated paper is larger than a normal coated grade and should be essentially non-porous. The standard deviation has not changed a large amount, which indicates that the size distribution of the features is not different.

The different result between the plastic film and the coated paper is hard to understand. The potential porosity of the coated sample could reduce the pressure distribution in the nip, causing cavitation to occur only in selected spots. The thickness of the substrates may cause these results also.

In figure **6.4** (a), the process ink is printed on newsprint with a speed of **4** m/s and an ink thickness of 3 microns. Filament remains are not seen on this substrate, either because no filaments are formed or they are too small that the remains are not visual. The features seen in figure **6.4** (a) are related to the structure of the newsprint, not the remains of filaments after printing. Figure **6.4** (b) is a process ink printed on a Mylar film with the same printing speed and ink film thickness as figure **6.4** (a); when comparing the images it is clear that the features are quite different.

Table 6.4: Filament Remains for two substrates.

	Plastic Film	Coated Paper
Ink Type	**Process Ink**	**Process Ink**
Time after print (sec)	*0.5*	*0.5*
Nip Loading (kg/cm)	100	100
Film Thickness (pm)	3.0	3.0
Average Size (μm)	46.4	63.5
Std. Dev. (pm)	18.6	17.0
Coef. Of Var. (%)	40.0	26.9

Porous substrates may reduce the pressure swings in the nip and change the film split conditions. Aspler *et. al.* (1994) shows that a porous substrate reduces the pressure pulse in the nip. The porous substrate may cause a shift in mechanism from a cavitation phenomena to a capillary film split as studied by Coyle *et. al.* (1986).

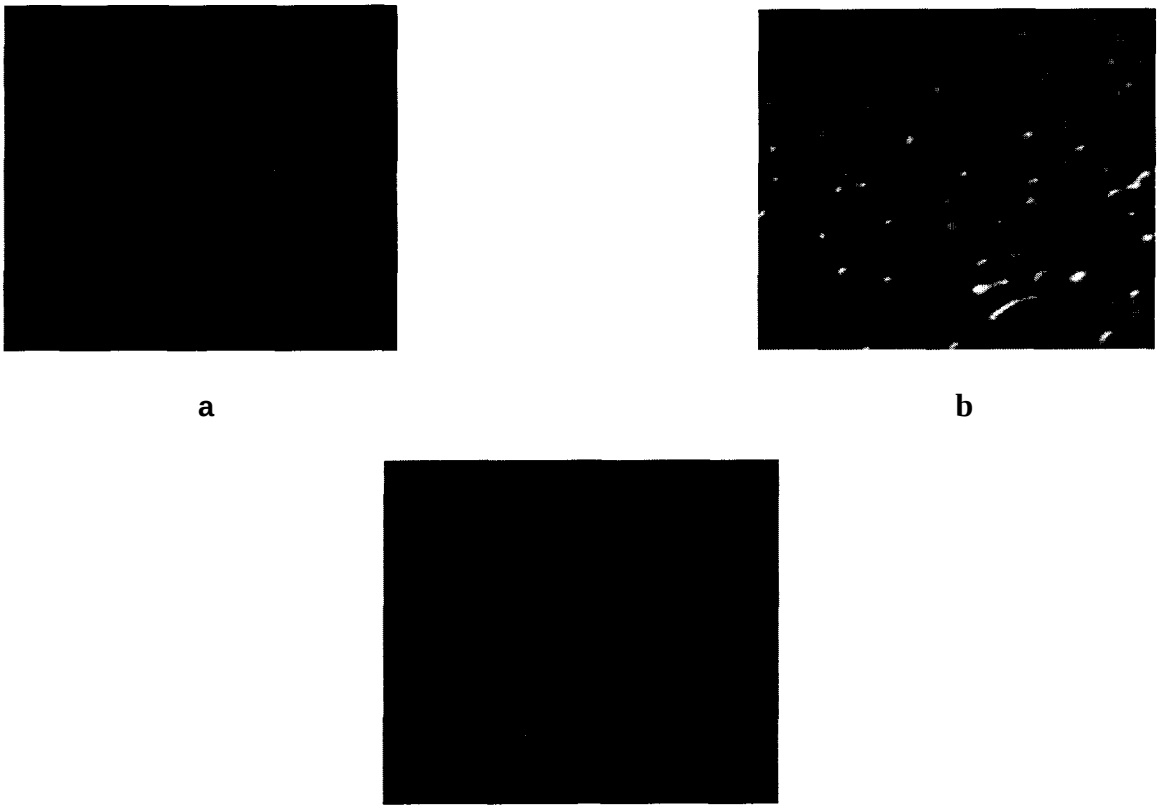

Figure 6.4. Pictures captured from video of process ink printed at 4 m/s with a film thickness of 3 microns. Frame (a) shows a newsprint substrate. Frame (b) shows a Mylar film substrate. Frame (c) shows a light weight coated basepaper substrate. The width of the images represents 2 mm. The time after printing is 0.5 seconds.

6.6 Summary

As the ink film thickness and printing speed increases, the size and the size distribution of filament remains increase. The nip loading, using plastic film as a substrate, did not have a significant effect on the size distribution for the range studied. Ink rheology is found to have a significant influence on filamentation and the resulting size distribution. The substrate did have a large influence on the size distribution. Porous substrates result in no

visible filament remains using our magnification and techniques. Only the less porous substrates exhibited filament remains with our technique.

CHAPTER 7: DIMENSIONAL ANALYSIS

Dimensional analysis can help reduce the complexity of a phenomena that depends on many variables. The generality of the method is both its strength and its weakness. The result of a dimensional analysis problem is a reduction of the number of variables in the problem. Dimensional analysis is a step toward the goal of describing a physical entity or phenomenon in terms of relationships between dimensionless groups. The net result is often an empirical expression that correlates the results.

7.1. Dimensional Analysis Results

For this research we have nine quantities and three fundamental units. Therefore, we have six dimensionless groups:

$$V^* = \frac{V}{h^3} \tag{7.1}$$

$$h^* = \frac{h}{D} \tag{7.2}$$

$$We = \frac{h \cdot u^2 \cdot \rho}{\sigma} \tag{7.3}$$

$$Re = \frac{h \cdot u \cdot \rho}{\mu} \tag{7.4}$$

$$De = \frac{\tau \cdot u}{h} \tag{7.5}$$

$$Tr = \frac{Pel}{\mu} \tag{7.6}$$

Where V is filament volume, h is film thickness, u is roll speed, D is roll diameter, ρ is the density, μ is the steady shear viscosity, μ_{el} is the elongational viscosity, τ is the relaxation time and σ is the surface tension of the fluids. Of course, there may be other variables or quantities that are not included here, such as cavitation pressure, shear-thinning index, or other unmeasured quantities such as the first normal stress coefficient. We obtain the following function fi-om our dimensional analysis:

$$V^* = f(h^*, We, Re, De, Tr) \tag{7.7}$$

we expect surface tension not to be a factor. Therefore, the Weber number is not included.

The function for V^* can be defined as follows:

$$V^* = A \cdot Re^b \cdot De^c \cdot Tr^d \tag{7.8}$$

A multivariable analysis may be done on the data obtained from the experiments performed to be able to determine the coefficient, A, and the powers, b, c, d. The dimensionless filament volumes are calculated by dividing the experimental volumes by the film thickness cubed. The Reynolds number is a function of film thickness and viscosity. The speed is constant at **0.34** m/s. The density does not vary much and is known for each fluid or calculated. For a shear-thinning fluid, the low shear viscosity is used. Therefore, the Reynolds number for all fluid may be determined. The Deborah number is a function of film thickness, speed of the roll, and the relaxation time of the

fluids. The parameter, τ, relaxation time, is obtained from the oscillatory experiments. The relaxation time is the inverse value of the frequency (f) multiplied by 2π at which the loss G'' modulus and storage G' modulus are equal as:

$$\tau = \frac{1}{2 \cdot \pi \cdot f} \tag{7.9}$$

For some fluids and inks, G' and G'' had to be fit to a function and f found due to extrapolation. Tr is calculated as defined above, by dividing the elongational viscosity of the fluid with the shear viscosity of the fluid gives this value. Knowing all of these values and applying a multivariable data analysis to this data we obtain a linear equation with respect to three variables. Now to be able to transform Eq. (7.7) to a linear equation the logarithm of both sides of the equation must be taken. Therefore Eq. (7.8) will become:

$$\mathrm{LogV^*} = \mathrm{LogA} + b\mathrm{Log\,Re} + c\mathrm{LogDe} + d\mathrm{LogTr} \tag{7.10}$$

Using the values found in table 7.1 the following equation is obtained for the fluids excluding the inks that are found at the bottom of the table.

$$\mathrm{LogV^*} = 50.0 \times 10^4 + 0.2\mathrm{Log\,Re} + 0.001\mathrm{LogDe} + 0.4\mathrm{LogTr} \tag{7.11}$$

This can be arranged to obtain Eq. (7.12)

$$V^* = 50.0 \times 10^4 \cdot Re^{0.2} \cdot De^{0.001} \cdot Tr^{0.4} \quad (7.12)$$

The R^2 value for the plot that fit this equation for all of the fluids except the inks is 0.38. For all fluids except the inks, increasing the elasticity decreases the filament size, but the extensional viscosity had the largest effect. The correlation is not good but shows the trends.

If this procedure is applied to only the Newtonian fluids the following equation is found with an R^2 value of 0.81:

$$V^* = 11.8 \times 10^7 \cdot Re^{0.85}\, De^{0.07} \cdot Tr^{0.91} \quad (7.13)$$

These fluids have the smallest dependence on the Deborah number but a very high dependence on both the Reynolds number and the Trouton ratio.

If we just take the non-Newtonian fluids into consideration, the V^* is:

$$V^* = 92.9 \times 10^3 \cdot Re^{-0.35} \cdot De^{-0.13} \cdot Tr^{0.16} \quad (7.14)$$

The R^2 value for the plot that fits this equation for the non-Newtonian fluids is 0.28. The Reynolds number is important for this set of fluids. The Trouton ratio shows a direct correlation where the other two are inversely related.

The same procedure as above is applied to the inks only and the equation obtained for that analysis is as follows:

$$V^* = 55.3 \times 10^{15} \cdot Re^{-1.14}\, De^{-5.9} \cdot Tr^{-0.05} \quad (7.15)$$

The R^2 value for the plot that fit the inks is 0.71. The Deborah number has a very high power value therefore, these fluids have a very high inversely proportionality to the relaxation time. From the Tr value we do see that elongational viscosity has an effect. This effect is not as high as the other two dimensionless parameters but the inks do have again an inverse relationship with their elongational viscosity.

When all of the fluids are taken into consideration, the coefficient and the powers of the dimensionless parameters are calculated as:

$$V^* = 975.72 \cdot Re^{-0.33} \cdot De^{0.35} \cdot Tr^{0.10} \quad (7.16)$$

The R^2 value for this analysis is low and found to be 0.16. This equation implies that all of the fluids are directly proportional to the Deborah number, and Trouton ratio with all of the fluids having a higher dependence on the Deborah number compared to the viscosity ratio, but again the R^2 value is quite low therefore a final conclusion cannot be made. All of the fluids have a dependence on the Reynolds number as much as a dependence they have on the Deborah number but in an inverse proportion.

The shear viscosity values used in this analysis are the low shear viscosity values, when the high shear viscosity values are used the R^2 value of the correlation does not have a significant increase as to which the high shear viscosity should be used. The R^2 values obtained using the high shear viscosity values is 0.29.

Table 7.1: Data used for multivariable linear analysis

Fluids	V*	Re	De	Tr
s o 1	77699	0.000105536	77095	0.584399912
SO2	9584.141	1.32E-05	433.075	0.785466976
SO3	11549.09	4.40E-06	368.73	3.650699602
SO4	15576.69	2.20E-06	295.12	9.853595281
PTO1	103014.9	9.68E-05	171.615	3.451500039
PT02	137243	1.21E-05	98.94	6.263199693
PT03	80316.08	2.42E-05	104.72	3.823999651
1.6% 9M8	493877.7	0.00289	2800	0.799671815
3.46% 9M8	513710.6	0.00019788	1870	262.2500266
6.15% 9MS	808634.4	1.07E-05	1702.078	304.930017
Boger Fluid 1	918974.1	0.00578	20570	23044.00206
Boger Fluid2	103720300	2.11E-05	2630.24	402.1157143
Polyacrylamide	477009.1	0.0003876	418710	495.5099367
Corn Syrup	543630.8	0.000184167	696.456	3.308333361
Model Ink A	8200000	1.02E-06	760.58	1.609774033
Model Ink B	1100000	1.07E-06	898.62	1.105670964
Model Ink C	2300000	2.82E-06	788.46	0.48499757
Model Ink D	8000000	5.69E-07	768.74	3.635518874
Model Ink E	1800000	1.35E-06	803.76	0.861783685
Model Ink I	4000000	1.26E-08	1902.64	1.350033974
Process Ink	4000000	2.22E-06	714.34	0.001284938

7.2. Summary

The dimensional analysis gives some trends in the data set. However, when all of the fluids are taken into consideration the equation fit to the data has a very low correlation. When the fluids are split up into groups, a better correlation is obtained. This result indicates that there is still at least one more parameter or fluid property that influences filament size that is not included here. For the Newtonian fluids, the dominating parameter is the elongational viscosity. The non-Newtonian fluids are dominated by the Reynolds number, and for the inks, the relaxation time is the dominating factor.

CHAPTER 8: MODELING OF FILAMENTATION

Cavitation and filament formation events are random three-dimensional transient events. Therefore, many assumptions are needed to reduce the complexity of the problem. Two approaches are proposed to model the filamentation process. The first approach is calculating the pressure profile in the nip to predict the conditions to produce filaments. The second approach is to calculate the pressure in a volume of fluid moving with the rolls to predict filament size. In the literature, the flow in this geometry has been described by Coyle ***et.*** *al.* (1987, 1990), but there is no attempt, to our knowledge, to model the filament formation process.

8.1. Pressure Distribution in Rolling Nip Geometry

Using the lubrication theory, the pressure distribution is estimated between the rolls. The gap between the two rolls is a function of **x,** the minimum gap found in between the two rolls is $2h_o$. The rolls are turning with a surface velocity of u and have a radius of R. **A** representation of this geometry is depicted in figure 8.1.

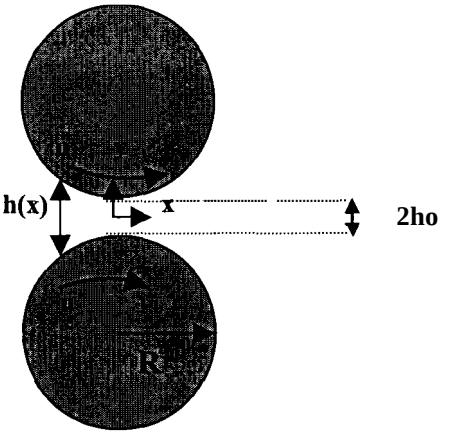

Figure 8.1: Rolling Nip Geometry

The momentum equations are:

$$\frac{dP}{dx} = \mu \cdot \frac{\partial^2 v_x}{\partial y^2} \tag{8.1}$$

$$\frac{dP}{dy} = 0 \tag{8.2}$$

where P is the fluid pressure, μ is the fluid viscosity, and v_x is the x directed fluid velocity. These equations show that pressure is not a function of the y position as finite element methods have confirmed.

Eq. (8.1) is integrated with the no slip boundary conditions. The conservation of mass equation is used to eliminate the velocity term. The ordinary differential equation for pressure is found as in Ninness ***et.*** *al.* (1998):

$$\frac{dP}{dx} = \frac{-3 \cdot \mu}{h(x)^3}\left(\frac{Q}{2} - u \cdot h(x)\right) \tag{8.3}$$

where Q is the volumetric flow rate per unit width, and must be equal to the volume fed to the nip.

The equation for the distance between the two rolls is:

$$h(x) = h_o + R \cdot (1 - \sqrt{1 - x^2}) \tag{8.4}$$

where R is the roll radius.

In the model by Ninness ***et. al.*** (1998) the following procedure and equations **(Eqs.** 8.5-**8.13)** are used to obtain exit and inlet locations. The inlet pressure for all cases is taken to be atmospheric (zero gauge pressure). For fluid flow with no penetration or filtercake formation, the exit pressure and location can be found using the "visco-capillary" technique in **Eqs.** (8.5-8.7).

$$P_e = \frac{-\sigma}{R_m} \tag{8.5}$$

where R_m is the radius of curvature of the film-split meniscus, and σ is the fluid surface tension. The radius of curvature is given by,

$$R, = \frac{Q_e}{2.68 Ca^{2/3} u} \tag{8.6}$$

with Q_e being the volumetric flow rate per unit length at the exit and Ca the capillary number $Ca=\mu_c u/\sigma$. For a speed ratio of unity the film-split height at the exit h_e is given by the following equation.

$$h_e = \frac{Q_e}{U}\left(1.644 + \frac{2}{2.68Ca^{2/3}\sqrt{1+.414(3Ca)^{2/3}}}\right) \tag{8.7}$$

$$Q_e = Q - uh_f - Lu\varepsilon_P \tag{8.8}$$

where Q_e is now the amount of "free" coating available to be split at the exit, and h_f and L are the filtercake thickness and depth of liquid penetration at the exit of the nip, respectively, and ε_p is the void fraction of the substrate. **A** mass balance at any location gives,

$$Q = h_i u = \int_{h_f}^{h} v_x dy + h_f(x)u + uL(x)\varepsilon_P \tag{8.9}$$

Q is the volumetric flow rate per unit width of the roll, and must equal the volume fed to the nip, $h_i u$. The integral is the "free" fluid layer between the filtercake and the backing roll. The second term is the volumetric flow rate of solid particles and liquid contained in the filtercake layer. The last term represents the liquid in the substrate.

Integrating Eq. (8.1) with the no-slip boundary condition at the roll and filtercake surfaces and inserting this result into Eq. (8.9) gives the pressure gradient for the flow in the nip

$$\frac{\partial P}{\partial x} = \frac{12 \mu_C u \left(h(x) + L(x)\varepsilon_p - h_i\right)}{\left(h(x) - h_f(x)\right)^3} \tag{8.10}$$

Eq. (8.10) is a modified lubrication expression which accounts for the penetration of fluid and requires knowledge of the filtercake thickness and penetration depth into the paper at each x location. A mass balance around the filtercake and paper gives the working equations for the filtercake growth and penetration depth:

$$\frac{\partial h_f}{\partial x} = \frac{v_y}{u}\frac{\phi_C}{\phi_F} \tag{8.11}$$

$$\frac{\partial L}{\partial x} = \frac{v_y}{\varepsilon_p u} \tag{8.12}$$

where v_y is the penetration velocity, ϕ_C and ϕ_F are the volume fraction of particles in the coating and the filtercake. The algorithm used in Ninness *et. al.* (1998) is as follows:

1. Select a trial entrance location.
2. Integrate Eqs. (8.10)-(8.12) to obtain pressure and penetration amount at the outlet.
3. Adjust entrance location until the exit pressure matches that of Eqs. (8.5)-(8.7)

4. Adjust the exit flow rate at exit in Eqs. (8.6) and (8.7) to account for penetration as in **Eq.** (8.8).
5. Repeat above until exit flow rate does not change.

Once the pressure field is found, the nip loading, or the force per unit width applied to the rolls is obtained by :

$$F = \int_{x_i}^{x_e} P dx \tag{8.13}$$

where x_e and x_i are the exit and entrance locations.

Input into the model include the viscosity, the surface tension, and the film thickness. The nip load value obtained from the model is adjusted to equal the experimental nip load and the minimum pressure to be just below subambient. The viscosity value for the specified film thickness, that gives the appropriate nip load and pressure value is considered to be the lowest viscsoity value of a fluid that would form a filament at that thickness, the critical viscosity. These calculations were done using a Newtonian model approximation. The experimental nip load is found by calculating the force the Plexiglas roll applies to the bottom roll. The weight of the Plexiglas roll, 161.73 grams, is converted into a force value. The force is applied to a **2** mm width strip and the experimental nip load is obtained by dividing the force with the width giving 793 N/m.

Table 8.1 : Model parameters used for the pressure profile model

Model Parameters	Value
R, roll radius	0.03 m
u, surface roll speed	0.34 m/s
μ, viscosity of fluid	Varies from fluid to fluid (Pa-s)
h_o, initial gap	Film thickness of fluid (m)
Q, Volumetric flow rate	Evaluated, (m^3/s)
F, Force	Evaluated, (N)
w, width	0.002 m
h(x), distance between rolls	Calculated (m)
P, initial pressure	0.0 Pa
x, initial x value	-1.0 cm
dx, increment in x	0.01 cm

The conditions to generate a pressure lower than the vapor pressure are compared to the conditions when filaments are formed in figure **8.2.**

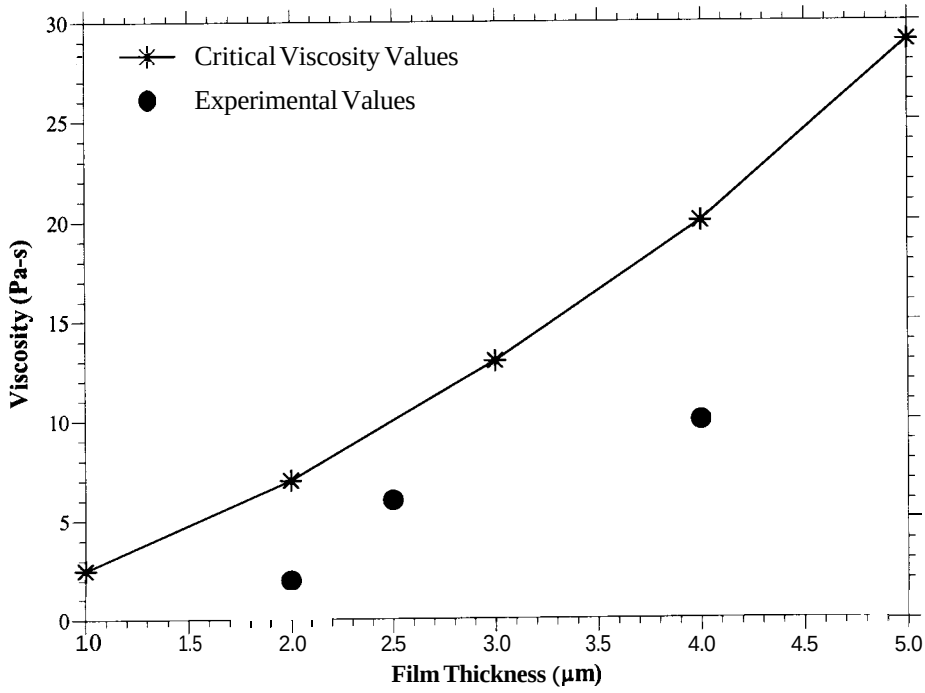

Figure 8.2: Lowest theoretical viscosity values that form filaments at the indicated film thickness for Newtonian fluids

The three points on the graph are the experimental film thickness and the lowest viscosities of Newtonian fluids that did form filaments. The experiments were done on the roll set-up as described in chapter **2** section 2.3. The experimental points are in a good range of error for the fluids to form filaments. Glycerin having a viscosity of 1 Pa-s at 1 μm film thickness did not form filaments: this result agrees with the model. Ethylene glycol having a viscosity of 16.1 mPa-s theoretically would not even be able to form filaments at a film thickness of 0.3 μm. Experimentally, this fluid was not able to form filaments.

8.2. Newtonian Prediction of Filament Size

Figure **8.3** illustrates a parallel disk geometry. The disk represents the top and bottom roll surfaces. This geometry represents a volume of fluid moving in the nip. The goal is to find the critical disk radius R_{disk} were cavitation occurs. This value should be related to the size of the filament formed, because if several bubbles are formed and coalesce, the fluid between these bubbles will be filaments, as depicted in figure 8.4.

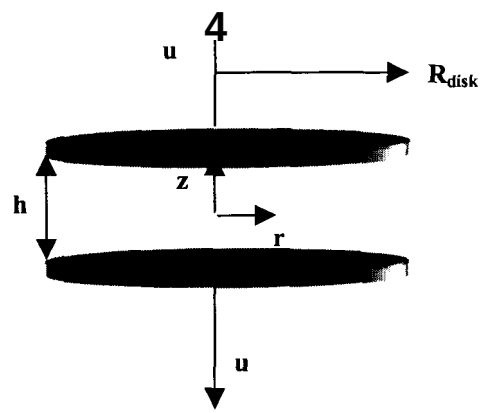

Figure 8.3: Parallel plate geometry depicting frame moving with fluid

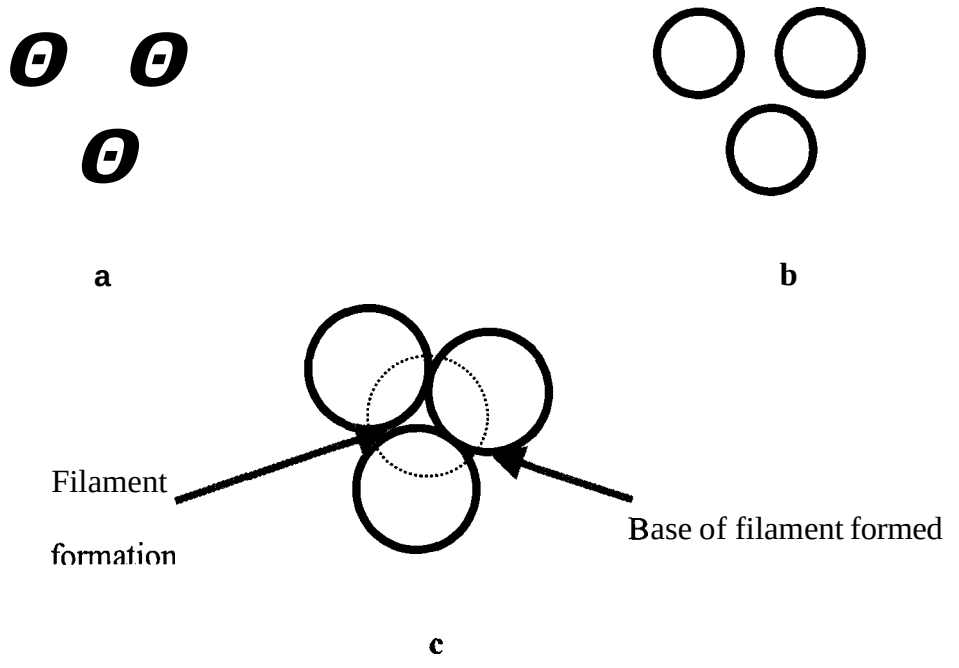

Figure 8.4: A schematic of the theoretical formation of a filament a) is the first stage of bubble formation b) bubbles grow to form filament c) when bubbles touch to form a filament

By applying the lubrication approximation to the Navier-Stokes equations, the r and z momentum terms are:

$$\frac{dP}{dr} = \mu \cdot \frac{\partial^2 v_r}{\partial z^2} \tag{8.14}$$

$$\frac{dP}{dz} = 0 \tag{8.15}$$

where P is the pressure, μ is viscosity, and v_r the velocity in the r direction.

The continuity equation is:

$$\frac{1}{r}\cdot\frac{\partial r v_r}{\partial r}+\frac{\partial v_z}{\partial z}=0 \tag{8.16}$$

Using the Lebnitz's Rule and the velocity boundary conditions of at z=0, v_z=-u, v_r=0 and at z=h, v_z=u, v_r=0, integrating Eq. (8.16) we obtain the ordinary differential equation for the pressure in the r-direction as follows:

$$\frac{dP}{dr}=\frac{12\cdot\mu}{h^3}\left(u\cdot r-\frac{C}{r}\right) \tag{8.17}$$

where P is pressure, **C** is an integration constant and is what is being found using the boundary condition at $r=R$, $P=0$. When h is constant, an expression is obtained for the pressure as a function of r.

$$P=\frac{6\cdot\mu\cdot u}{h^3}\cdot(r^2-R^2) \tag{8.18}$$

The final equation to obtain the disk radius, R_{disk}, at the point of minimum pressure at $r=0$ being equal to the atmospheric pressure is:

$$R_{disk}=\sqrt{\frac{P_{atm}\cdot h^3}{6\cdot\mu\cdot u}} \tag{8.19}$$

If every vapor bubble formed coalesced with two others, a filament would be formed. That filament volume should scale as the volume between the disks. Figure 8.5 shows the results for this situation.

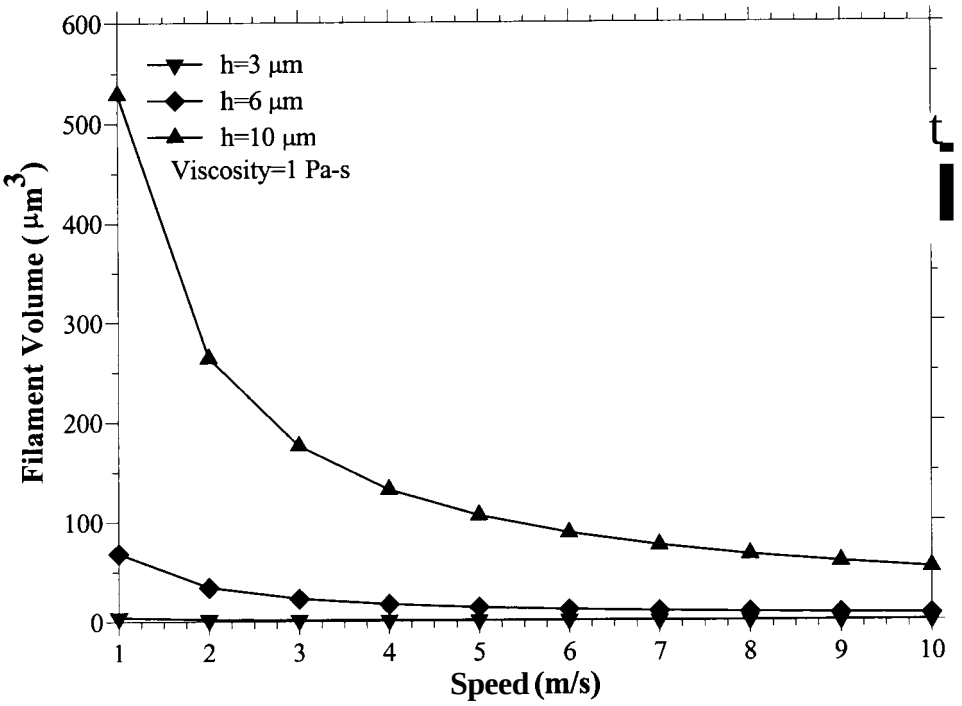

Figure 8.5: Graph of filament volume versus speed for viscosity of 1.0 Pa-s and three different thickness

In the actual case the separation velocity increases as the fluid exits the nip. If this velocity change is taken into account, the axial directed velocity and gap as a function of the roll surface velocity u_r are:

$$u(t) = \frac{2 \cdot u_r^{\,2} \cdot t}{R_r} \tag{8.20}$$

$$h(t) = h_o + \frac{u_r^{\,2} \cdot t}{R_r} \tag{8.21}$$

where R_r is the roll radius and h_o is the gap at the roll center.

The force is found by integrating the pressure in Eq. (8.18). The pressure, at r=0, and the force become:

$$P(t) = \frac{-3 \cdot \mu \cdot u(t) \cdot R_{disk}^{\,2}}{h(t)^3} \tag{8.22}$$

$$F(t) = \frac{-3 \cdot \pi \cdot \mu \cdot u(t) \cdot R_{disk}^{\,4}}{2 \cdot h(t)^3} \tag{8.22}$$

Now the pressure will start at zero pressure gauge at the nip center because the separation velocity, u(t), is zero. The pressure decreases as separation occurs. Figure **8.6** shows the results of the calculation for roll radius and speed that resemble the experiments with viscosity of 12 Pa-s for a few disk radii. For the disk radius that causes the pressure to drop to −100 kPa, the length scale of bubble formation is found.

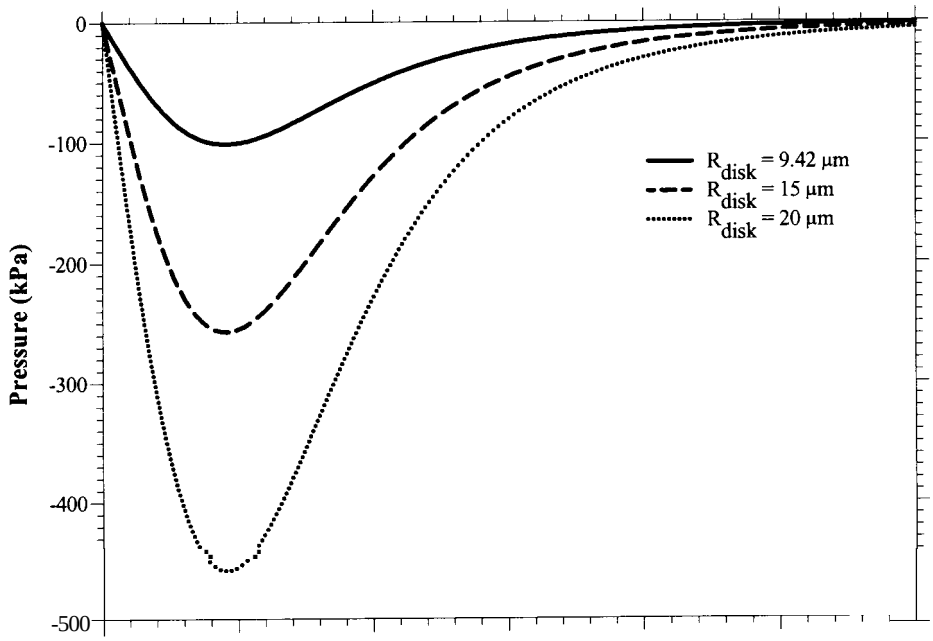

Figure 8.6: Graph of pressure versus time for three different R_{disk} values.

8.3. Maxwell Fluid

Most of the fluids tested have an elastic nature and a relaxation time. Therefore, a linear Maxwell constitutive equation was used to give an indication of the effect of viscoelasticity.

Starting with the momentum equation in the cylindrical coordinate system:

$$\frac{\partial \tau_{rz}}{\partial z} = \frac{\partial P}{\partial r} \tag{8.23}$$

$$P \neq f(z) \tag{8.24}$$

and using the equation for a linear Maxwell fluid:

$$\tau_{rz} + \lambda \cdot \frac{\partial \tau_{rz}}{\partial t} = \mu \cdot \frac{\partial v_r}{\partial z} \tag{8.25}$$

the time dependent Maxwell fluid pressure profile is obtained.

Taking the integral of Eq. (8.23) with respect to z we obtain:

$$\tau_{rz} = \frac{\partial P}{\partial r} \cdot z + C_1 \tag{8.26}$$

the time dependent derivative of Eq. (8.26) gives Eq. (8.27):

$$\frac{\partial \tau_{rz}}{\partial t} = \frac{\partial^2 P}{\partial t \partial r} \cdot z + \frac{\partial C_1}{\partial t} \tag{8.27}$$

Inserting Eq. (8.26) and (8.27) in to Eq. (8.25) the following is found:

$$\frac{\partial P}{\partial r}\cdot\frac{z}{\mu}+\frac{C_1}{\mu}+\frac{\lambda}{\mu}\cdot\frac{\partial^2 P}{\partial t\partial r}\cdot z+\frac{\lambda}{P}\cdot\frac{\partial C_1}{a}=\frac{\partial v_r}{\partial z} \tag{8.28}$$

Integrating Eq. (8.28) with respect to z and using the boundary condition at $z=0$ $v_r=0$

$$\frac{\partial P}{\partial r}\cdot\frac{z^2}{2\cdot p}+\frac{C_1\cdot z}{\mu}+\frac{\lambda}{2\cdot\mu}\cdot\frac{\partial^2 P}{\partial t\partial r}\cdot z^2+\frac{\lambda}{P}\cdot\frac{\partial C_1}{a}\cdot z=v_r+C_2 \tag{8.29}$$

from Eq. (8.29) C_2 becomes equal to zero. Using the boundary condition at $z=0$ $v_r=0$

$$C_1=-\frac{\partial P}{\partial r}\cdot\frac{h}{2}-\frac{\lambda}{2}\cdot\frac{\partial^2 P}{\partial t\partial r}\cdot h+\lambda\cdot\frac{\partial C_1}{\partial t} \tag{8.30}$$

Inserting **Eq.** (8.30) into Eq. (8.29) and using the $C_2=0$ v_r becomes:

$$v_r=\frac{1}{2\cdot\mu}\frac{\partial P}{\partial r}(z^2-h\cdot z)+\frac{\lambda}{2\cdot\mu}\cdot\frac{\partial^2 P}{\partial t\partial r}\cdot(z^2-h\cdot z) \tag{8.31}$$

Using the concept of the conservation of mass:

$$\pi\cdot u\cdot r^2=-\int_0^h v_r\cdot 2\cdot\pi\cdot r\cdot dz \tag{8.31}$$

inserting the equation for v_r into Eq. (8.31), and taking the integral, using the boundary conditions at r=R P=O and $\partial P/\partial t = 0$ the final pressure profile equation for a Maxwell fluid to be:

$$P + \lambda \cdot \frac{dP}{dt} = \frac{3 \cdot \mu \cdot u}{h^3} \cdot \left(r_2 - R^2\right) \tag{8.32}$$

Using the definition for force where:

$$F = \int_0^R P \cdot 2 \cdot \pi \cdot r \cdot dr \tag{8.33}$$

The equation for force is:

$$F + \lambda \cdot \frac{dF}{dt} = \frac{-3 \cdot \mu \cdot u \cdot R^4}{2 \cdot h^3} \tag{8.34}$$

The pressure at the disk center is found by the expression:

$$\frac{dP(t)}{dt} = \left(\frac{-3 \cdot \mu \cdot u(t) \cdot R_{disk}^{\ 2}}{h(t)^3} - P(t) \right) \cdot \frac{1}{\lambda} \tag{8.35}$$

A FORTRAN program was prepared to use the Euler's method to calculate the pressure-time relationship for a separating disk system. Figure 8.7 shows how the relaxation time changes the results. Increasing the disk radius causes the minimum pressure to become lower. The disk radius value that produces a pressure lower than the fluid vapor pressure should give the length scale of the filament.

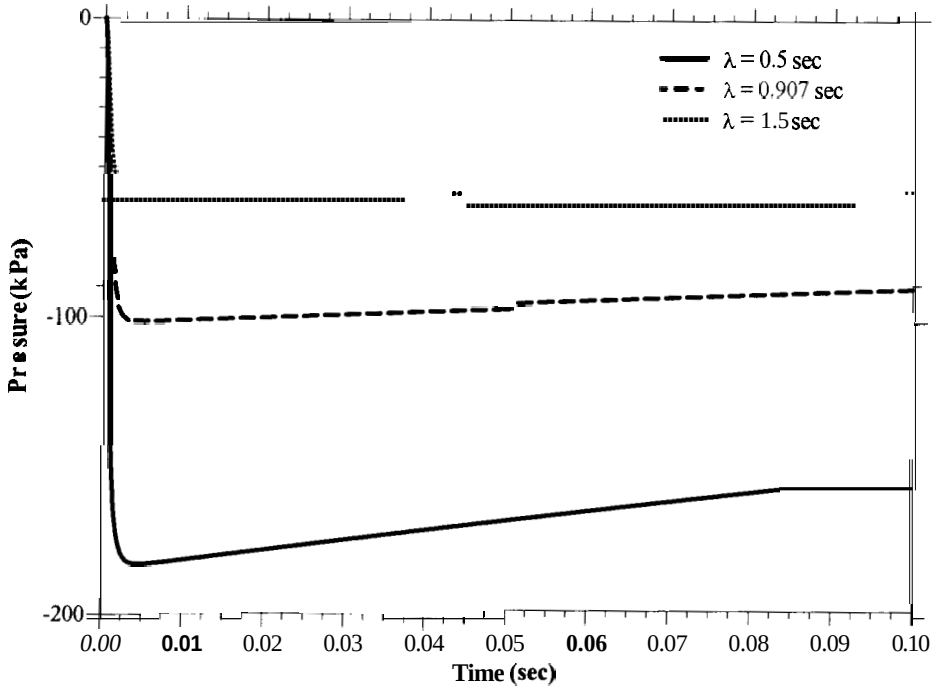

Figure 8.7: Graph of pressure versus time for three different relaxation time values for parameters in table **8.2** for $R_{disk} = \mathbf{9.42}\,\mu m$

Table 8.2: Model parameters used for the Newtonian and Maxwell Model approximation

Model Parameters	Value
R, roll radius	0.03 m
u_r, surface roll speed	0.34 m/s
u(t), disk separation velocity at time t	Calculated *(d s)*
μ, viscosity of fluid	Varies from fluid to fluid (Pa-s)
h_o, initial gap	Film thickness of fluid (m)
h(t), disk separation at time t	Calculated (m)
R_{disk}, disk radius	Evaluated m
λ, relaxation time (Maxwell)	Varies from fluid to fluid sec

8.4. Comparison with Data

The model parameters used in this program are given in table 8.2. By looking at the volumes predicted for the Newtonian and Maxwell cases as in figures 8.5 and 8.6, it seems clear that if these calculations represent the pressure history of the fluid and the formation of vapor bubbles, a large fraction of these bubbles collapse and do not coalesce to form filaments. If the fraction of bubbles that do form filaments is F, then the filament volume is given by:

$$V^* = \frac{V_p^*}{F} \tag{8.36}$$

where V_p is the value predicted by either the Newtonian or Maxwell cases where $V_p=\pi*R_{disk}^2*h(t)$.

The elongational viscosity may influence the fraction of bubbles that coalesce. **A** high elongational viscosity should decrease the fraction coalesced, resulting in larger filaments. In a simple way, the increase of filament volume may be linear with elongational viscosity. **A** more complex relationship probably exists, but this will give a first attempt. The "F" factors are no longer the fraction of bubbles that coalesce to form filaments.

We can make dimensionless quantities by dividing the volumes by the cube of the film thickness. Elongational viscosities are made dimensionless with the shear viscosities. The fraction of bubbles coalescing adjusts to attempt to fit the data by a least squares method. Four forms emerge to describe the filament size.

$$V_{1N}^{*} = \frac{V_N^{*}}{F_{1N}} \tag{8.37}$$

$$V_{1M}^{*} = \frac{V_M^{*}}{F_{1M}} \tag{8.38}$$

$$V_{2N}^{*} = \frac{Tr \cdot V_N^{*}}{F_{2N}} \tag{8.39}$$

$$V_{2M}^{*} = \frac{Tr \cdot V_M^{*}}{F_{2M}} \tag{8.40}$$

Table 8.3: Results of experimental V^* values and the V_{1N}^*, V_{1M}^* values

Fluid	Vis. (Pa-s)	λ (sec)	Tr	Exp. V^*	V_N^*	V_M^*
s o 1	12	0.9070	0.584	78000	20.94	42343
SO2	106	0.0035	0.785	10000	2.375	29.69
SO3	300	0.0043	3.651	12000	0.84	13.53
SO4	600	0.0051	9.854	16000	0.42	8.16
PTO1	10	0.0020	3.452	103000	25.16	175
PT02	126	0.0012	6.263	170000	2	8.66
PT03	50	0.0012	3.824	80000	5.03	20.78
1.6% 9M8	0.2	0.0014	0.800	494000	818.237	97089.35
3.5% 9M8	3	0.0090	262.250	514000	56.07	3617.97
6.2% 9M8	64	0.0011	304.930	809000	2.7875	216.25
Polyacrylamide	2	2.4630	495.510	477000	88.625	1.18E7
Corn Syrup	6	0.0051	3.308	544000	33.024	857.6
BF 1	0.1	0.1210	23044.002	919000	1775	3525000
BF 2	7	0.0039	402.116	104000000	12.72	629.6
Model Ink A	33	0.0023	1.610	8200000	0.377	6.39
Model Ink B	318	0.0022	1.106	1100000	0.369	6.58
Model Ink C	121	0.0026	0.485	2300000	1.04	21
Model Ink D	598	0.0024	3.636	800000	0.21	3.75
Model Ink E	251	0.0023	0.862	1800000	0.502	8.69
Model Ink I	25760	0.0056	1.350	4000000	0.0049	0.249
Process Ink	147	0.0021	0.001	4000000	0.859	13.2

Table 8.4: Results of predicted V^* values and factored V^* values using the optimum F factor

Fluid	V_N^*	V_M^*	V_{1N}^*	V_{1M}^*	V_{2N}^*	V_{2M}^*
s o 1	20.94	42343	19036.36	2490.77	0.28	0.28773
SO2	2.375	29.69	2159.09	1.75	0.04	0.00027
SO3	0.84	13.53	763.64	0.80	0.07	0.00057
SO4	0.42	8.16	381.82	0.48	0.09	0.00093
PTO1	25.16	175	22872.73	10.29	1.97	0.00702
PT02	2	8.66	1818.18	0.51	0.28	0.00063
PT03	5.03	20.78	4572.73	1.22	0.44	0.00092
1.6% 9MS	818.237	97089.35	743851.82	5711.14	14.87	0.90278
3.5% 9M8	56.07	3617.97	50972.73	212.82	334.19	11.0327
6.2% 9M8	2.7875	216.25	2534.09	12.72	19.32	0.76675
Polyacrylamide	88.625	1.18E7	80568.18	694117.6	998.06	67988.5
Corn Syrup	33.024	857.6	30021.82	50.45	2.48	0.03299
BF 1	1775	3525000	1613636.3	207352.9	929616	944536
BF 2	12.72	629.6	11563.64	37.04	116.25	2.94386
Model Ink A	0.377	6.39	342.73	0.38	0.015	0.00012
Model Ink B	0.369	6.58	335.45	0.39	0.009	8.45E-5
Model Ink C	1.04	21	945.45	1.24	0.01146	0.00012
Model Ink D	0.21	3.75	190.91	0.22	0.017	0.00015
Model Ink E	0.502	8.69	456.36	0.51	0.00983	8.71E-5
Model Ink I	0.0049	0.249	4.45	0.015	0.00015	3.90E-6
Process Ink	0.859	13.2	780.91	0.78	2.51E-5	1.97E-7

where V_N^* is the predicted Newtonian dimensionless volume and V_M^* is the predicted Maxwell dimensionless volume. Subscript 1 denotes the simple case and 2 denotes the elongational case.

Table 8.5: Optimum F values obtained from the analysis for fluids

	Newtonian	Maxwell		Maxwell
Simple Case	F_{1N}	F_{1M}	**Simple Case**	F_{1M}
All fluids	0.0011	17	**Excluding High V_P^***	0.0005
Elongational Case	F_{2N}	F_{2M}	**Elongational Case**	F_{2M}
All fluids	44	86,000	**Excluding High V_P^***	0.04

When the analysis was being done it was noticed that three fluids, Boger fluid 1, 1.6% CMC 9M8 and Polyacrylamide gave high V_M^* values compared to the others seen in table 8.3, therefore, another factor analysis excluding these three fluids were done. In both situations given above, where all of the fluids were taken into account the simple case, and when three were excluded the elongational case gives the optimum fraction values. For all of the fluids the Newtonian simple case seems to predict the best values and gives a minimum error value of 104523066 whereas the Newtonian elongational case predicts the closest values for the situation where some fluids were excluded with a minimum error of 98682669.13. This concludes that elongation has a large influence on the filamentation event.

8.5. Summary

The conditions for onset of filamentation is somewhat over predicted by the lubrication theory for Newtonian fluids, but the correct trend and order of magnitudes are predicted. The predictions may be improved by accounting for other effects such as the process parameters or other characteristics of the fluid as the relaxation time of the fluids.

A model to predict the filament size from the fluid rheological properties and the process conditions is proposed. The model follows a volume of fluid as it exits the nip. The length scale associated with the pressure decreasing to the vapor pressure is predicted. This length scale, along with **an** empirical factor that represents the fraction of bubbles that coalesce, are used to predict filament size. While some trends in the data are correctly predicted, a clear agreement between the model and the experiments is lacking. Several reasons for this lack of agreement are possible. The relaxation time for each fluid was evaluated from an extrapolation of equating the fitted equations of the loss and storage modulus of each fluid. If a nice trend is not obtained for one of these moduli the mathematical evaluated relaxation time may not be as precise as some of the fluids which would effect the predicted filament size. The elongational viscosity values found for each fluid were not steady. The data obtained from this procedure, may have some experimental errors corresponding to deviate them from the actual elongational viscosity values of the fluids. The steady shear viscosity values for the fluids were taken to be constant; the viscosity values for some fluids do change with a change in shear, as indicated in previous chapters. This value might not directly be corresponding to the viscosity effect to these fluids. The gap used in the model was assumed to be equivalent to the experimental film thickness. This assumption is considered to be good, but may

effect the final model prediction. The model was prepared by assuming the two roll radii were equal; experimentally, one roll had a larger radius compared to the other.

CHAPTER 9: CONCLUSIONS AND RECOMMENDATIONS

9.1. Conclusions

This study leads to conclusions, contributing to the literature.

- The filamentation behavior can not be directly correlated to the broken filaments, filament "remains", on the surface as the recoiling process differs from fluid to fluid.
- **A** novel procedure to characterize the cavitation ability of a fluid is developed, but no clear dependence of filament size on cavitation was observed.
- **A** technique to determine the influence of printing speed, nip loading, and substrate on filament "remains" was developed.
- Fluid rheology is found to have a significant effect on filamentation and the resulting size distribution in a complex manner.
- For all fluids, increasing the elastic nature of the fluid resulted in smaller filaments.
- Porous substrates must alter the pressure field and reduce or eliminate filaments.
- An empirical correlation is proposed between Reynolds number, Deborah number and Trouton ratio and the filament volume.
- The proposed model predicts a first approximation of filament volume.
- Other parameters or fluid properties besides the ones analyzed in this research must have an effect on filamentation.

9.2. Recommendations

Some other investigations to develop this research may be conducted. The effect of a substrate on filamentation in the rolling nip may be analyzed by placing a substrate on the Plexiglas roll and start recording right after the Plexiglas roll is in contact with the other rolls. **A** better technique may be thought of to be able to predict the actual film thickness of the fluid that is on the roll or substrate. An appliance that can actually measure the pressure of the fluid that is found in the vacuumed syringe would be a more precise value for cavitation pressure. The effect of resistance that might occur during the pull of the plunger will be neglected this way. Any pressure leakage occurring can also be analyzed better in this type of technique. **A** pressure analysis during printing would even be a better way to predict exactly where cavitation occurs which would be the beginning of filamentation. Finding the exact point of where the final filament breaks would help in being able to model the whole filamentation process with average filament volume values. The elongational viscosities may be analyzed with a precise apparatus that would calculate the elongational viscosities as elongating the fluids. The apparatus used here is a novel apparatus that is dependent on too many parameters that might effect the results from the environment. **A** procedure to be able to obtain the exact and precise relaxation time may be thought of being developed to accurately analyze the effect of elasticity and relaxation time on the filamentation behavior. The results found in this research indicate that other parameters or fluid properties, besides the ones analyzed in this research, do influence filamentation. The analysis of other parameters or fluid propertiesdirectly on to the filamentation process may be done, such as the fluid component interactions. The modeling that was developed in this research took the Newtonian and Maxwell models

into consideration. Developing an algorithm that uses other models might be considered. Developing a model that takes all of the significant parameters and properties into consideration may be thought of. In this research the effect of substrate on the filamentation process was not modeled. The effect of a substrate, porosity, roughness, etc., may be analyzed in a modeling point of view.

REFERENCES

Amari, T., Xianfu, W., Hayashi, T., Morita, K., "Dynamics and Rheology of Inks including Various Types of Gelling Agents", *TAGA Proceeding,* 354-367, 1994.

Aspler, J. **S.,** Lyne, M. B., Dealy, J. M., Pangalos, G. C., "Rheological Properties of News inks and Surface Strength Test Liquids", *Advances in Printing Science and Technology,* 235, 1982.

Aspler, J. **S.,** Lepoutre, P., "The Transfer and Setting of Ink on Coated Paper", *Progress in Organics Coatings,* 19,333, 1991.

Aspler, J. **S.,** Taylor, **S.,** "Tack Development in Water-Based Inks", *Nordic Pulp and Paper Research Journal,* **1,** 4, 1991.

Aspler, J. S., "NMR Spectroscopy, Ploymer Motion, and "Tack" of Model Printing Inks", *Polymer Engineering and Science,* 32, 18, 1992.

Aspler, J. **S.,** De Grâce Y. H., Béland, M. C., Maine, C., Piquard, L., "Transfer and Setting of Water-Based Ink, Part 11: Water Absorbency and Uncoated Paper Structure", *I992 International Printing & Graphics Arts Conference,* 251, 1992.

Aspler, J. **S.,** "Interactions of Ink and Water with the Paper Surface in Printing", *Nordic Pulp and Paper Research Journal,* **1,** 68, 1993.

Aspler, J. **S.,** Maine, C., De Grâce, Y. H., Zang, Y. H., Taylor **S.,** "Printing Tack, Part I: Influence of Paper Structure on Ink 'Tack' Measured in a Printing Nip", *Advances in Printing Science and Technology,* 22, 139, 1994.

Aurenty, P., Palierne, J. F., Gandini A., "Viscoelasticity of Water/Ink Emulsions at Low and High Frequency", *TAGA Proceeding,* 638-659, 1998.

Barnes, H. A., Hutton, J. F., Walters, K., *An Introduction to Rheology,* Elsevier Science Publishers B. V., Amsterdam, The Netherlands, 1989.

Benjamin, D. F., Roll Coating Flows and Multiple Roll Systems, University of Minnesota, PhD. Dissertaion, March **1994.**

Benjamin, D. F., Carvalho, M. S., Anderson, T. J., Scriven, L. E., "Forward Roll Film Splitting: Theory and Experiment" *1994 Coating Conference,* **109, 1994.**

Benkreira, H., Edwards, M. F., Wilkinson, W. L., "Roll coating of purely viscous fluids" *Chemical Engineering Science,* **36,429-434 1981.**

Bennett, C. **O. ,** Myers, J. E., *Momentum, Heat and Mass Transfer,* McGraw-Hill, New York, **1974.**

Bery, Y. **A.,** Loel. P. **A.,** "Nature of Ink Film Splitting", *1992 International Printing & Graphics Arts Conference, 53,* **1992.**

Blayo, B., Fang, **S.** W., Gandini, **A.,** Le Nest, J. F., "Study of Ink Misting Phenomena", *TAGA Proceeding,* **791-806, 1997.**

Bousfield, D. W., "Filament Splitting Between Separating Plates", *Chem. Eng. Comm.,* **73, 19, 1988.**

Bousfield, D. W., "Thinning of a Viscoelastic Film", *Chemical Engineering Science,* **44, 3,763, 1989.**

Brennen, C. E., *Cavitation and Bubble Dynamics,* Oxford University Press, New York, **1995.**

Browne, T.C., Crotogino, R. H., Douglas, W. J. M., "Viscoelastic Modeling of Paper in a Calender Nip" *Journal of Pulp and Paper,* **22,** *5,* **170, 1996.**

Carvalho, M. **S.,** Dontula P., Scriven , L. E., "Non-Newtonian Effects on the Ribbing Instability" *1995 Coating Conference,* **223, 1995.**

Chen, K. S. A., Scriven, L. E., "Liquid penetration into a deformable porous substrate" *TAPPI Journal*, **73,** 1, **151, 1990.**

Chhabra, R. P., *Bubbles, Drops, and Particles in Non-Newtonian Fluids,* CRC Press, Ann Arbor, U.S.A., **1993.**

Chou, S. M., "A Study of Ink Formulation Versus Ink Properties: I. Steady-Shear Rheological Properties", *1994 International Printing & Graphics Arts Conference,* **97-100,1994.**

Chou, S. M., "A Study of Ink Formulation Versus Ink Properties: II. Ink Transfer and Ink Mileage", *1994 International Printing & Graphics Arts Conference,* **101-104, 1994.**

Cohu, O., Magnin,A., "Rheometry of paints with regard to roll coating process", *The Jorurnal of Rheology,* **39, 4, 1995.**

Coyle, D. J., Macosko, C. W., Scriven, L. E., "Film-splitting flows in forward roll coating", *Journal of Fluid Mechanics,* **171, 183, 1986.**

Coyle, D. J., Macosko, C. W., Scriven, L. E., "Film-splitting flows of shear thinning liquids in forward roll coating", *AIChE Journal,* **33,741-746, 1987.**

Coyle, D. J., Macosko, C. W., Scriven, L. E., "Stability of symmetric film-splitting between counter-rotating cylinders", *Journal of Fluid Mechanics,* **216,437, 1990.**

Creasy, T. S., Advani, S. G., Okine, R. K., "Non-linear reponse of a long, discontinuous fiber/melt system in elongational flows", *Rheol. Acta*, **35, 345-355, 1996.**

Debenedetti, P. G., D'Antonio, M. C., "Stability and Tensile Strength of Liquids Exhibiting Density Maxima", *AIChE Journal,* **34, 3, 447-464, 1988.**

De Grâce, Y. H., Dalphond, J. E., Mangin, P. J., "A Mechanistic Approach to Ink Transfer, Part III: Properties of Ink Filaments in Printing Nips", *Advances in Printing Science and Technology,* **21,312, 1992.**

Desjumaux, D. Bousfield, D. W., Aurenty, P., "Dynamics of Ink Gloss: Influence of Ink Rheology on Leveling", *TAGA Proceeding,* 618-637, 1998.

Ercan, S. N., Investigation of Steady Shear Rheology of Hazelnut Paste and Peanut Paste, Bogazici University, Masters Thesis, 1996.

Ercan, **S.** N., Bousfield, D. W., "Influence of Process Parameters on Filament Size Distribution", *1998 Pan-Pacific and International Printing & Graphic Arts Conference,* 111,1998.

Everage, Jr. A. E., Gordon, R. J., "On the Stretching of Dilute Polymer Solutions", *AIChE Journal,* **17**, 5, 1257-1259, 1971.

Fernando, R. H., "Rheological Aspects of Misting Mechanisms in Roll Applied, Non-Newtonian Paper Coatings and Inks" *1999 Coating Conference,* 1, 1999.

Fernando, R.H., Glass, J. E., "Dynamic Uniaxial Extensional Viscosity (DUEV) Effects in Roll Application 11. Polymer Blend Studies", *Journal of Rheology,* **32,** 2, 199-213, 1988.

Fu, T. Z., James, D. F., Lyne, M. B., "Measuring the Extensional Rheology of Printing Inks", *1994 International Printing & Graphic Arts Conference,* 3, 1994.

Gaskell, P.H., Savage, M.D., Summers, J.L., Thompson, H.M., "Modeling and Analysis of Meniscus Roll Coating", *Journal of Fluid Mechanics.,* 298: 113-137, 1995.

Gavis, J., Gill, S. T., "Tensile Stress in Jets of Viscoelastic Fluids II", *Journal of Polymer Science,* **21,** 353-362, 1956.

Glass, J. E., "Dynamics of Roll Spatter and Tracking: Part I: Commerical Latex Trade Paints", *Journal of Coating Technology,* Reprint of May and June 1978 issue.

Glass, J. E., "Dynamics of Roll Spatter and Tracking: Part 11: Formulation Effects in Experimental Paints", *Journal of Coating Technology,* Reprint of May and June 1978 issue.

Glass, J. E., "Dynamics of Roll Spatter and Tracking: Part III: Importance of Extensional Viscosities", *Journal of Coating Technology,* Reprint of May and June **1978** issue.

Glass, J. E., "Dynamics of Roll Spatter and Tracking: Part IV: Importance of G* Recovery and N_1 in Tracking", *Journal of Coating Technology,* Reprint of May and June **1978** issue.

Glatter, T., Bousfield, D., "Print Gloss Development on a Model Substrate", *1996 International Printing & GraphicArts Conference,* **141, 1996.**

Glatter, T., Print Gloss Development on a Model Substrates, University of Maine, Masters Thesis, **1996.**

Hayashi, T., Amari, T., "Dynamics of Transfer and Splitting of Emulsified Ink", *1992 International Printing & GraphicArts Conference,* **75, 1992.**

Hayashi, T., Kotaro, M., Amari, T., "Rheological Properties and Printabilities of Polybutadiene/Carbon Black Ink", *J. Jpn. Soc. Colour Muter.,* **66,** 1**1,655-664, 1993.**

Ilano, A. L., Williams, M.C., Greens, E. A., "Degradation of Polymers During Aerosol Formation from Antimisting Polymer Solutions", *Journal of Applied Polymer Science,* **32,3649-3656, 1986.**

Isono, H., Hasuike, M., "Effects of Paper Structure on Print Quality", *1992 International Printing & GraphicArts Conference,* **197, 1992.**

Iyer, R. R., Bousfield, D. W., "The leveling of coating defects with shear thinning rheology" *J. Chem. Eng. Sci.,* **51,4611, 1996.**

Jones, W. M., Williams, P. R., Virdi, T. **S.,** "The Elongation of Radial Filaments of a Boger Fluid on a Rotating Drum", *Journal of Non-Newtonian Fluid Mechanics,* **21, 51-64, 1986.**

Kolte, M. I., Szabo, P., "Capillary thinning of polymeric filaments", *Journal of Rheology,* **43, 3, 609, 1999.**

Langhaar, H. L., *Dimensional Analysis and Theory of Models,* R. E. Krieger Pub. Co., New York, 1980.
Letzelter, P., Eklund, D., "Dewatering of Coating Color in the Film Press" *1996 Tappi Coating Conference Proceedings,* 269-281, 1996.

Lim, C. H., Bohan, M. F. J., Claypole, T. C., Gethin, D. T., Roylance B. J., **"A** finite element investigation into a soft rolling contact supplied by a non-Newtonian ink." *Journal of Physics, **29,*** 1894-1903, 1996.

Lindholm, G., "Dimensional stability and the influence of conditions in the printing nip", *1996 International Printing & Graphic Arts Conference,* 55, 1996.

Lyne, M. B., "The Importance of Extensional Viscosity in the Impression of Ink into Paper during Printing", *Advances in Printing Science and Technology,* 236-248, 1990.

MacGregor, M. **A.,** Johansson, P., "Image Analysis Techniques for Studying 'Orange Peel' Gloss Effects in LWC Paper", *1990 Coating Conference,* 125, 1990.

MacPhee, J., **"A** Unified View of the Film Splitting Process, Part I", *American Ink Maker,* 75, 1, 42-49, 1997a.

MacPhee, J., **"A** Unified View of the Film Splitting Process, Part 11", *American Ink Maker,* **75**, 2, 51-56, 1997b.

Matta, J. E., Tytus, R. P., "Liquid Stretching Using **A** Falling Cylinder", *Journal of Non-Newtonian Fluid Mechanics,* 35,215-229, 1990.

Nguyen, D. **A.,** Sridhar, T., "Preparation and Some Properties of M1 and its Constituents", *Journal of Non-Newtonian Fluid Mechanics,* **35**, 93-104, 1990.

Nguyen, N., Jordan, B., De Grâce, J., "Measurements of Ink Filament Splitting Patterns by Image Analysis", *Journal of Pulp and Paper Science,* **20**, 3, J87, 1994.

Ninness, B, Bousfield, D. W., Triantaafillopoulos, N. G., " Fluid Dynamics Mode if the Film-Fed Rolling Nip with a Porous Substrate" 1998 *Coating Conference,* 515, 1998.

Nixon, K. E., "Inks Under Pressure Part 11",*American Ink Maker*, 34-44, 1995.

Olagunju, D. O., **"A** 1-D theory for extensional deformation of a viscoelastic filament under exponential stretching", *Journal of Non-Newtonian Fluid Mechanics,* 87, 27-46, 1999.

Pangolos, G., Dealy, J. M., Lyne, M. B., "Rheological Properties of News Inks", *Journal of Rheology,* 4,471, 1985.

Patel, N., Dealy, J., M., "Measurement of Tensile Stress at the Exit of a Printing Nip", *Journal of Non-Newtonian Fluid Mechanics,* 22,245-252, 1987.

Petrie, C. J. **S.,** *Elongational Flows,* Pitman Publishing Limited, London, 1979.

Pitts, E., Greiller, J., "The Flow of Thin Liquid Films Between Rollers" *Journal of Fluid Mechanics,* **11**, 33, 1961.

Riise, B. L., Mikler, N., Denn, M. M., "Rheology of liquid crystalline polymer dispersed in a flexible polymer matrix", *Journal of Non-Newtonian Fluid Mechanics,* 86, 3-14, 1999.

Rodrigue, D., De Kee, D., Chan Man Fong, C. F., "The slow motion of a single gas bubble in a non-Newtonian fluid containing surfactants", *Journal of Non-Newtonian Fluid Mechanics,* **86**, 211-227, 1999.

Rood, E.P., "Review-Mechanisms of Cavitation Inception", *Journal of Fluids Engineering,* 113, 163, 1991.

Roper 111, J. **A.,** Bousfield, D. W., Urscheler, R., Salminen, P., "Observations and Proposed Mechanisms of Misting on High-speed Metered Size Press Coaters", 1997 *Coating Conference,* pg. 1, 1997.

Smith, D., Engle, L. S., Howard, J., Jones, W., "Film Splitting on Rotating Rollers", *TAGA Proceeding,* 147-151, 1956.

Soules, D. A., Fernando, R.H., Glass, J. E., "Dynamic Uniaxial Extensional Viscosity (DUEV) Effects in Roll Application I. Rib and Web Growth in Commercial Coatings", *Journal of Rheology*, **32**, 2, 181-198, 1988.

Steiert, Ph., Wolff, C., "Rheological Properties of a Polyisobutylene in a Kerosene/Polybutene Mixture in Simple Shear Flow", *Journal of Non-Newtonian Fluid Mechanics,* 35, 189-196, 1990.

Strauss, V., *The Printing Industry,* Printing Industries of America, Inc., 1967.

Taylor, E. S., *Dimensional Analysis for Engineers,* Clarendon Press, Oxford, 1974.

Taylor, J., H., Zettlemoyer, A. C., "Hypothesis on the Mechanism of Ink Splitting During Printing" *TAPPI,* **41,** 12, 749, 1958.

Thomson, I. G., Young, F. R., "High-speed photographic studies of ink filamentation", *Jour. Oil Col. Chem. Assoc.,* 58,389, 1975.

Toivakka, M. O., Bousfield, D. W., "Levelling of Coating Supensions" *Journal of Pulp ans Paper Science,* **25,** *5,* 183-188, 1999.

Trefz, M., "Theoretical Aspects and Practical Experiences for Film Coated Offset Grades", *TAPPI Journal,* **79,** 1,223-230, 1996.

Van der Meulen, W. M. , "Misting of Printing Inks", *American Ink Maker,* ***65,*** 6, 86, 1987.

Voet, A., "Ink Misting and Its Prevention", *American Ink Maker*, **34,** *2,* 32, 1956.

Xiang, Y., Desjumaux, D., Bousfield, D. W., Forbes, M. F., "Relationship Between Coating Layer Composition, Ink Setting Rate, and Offset Print Gloss", *1998 Pan-Pacific and International Printing & Graphic Arts Conference,* 85-91, 1998.

Zang, Y. H., "Asymmetric Splitting and Ink Transfer: A new Ink Transfer Model", *1992 International Printing & Graphics Arts Conference,* 103, 1992.

Zang, Y. H., Aspler, J. S., Boluk, M. Y., De Grâce, J. H., "Direct measurements of tensile stress ("tack") in thin ink films", *Journal of Rheology,* **35,** 3, 1991.

Zang, Y. H., Aspler, "The Influence of Coating Structure on the Ink Receptivity and Print Gloss Development of Model Clay Coatings", *1994 International Printing & Graphic Arts Conference,* 193, 1994.

Zettlemoyer, A. C., *Nucleation,* Marcel Dekker Inc. 1969.

Zettlemoyer, A. C., Myers, R. R., "The Rheology of Printing Inks", *Rheology Theory and Application* Vol. 3 Academic Press, New York, 1960.

Zimsak, M. A., Boger, D. V., Tirtaatmadja, V., "Steady shear and dynamic rheological properties of xanthan gum solutions in viscous solvents", *Journal of Rheology,* **43,** 3, 627,1999.

APPENDIX A: CALCULATIONS OF ELONGATIONAL VISCOSITY

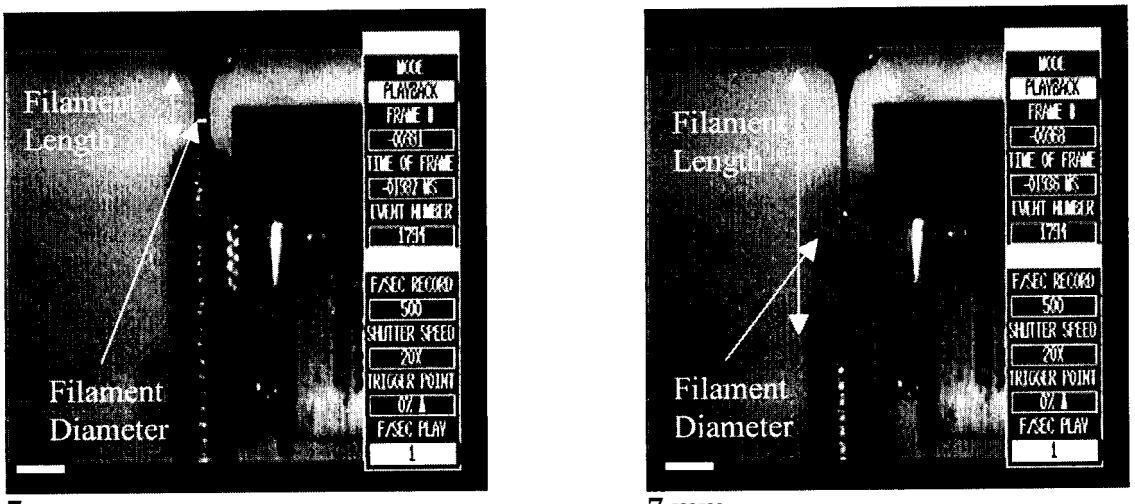

7 mm **7 mm**

a **b**

time = 164 ms **time = 210 ms**

Figure A.l: Images for elongational calculations

Table A.l: Excel sample spread sheet for calculating elongational viscosity

Procedure For Apparent Elongational Viscosity Calculation via Falling Cylinder Method

- Record Time, Filament Length, and Filament Diameter data from image analysis
- Plot (L-Lo) vs. Time and R vs. Time
- Fit Polynomials to these two curves
- Calculate first derivatives for these functions
- Calculate second derivative of Bob Velocity to get Bob Acceleration
- Calculate Bob Velocity, Bob Acceleration, and Radial Velocity
- Calculate Elongation Rate (epsilon dot) via Eq. 2 in Matta & Tytus
- Calculate Apparent Elongational Viscosity via Eq. 7 in Matta & Tytus

Bob Velocity Function

Polynomial Order	4	3	2	1	0
Coefficients	0	1822.1	-226.81	9.8602	-0.099
1st Deriv.	0	5466.3	-453.62	9.8602	0

Bob Acceleration Function

Polynomial Order	3	2	1	0
Coefficients	0	5466.3	-453.62	9.8602
1st Deriv.	0	10932.6	-453.62	0

Radial Velocity Function

Polynomial Order	3	2	1	0
Coefficients	180.11	-39.724	-0.0723	0.3449
1st Deriv.	540.33	-79.448	-0.0723	0

Table A.2: Excel sample spread sheet for calculating elongational viscosity

Time (s)	Filament Length (L) (mm)	L (cm)	L-Lo (cm)	Filament Diameter (mm)	Filament Radius (R) (cm)
0	2.3	0.23	0	6.991103	0.34955515
0.012	2.356552	0.2356552	0.0056552	6.755448	0.3377724
0.024	2.435103	0.2435103	0.0135103	6.519793	0.32598965
0.036	2.670759	0.2670759	0.0370759	5.891379	0.29456895
0.048	2.827862	0.2827862	0.0527862	5.420069	0.27100345
0.06	3.063517	0.3063517	0.0763517	4.791655	0.23958275
0.072	3.534828	0.3534828	0.1234828	4.006138	0.2003069
0.084	4.477448	0.4477448	0.2177448	3.300107	0.16500535
0.096	5.969931	0.5969931	0.3669931	2.592207	0.12961035
0.108	8.483586	0.8483586	0.6183586	1.963793	0.09818965
0.12	11.86131	1.186131	0.956131	1.571034	0.0785517
0.132	16.57516	1.657516	1.427516	1.178276	0.0589138
0.144	23.01619	2.301619	2.071619	0.9426207	0.047131035

Table A.3: Excel sample spread sheet for calculating elongational viscosity

Bob Velocity (V) (cm/s)	Radial Velocity (Vr) (cm/s)	Bob Acceleration (a) (cm/s^2)	Elongation Rate (epsilon dot) (1/s)	App. Elongational Viscosity (eta) (Pa-s)	Shear Viscosity (Pa-s)
9.8602	-0.0723	-453.62	0.41366863	19100.41997	320
5,2039072	-0.94786848	-322.4288	5.612468514	1369.856608	320
2.1219088	-1.66782192	-191.2376	10.23236118	725.4745736	320
0.6142048	-2.23216032	-60.0464	15.15543522	532.7430269	320
0.6807952	-2.64088368	71.1448	19.48966834	427.7679344	320
2.32168	-2.893992	202.336	124.15860073	377.8829196	320
5.5368592	-2.99148528	333.5272	29.86901879	363.5789962	320
10.3263328	-2.93336352	464.7184	35.55476862	358.9076973	320
16.6901008	-2.71962672	595.9096	41.96619668	367.5985138	320
24.6281632	-2.35027488	727.1008	47.87215109	370.2004985	320
34.14052	-1.825308	858.292	46.47405467	287.9659706	320
45.2271712	-1.14472608	989.4832	38.86105055	-42.32540575	320
57.8881168	-0.30852912	1120.6744	13.0923974	-3232.017581	320

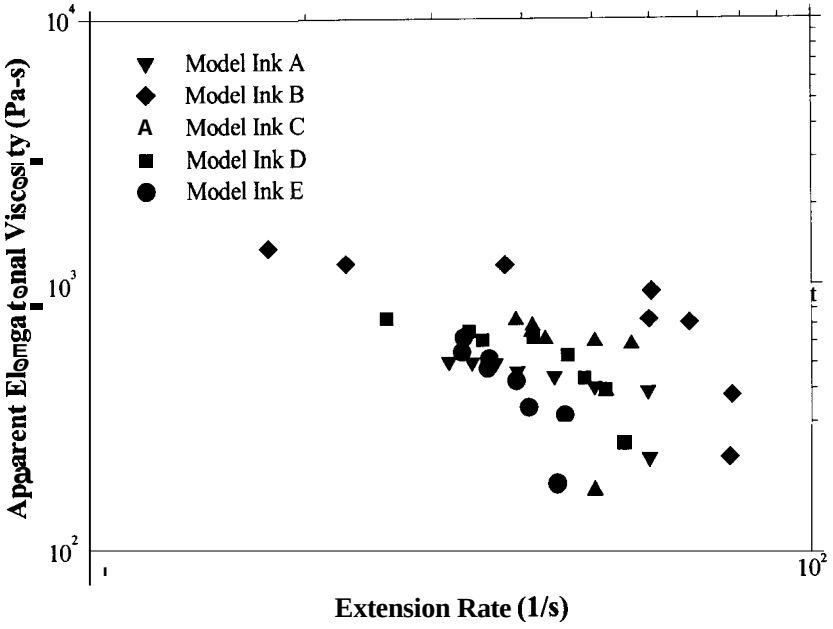

Figure **A.2:** Apparent elongational viscosities for the five model inks

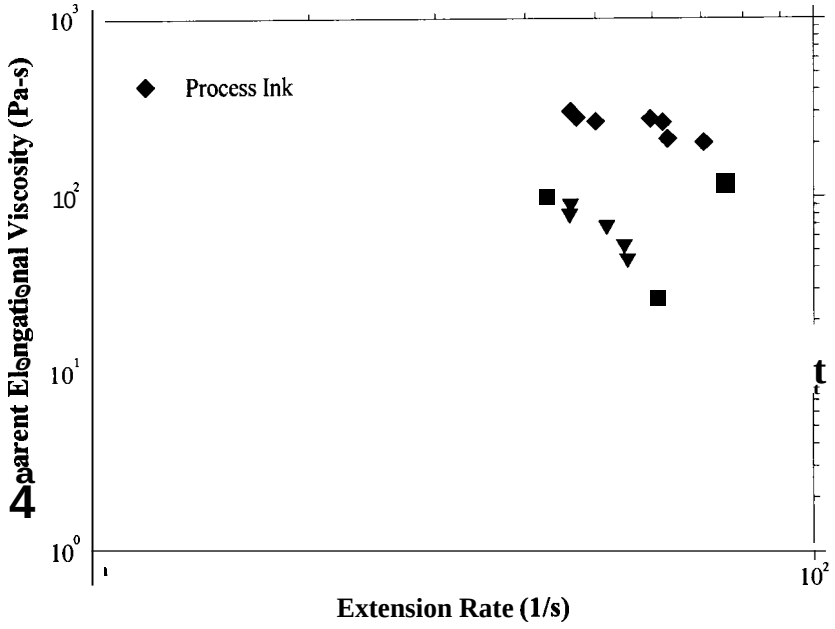

Figure A.3: Apparent elongational viscosities for the process ink and model ink I

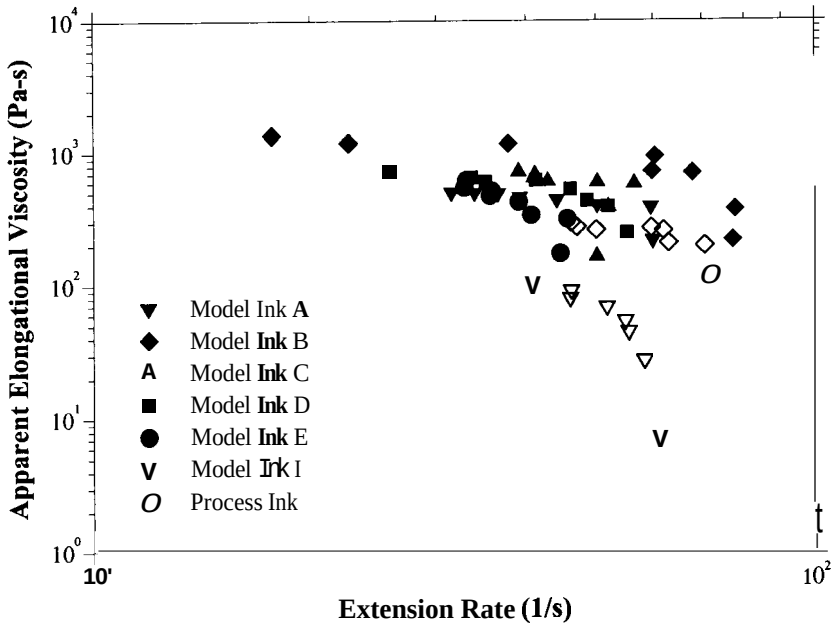

Figure A.4: Apparent elongational viscosities for all inks

APPENDIX B: CALCULATIONS OF FILAMENT VOLUMES

An image of the tip of a paper clip is used to calibrate the images measured to a realistic dimension. In the image below, the real width of the end of the paper clip is 0.8 mm. Knowing this and before each filamentation experiment measuring this width with a ruler on the screen gives us our calibration ratio. Since the camera position was kept in the same position the calibration ration came out to be the same for each experiment, 0.8 mm corresponded to 35 mm measured by the ruler.

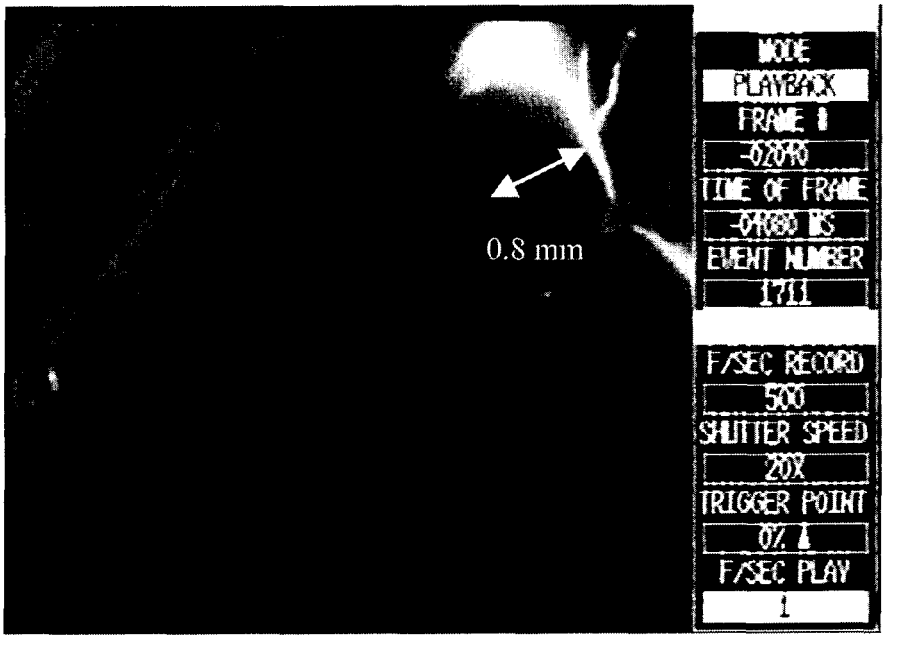

Figure B.1: Calibration image used for filament volume calculations

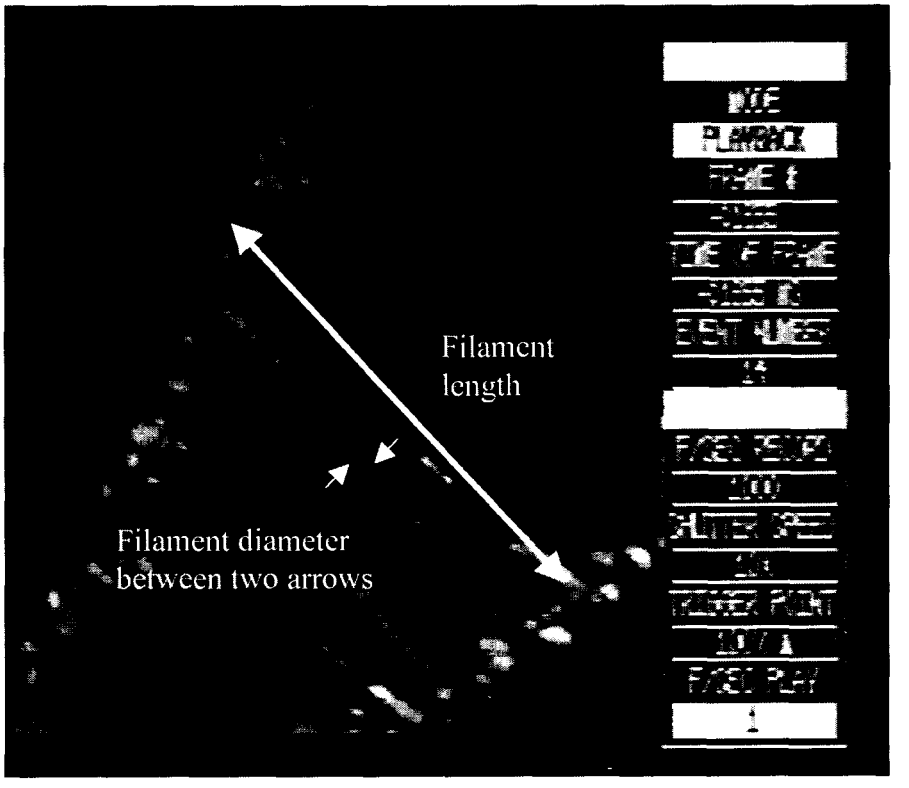

Figure B.2: Filament length and width measurements

Knowing the ratio above after each manual measurement of filament using a ruler a spread sheet shown below is prepared. Where the measured length and width are entered as data and the actual length and width of the filament are obtained, which is considered the calculated width and length. Assuming the filament is a cylinder the volume for each of the filaments measured are measured and an average is obtained. **A** standard deviation value is also calculated. These measurements are done using a ruler so errors may occur during prediction of width and length measurements occurring from the bare eye. The filaments measured are selected randomly, making sure the filament is clear is a key issue to be able to obtain a precise measurement of width and length. Filaments of all lengths, very small, as close into the nip as possible, and very long, as far out of the nip as the fluid elongates, were measured to be able to obtain a reliable average filament volume.

As many filaments as possible were measured and calibrated to obtain an average filament volume. In some cases, very many filaments were not seen and the comparisons after that were done using the same basis filament number.

Table B.1: Sample Excel spread sheet for calculating filament volume

Silicone Oil 1		0.8/3.5-cal	0.8/3.5-cal	Cylinder	Cylinder
L (measured)	**W (measured)**	**L (calculated)**	**W (calculated)**	**Volume (mm^3)**	**Volume (mm^3)**
3	0.3	0.685714286	0.068571429	0.002532325	2532325.18
3.5	0.4	0.8	0.091428571	0.00525223	5252230.004
4	0.5	0.914285714	0.114285714	0.009378982	9378982.149
3	0.5	0.685714286	0.114285714	0.007034237	7034236.612
3	0.7	0.685714286	0.16	0.013787104	13787103.76
3.4	0.3	0.777142857	0.068571429	0.002869969	2869968.538
3	0.3	0.685714286	0.068571429	0.002532325	2532325.18
2.7	0.5	0.617142857	0.114285714	0.006330813	6330812.951
1.5	0.7	0.342857143	0.16	0.006893552	6893551.88
3	0.2	10.685714286	0.045714286	0.001125478	1125477.858
2.5	0.3	0.571428571	0.068571429	0.002110271	2110270.984
3	0.5	0.685714286	0.114285714	0.007034237	7034236.612
2.5	0.6	0.571428571	0.137142857	0.008441084	8441083.935
3	0.3	0.685714286	0.068571429	0.002532325	2532325.18
3.5	0.3	0.8	0.068571429	0.002954379	2954379.377
3.5	0.4	0.8	0.091428571	0.00525223	5252230.004
2	0.5	0.457142857	0.114285714	0.004689491	4689491.075
4	0.2	0.914285714	0.045714286	0.001500637	1500637.144
3	0.4	0.685714286	0.091428571	0.004501911	4501911.432
1.8	0.4	0.411428571	0.091428571	0.002701147	2701146.859
			Avg. Vol.	0.004972736	
			Std. Dev.	0.003163958	

Table B.2: Film thickness, average filament volume and standard deviation values of fluids

Fluid	(μm)	Volume (mm^3)	Standard Deviation (mm^3)
s o 1	4	*0.005*	*0.003*
SO2	4	0.0006	0.0003
SO3	4	0.0007	0.0006
SO4	4	0.001	0.0007
PTO1	4	0.007	0.004
PT02	4	0.011	0.009
PT03	4	0.005	0.004
1.6% 7H	2	0.004	0.003
1.6% 9MS	1.7	0.002	0.001
35% 9MS	1.8	0.003	0.003
6.2% 9MS	2	0.006	0.009
Corn Syrup	2.5	0.009	0.008
Polyacrylamide	2	0.004	0.003
BF 1	2	0.007	0.008
BF 2	0.5	0.013	0.012
Model Ink A	1	0.008	0.007
Model Ink B	1	0.001	0.0006
Model Ink C	1	0.002	0.0015
Model Ink D	1	0.0008	0.0004
Model Ink E	1	0.002	0.001
Model Ink I	1	0.004	0.003
Process Ink	1	0.004	0.002

BIOGRAPHY OF THE AUTHOR

Saybil Nuray Ercan was born in Chicago, Illinois on February 23, 1972. She was raised in Highland Park, Illinois until 1984, moved to Istanbul, Turkey and was raised there after. She graduated as valedictorian from Ozel Dost High School, Istanbul, Turkey in June 1990. She attended the Chemical Engineering Department at Boğaziçi University in October 1990. She graduated with a Bachelor of Science degree from the Chemical Engineering Department of Boğaziçi University in July 1994. Ercan continued at the same university and same department with a teaching and research assistantship for her Masters of Science degree and obtained her degree in June 1996. She joined the Paper Surface Science Program of the Chemical Engineering Department at The University of Maine in the fall of 1996 with the hope of obtaining a degree of Doctor of Philosophy.

Saybil Nuray Ercan is a candidate for the Doctor of Philosophy degree in Chemical Engineering from The University of Maine in May, 2001.